Ordered And Disordered Porous Materials

For Nanofiltration Application

Graduation committee:

Chairman:	Prof. dr. ing. M. Wessling	University of Twente
Promotor:	Prof. dr. ing. D.H.A. Blank	University of Twente
Assistant promotor:	Dr. ir. J.E. ten Elshof	University of Twente
Committee members:	Dr. ir. K. Keizer	University of Twente
	Prof. dr. ir. L. Lefferts	University of Twente
	Prof. F. Mugele	University of Twente
	Prof. A. Ayral	University of Montpellier II
	Dr. A. Buekenhoudt	VITO, Mol

The research described in this thesis was carried out in the Inorganic materials science group at the University of Twente. Financial support is provided by The Commission of the European Communities in the framework of the Growth Programme, "SUSTOX - Catalytic Oxidation as Tool for Sustainable Fine Chemicals Manufacture", contract no. GRD1-2000-25053.

Ordered and disordered porous materials for nanofiltration application

Sankhanilay Roy Chowdhury

ISBN 90-365-2178-5

Printed by Print Partners Ipskamp, Enschede, The Netherlands.

ORDERED AND DISORDERED POROUS MATERIALS FOR NANOFILTRATION APPLICATION

DISSERTATION

to obtain
the doctor's degree at the University Twente,
on the authority of the rector magnificus,
prof. dr. W.H.M. Zijm,
on account of the decision of the graduation committee,
to be publicly defended
on Wednesday, April 6, 2005 at 15.00

by

Sankhanilay Roy Chowdhury

born on 12th April 1972

in Chandannagar, India

The dissertation is approved by the promotor
Prof. dr. ing. D.H.A. Blank and the assistant promotor Dr. ir. J.E. ten Elshof

This thesis is dedicated to

You

Table of Contents

Summary

This Ph.D. dissertation elaborates on the use of porous materials in fluid separation technology. Two different types of porous materials, namely surfactant templated silica and alumina have been used to prepare flat plate geometry porous membranes.

Two different synthesis routes of surfactant templated silica materials have been presented. Silica sol formulations have been taken from literature. Powders derived from sol 1 did not show any sign of an ordered mesoporous structure, however films derived from sol 1 on different supports did contain ordered mesoporous domains. It has also been shown that the ordered silica layer does not grow directly on the mesoporous substrate. Instead it grows on a structurally disordered silica-rich interface of thickness ~20 nm. Defect free layers could be formed from sol 1 both on macroporous and mesoporous supports. Powders and thin films grown on dense support, derived from sol 2, showed indications of an ordered mesoporous structure, but there was no sign of an ordered porous structure on porous substrates. Defect-free silica layers could be formed on mesoporous supports but not on macroporous supports. Water transport experiments showed that a silica layer deposited on an α-alumina support has the highest water permeability among all the silica layers, but the intrinsic permeability of the silica layer deposited on α-alumina support showed the lowest value. This is probably due to the microporous nature of the silica layer. Non-aqueous solvent permeation through the γ-alumina supported silica layer from sol 2 showed that hydrophilic liquids have a higher permeability coefficient than hydrophobic solvents.

Fluid flow through porous media receives considerable attention in this thesis. Three different pore sized γ-alumina membranes were prepared by calcining the membranes at three different temperatures namely 450°C, 600°C and 800°C. Fluid flow through porous media could be described in a very simple manner with Darcy's law. It was found that the behaviour of all liquids (hydrophilic or hydrophobic) except water deviates from Darcy's law (e.g. pressure vs. flux plot gives a positive x-axis intercept) below some critical average diameter of the porous medium. The critical pore diameter is not the same for each and every liquid. To understand this behaviour we took into account two structural factors, namely porosity and tortuosity of the porous medium, which can affect the permeability of the liquids, and a physical parameter, namely the viscosity of the liquids. It has been found that the presence of water as a secondary minority species in the solvents plays an important role in the mechanism of solvent transport through porous media. Based on the observed phenomena and available literature a hypothesis of liquid transport through porous media has been proposed.

The recovery of an industrially important poly-oxo-metalate (POM) catalyst using two types of γ-alumina membranes is also discussed. Nanofiltration experiments

were carried out on aqueous solutions of $Na_{12}POM$ and an organic liquid mixture containing $Q_{12}POM$ (Q=quarternary ammonium ion). The γ-alumina membrane calcined at 600°C showed > 96% retention of POM ions, regardless of the nature of the counter ions and the nature of the solvent. γ-Alumina membranes calcined at 900°C showed a lower level of retention for toluene soluble $Q_{12}POM$. The analysis showed that the retention of the catalyst is due to both double layer overlap and size exclusion for both water-soluble $Na_{12}POM$ and toluene soluble $Q_{12}POM$. Liquid permeability studies showed that aqueous POM solutions obey Darcy flow behaviour, while a non-zero threshold pressure needs to be exceeded before (non-aqueous) hydrophobic liquid transport takes place. This threshold pressure was absent for γ-alumina membranes calcined at 900°C, and this is most likely due to the larger pore size in the latter system. NMR and IR investigations on the final reaction mixture showed that the POM catalyst is stable under the used reaction and permeation conditions. XPS measurements together with experimental data showed that the POM did not enter the pores of the membrane, and thus it could be recovered easily. It has also been shown that the catalytic activity of the POM moiety increased with the number of membrane recycles.

Chapter 1

General introduction

There are two essential basic strategies for success in business:

1. Never reveal all you know

1. Introduction

Membrane separation / transport is one of the most primitive chemical process known on Earth. Examples of the earliest membranes are the biological cell membranes. Membrane separation processes have become an important industrial tool to obtain high purity products after the discovery of the first practical synthetic membrane process, reverse osmosis process using cellulose acetate membrane, by Sourirajan and Loeb at University of California, Los Angeles in 1960. Driving force for a membrane separation process can be a thermal energy gradient (membrane distillation), a concentration gradient (pervaporation, dialysis) or pressure (reverse osmosis, nanofiltration, untrafiltration). All these driving forces are manifestations of a difference of chemical potential of the permeating species between the feed side and the permeate side.

Membrane science is an interdisciplinary research area for scientists coming from chemistry, physics, materials science, chemical engineering, mechanical engineering and biology. Knowledge from some unrelated research fields like geology might also contribute to a large extent to the understanding of fluid flow through porous membranes.

Nanofiltration membranes are used to separate multivalent ions and small organic molecules from a solvent. Nanofiltration membranes can be divided into two groups depending on their structure, namely porous membranes and dense membranes with a swollen network. The first category comprises mainly inorganic membranes and the second category membranes polymeric materials. Both types can be either charged or uncharged, although no uncharged porous membranes are known that show nanofiltration properties. Ceramic nanofiltration membranes can have a wide range of pore diameters, from 1 nm to 7 nm depending upon the material and preparation procedures. Polymeric nanofiltration membranes can be porous or dense. A large number of organo-mineral membrane systems are also available for nanofiltration processes. Promising membrane materials for separation of highly charged large molecules are discussed briefly in the next sections.

2. Nanofiltration membrane materials

2.1 Inorganic nanofiltration membranes

A connected microporous structure in supported ceramic films can be created from a non-aggregated nanoparticulate sol with individual nanoparticles of less than 10 nm size. Such membranes offer attractive properties when used as ceramic nanofilters. Ceramic nanofilters are being recognized as being of growing importance due to the increasing demands of membrane systems that are able to separate ions and small molecules in harsh working conditions.

Macroporous α-alumina supported mesoporous γ-alumina is one of the important types of stacked ceramic nanofiltration membranes (1). These alumina membranes have good thermal and mechanical stability. These membranes have good

structural stability towards organic solvents but in very acidic (pH < 4) or alkaline (pH > 10) aqueous solutions the membrane system becomes chemically unstable (2). To improve the pH stability of ceramic membranes, zirconia and titania membranes have been developed (4,5). These two membrane systems can work in the pH window 0-12. Doping zirconia with magnesium oxide can even result in stable membranes through the whole pH range (3).

These membranes are usually prepared from their respective alkoxides. Hafnia nanofiltration membranes have been prepared by hydrolysis of hafnium alkoxide precursors (5). The water permeability through these membranes was found to be quite high. Silica-zirconia composite membranes have been prepared by the colloidal sol-gel method. The average pore size of this membrane varied from 1-4 nm. The polarity of the solvent was found to play a major role in the rejection characteristics of this system (6).

Sol-gel derived inorganic nanofiltration membranes can be thought of as a very thin packed bed of fine particles. The solvent permeation through these membranes is often described in terms of classical fluid mechanics (7). But nowadays some non-classical concepts like boundary slip (8,9) and the behaviour of fluids in confined media with dimensions of the order of the fluid molecules (10) are being applied to describe the permeability through the membranes (11).

2.2 Polymeric nanofiltration membranes

There are a few polymers that can be used as nanofiltration membranes, such as polyethersulfone (PES), sulfonated polysulfone, and polypiparazine amide (12) polydimetheyl siloxane (PDMS) (13), cellulose acetate (CA) (7), polysulfone (PS), (14) polyamides (PA)(15). These membranes can be dense or porous. The pore size of these membranes may vary from 0.43 nm to 4 nm (12). Cellulose esters like cellulose acetate (CA) are very suitable for desalination applications

because of their high permeability towards water in combination with a very low solubility towards salt (7). However, the chemical and thermal stability of these membranes is quite poor and therefore cleaning of the membrane modules is difficult. PA has better chemical stability compare to CA but it degrades in presence of an oxidizer like chlorine. PS, PES and polypiparazine amide has been used successfully for water treatment to remove multivalent ions. PDMS membrane has been used for solvent resistant nanofiltration (SRNF) (13). Generally inorganic membranes have higher water permeability than polymeric membranes due to larger pores (16).

2.3 Hybrid organic- inorganic membranes

Hybrid organic- inorganic materials offer a consistent and unique opportunity to combine the specific transport properties of organic and inorganic materials in

order to develop highly permselective membranes. Hybrid organic-inorganic materials are usually classified into two categories.

In the first category only interactions like Van der Waals forces and/or hydrogen bonds exist between the organic and inorganic parts. Such hybrid materials can be described as micro- or nanocomposites in which one part is dispersed in the other part that acts as host matrix.

In the other category a covalent bond exists between the organic and inorganic parts, resulting either in a homogeneous hybrid material on the molecular level, or in high surface area inorganic materials modified through surface grafting of organic groups. Examples of organic and inorganic hybrid membranes are the polysulfone – zirconia (Zirfon) system (17) and the Nafion-silica system (18). Nafion is a polymer having $–CF_2-CF_2-$ backbone with SO_3^- groups grafted on it.

Zirfon membranes are prepared by a phase inversion technique. In this system zirconium oxide grains are directly added to a polysulfone solution in N-methyl pyrrolidone and then the membrane is prepared by casting process. No chemical reaction is involved in this process.

Nafion-silica composite membranes can be prepared by introducing a silica precursor into a Nafion membrane. Silica forms the inside of the Nafion matrix due to hydrolysis and condensation of the precursor molecules. These hybrid membranes are more hydrophilic than the original Nafion membranes.

3. Important factors for separation mechanism of nanofiltration

Separation of solutes in nanofiltration processes is governed by two distinct factors, namely a) size exclusion (steric hindrance) by the membrane pores, and b) electrostatic interactions between charged solutes and the native surface charge on the membrane pore walls. The sign and magnitude of the solute charge determines the degree of electrostatic exclusion (19).

The Donnan potential governs the electrostatic exclusion in a membrane process. If a salt solution is in contact with a charged membrane, the membrane will repel ions with same charge of the membrane surface and attract ions with opposite charge. This process generates concentration gradients of all ions at the membrane/solution interface. Due to these concentration gradients a potential difference will be generated at the membrane/solution interface. This potential is known as Donnan potential. According to the original Donnan formula (20)

$$E = \frac{RT}{F} \log \frac{x}{y} \qquad [1]$$

where E is the Donnan potential, R the universal gas constant, T the absolute temperature, F the Faraday constant, x the co-ion concentration in the bulk solution, and y the co-ion concentration in the membrane. This potential prevents the diffusion of co-ions from the solution into the membrane. The Donnan potential difference is responsible for the repulsion of co-ions (i.e. ions with the same charge

as the membrane surface). Due to the requirement of electroneutrality, the counter ions are also rejected and thus separation of ionic solutes from the uncharged solutions occurs. For the salt A_xB_y, which ionises into A^{y+} and B^{x-}, the salt distribution coefficient *K* at equilibrium is given by

$$K = \frac{[B]_{membrane}}{[B]_{bulk}} \qquad [2]$$

The rejection (R) of the salt is then approximated by (1-K). This equation applies to negatively charged membrane (as in the case of inorganic nanofiltration membranes above their iso-electric points) used in nanofiltration.

Steric factors become important particularly for uncharged solute separation from solutions.
There are several theoretical models like the solution diffusion model (21), Maxwell-Stefan model (22), the dielectric exclusion model (23), available to describe solute rejection in nanofiltration membranes.

4. Polyoxometalate (POM) catalysts

POMs (polyoxometalates) are well known catalysts for the production of fine chemicals via oxidative methods (24). POMs are formed by a small number of metal clusters (typically 6-18 W, Mo or V atoms) coordinated by bridging oxygen atoms. They are stable at low pH ~ (2 – 4.5), highly soluble in water and very stable from redox point of view. These properties make it difficult to deal with the pure POMs. The structure of POMs range from simple to extremely complex, such as the wheel shaped and ball shaped structures shown below in Figure 1. The diameter of these molecules varies from 2.3 nm to 3 nm with a cage thickness of 2Å.

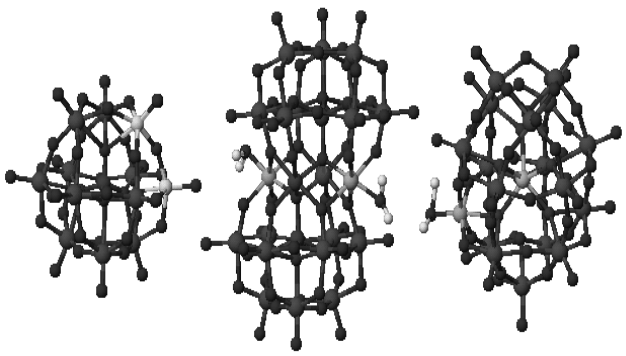

Figure 1. Schematic representations of different polyoxometalate (POM) molecules.

$[PV_2Mo_{10}O_{40}]^{5-}$(Left), $[M_2ZnW(ZnW_9O_{34})_2]^{q-}$(middle), $[MW_{17}O_{56}F_6NaH_2]^{q-}$(right). M (transition metal such as Mn, Ru, V etc.)

5. Scope of the thesis

The development of non-destructive recycling technologies for homogeneous catalysts is currently receiving strong interest. In particular, nanofiltration is emerging as a powerful technology for non-destructive homogeneous catalyst

recycling. For industrial use, especially under continuous conditions, very high catalyst retentions are required for valuable catalysts (generally well above 99%). The usual approach to achieve such very high retentions is based on the design of enlarged homogeneous catalysts with a rigid, shape-persistent molecular structure (25). Such catalysts are commonly prepared through a lengthy, and accordingly costly, multi-step organic synthetic procedure, which lowers the industrial feasibility of such catalyst systems. In this thesis we show that an inorganic, "sandwich" type polyoxometalate oxidation catalyst can be recycled very efficiently with near-quantitative retentions using nanofiltration. Till date in literature usefulness of polymeric membranes to recover homogeneous catalysts have been demonstrated. In this thesis the usefulness of inorganic γ-alumina membranes for catalyst recycling in organic medium will be demonstrated.

It is important to know the solvent–membrane interactions and solvent permeability through these membranes. Systematic studies of solvent permeation through organic polymeric membranes are known in literature, but for inorganic membranes this is still a largely unexplored field. Most inorganic nanofiltration membranes are mesoporous, i.e., pore diameters may vary from 2 to 50 nm. Here the lower pore size range equals just a few molecular diameters and there is still an open debate in literature on the physical state of liquids when they are confined to spaces of such molecular dimensions (10). It is thus important to know what are the important factors that govern the mechanism and rate of solvent permeation through pores of nanometer range size.

Another aspect of this thesis concerns the development of a mesoporous membrane, which could overcome some of the disadvantages of conventional inorganic membranes. Conventional sol-gel derived membranes like γ-alumina, have a relatively wide pore size distribution and a high tortuosity of the separating layer, which affects the intrinsic separation selectivity and permeability, respectively, negatively. These disadvantages may be overcome by employing template-directed synthesis methods for the formation of the mesoporous top layer. A well-known example of a templated inorganic material is mesostructured silica. Templated silicas can be synthesized using arrays of self-assembled surfactant molecules as structure directing templates, around which the inorganic precursor species are polymerized. In view of their high porosity and well-ordered pore geometries with narrow pore size distributions and low tortuosities, thin films of templated mesoporous materials are potential candidates for membrane applications (26). The cubic MCM-48 silica phase has an interconnected 3D channel system so that a low tortuosity in all directions is expected. This feature should lead to a high permeability of the layer.

6. Thesis structure

Chapter 2 gives an overview of the background and recent developments in the development of mesoporous inorganic membranes using soft chemical methods like micellar templating techniques.

Chapter 3 describes the preparation and characterization of ordered mesoporous silica thin films using surfactant templating techniques. The films were grown on structurally different substrates, i.e., both dense and mesoporous. The effect of substrate structure on the film is also investigated.

Chapter 4 describes the transport of hydrophilic liquids through mesoporous γ-alumina membranes derived from boehmite sols. The pore size of the γ-alumina membrane was varied systematically by choosing different firing temperatures. The influence of pore size on the permeability of different hydrophilic liquids is discussed.

Chapter 5 describes the transport of hydrophobic organic liquids through γ-alumina membranes with different pore sizes. The effect of dissolved water on the permeability of hydrophobic solvents is discussed.

Chapter 6 describes the application of mesoporous γ-alumina membranes for the recovery and subsequent re-use of polyoxometatale catalysts from aqueous and non-aqueous media.

Chapter 7 gives an evaluation of the results obtained in this thesis, and presents some recommendations for further study.

References:

1. A. Larbot, S. Alami- Younissi, M. Persin, J. Sarrazin, L. Cot, Preparation of γ-alumina nanofiltration membrane, *J. Membr. Sci.*, **97** (1994) 167.
2. T. Van Gestel, C. Vandecasteele, A. Buekenhoudt, C. Dotremont, J. Luyten, B. Van der Bruggen, G. Maes, Corrosion properties of alumina and titania NF membranes**,** *J. Membr. Sci.,* **214** (2003) 21.
3. R. Vacassy, C. Guizard, V. Thoraval, L. Cot, Synthesis and characterization of microporous zirconia powders: Application in nanofilters and nanofiltration characteristics**,** *J. Membr. Sci.,* **132** (1997) 109.
4. J. Sekulic, J.E. ten Elshof, D.H.A. Blank, A microporous titania membrane for nanofiltration and pervaporation, *Adv. Mater.*, **16** (2004) 1546.
5. P. Blanc, A. Larbot, J. Palmeri, M. Lopez, L. Cot, Hafnia ceramic nanofiltration membranes. Part I: Preparation and characterization**,** *J. Membr. Sci.,* **149** (1998) 151.
6. T. Tsuru, H. Kondo, T. Yoshioka, M. Asaeda, Permeation of nonaqueous solution through organic/lnorganic hybrid nanoporous membranes, *A.I.ChE J.*, **50** (2004) 1080.
7. M. Mulder, *Basic principles of membrane technology*; Kluwer Academic Press; Dordrecht, the Netherlands, 1996.
8. V.S.J. Craig, C. Neto, D.R.M. Williams, Shear-dependent boundary slip in an aqueous Newtonian liquid, *Phys. Rev. Lett.* **87** (2001) 30.
9. V.P. Sokhan, D. Nicholson, N. Quirke, Fluid flow in nanopores: Accurate boundary conditions for carbon nanotubes, *J. Chem. Phys.* **117** (2002) 8531.

10. M.L. Gee, P.M. McGuiggan, J.N. Israelachvili and A.M. Homola, Liquid to solidlike transitions of molecularly thin films under shear, *J. Chem. Phys.,* **93** (1990) 1895.
11. S. Roy Chowdhury, K. Keizer, J.E. ten Elshof and D.H.A. Blank, Effect of trace amounts of water on organic solvent transport through gamma-alumina membranes with varying pore sizes, *Langmuir*, **20** (2004) 4548.
12. K.H. Choo, D.J. Kwon, K.W. Lee, S.J. Choi, Selective removal of cobalt species using nanofiltration membranes, *Enviro. Sci. and Tech.,* **6** (2002) 1330.
13. N. Stafie, Poly (dimethyl siloxane) - based composite nanofiltration membranes for non-aqueous applications, PhD thesis, University of Twente. The Netherlands, 2004.
14. P.R. Lakshminarayan, M.Cheryan, N. Rajagopalan, Consider nanofiltration for membrane separation, *Chem. Eng. Proc.*, **68** (1994) 74.
15. R. Rautenbach, A.Gröschl, Separation Potential of Nanofiltration Membranes, *Desalination*, **77** (1990) 73.
16. W.B.S. de Lint, Transport of electrolytes through ceramic nanofiltration membranes, PhD thesis, University of Twente. The Netherlands, 2003.
17. I. Genne, Formation and characteristics of organo-mineral ultrafiltration membranes, PhD Thesis, Katholieke Universiteit Leuven, Belgium, 1996.
18. K.A. Mauritz and I.D. Stefanithis, Microstructural evolution of a silicon oxide phase in perflurosulfonic acid ionomer by an in situ sol-gel reaction. 2. dielectric relaxation studies, *Macromolecules*, **23** (1990) 1380.
19. J.M.M. Peeters, Characterization of nanofiltration membranes, PhD thesis, University of Twente. The Netherlands, 1997.
20. F.G. Donnan, Theory of membrane equilibria, *Chem. Rev.* **1** (1924) 73.
21. H. Lonsdale, U. Merten, R. Riley, Transport of cellulose acetate osmotic membranes, *J. Appl. Poly. Sci.*, **9** (1965) 1341.
22. R. Krishna, J.A.Wesselingh, The Maxwell-Stefan Approach to Mass Transfer, *Chem. Eng. Sci.*, **52**, 861 (1997).
23. A.E.Yaroshchuk, Dielectric Exclusion of ions from membranes, *Adv. Colloid Interface Sci.*, **85** (2000) 193.
24. A.M. Khenkin, R. Neumann, A.B. Sorokin and A. Tuel, Aerobic hydrocarbon oxidation catalyzed by the vanadomolybdophosphate polyoxometalate, $H_5PV_2Mo_{10}O_{40}$, supported on mesoporous MCM-41, *Catal. Lett.,* **63** (1999) 189.
25. D. Nair, J.T. Scarpello, I.F.J. Vankelecom, L.M. Freitas dos Santos, L.S. White, R.J. Kloetzing, T. Welton and A.G. Livingston, Increased catalytic productivity for nanofiltration-coupled Heck reactions using highly stable catalyst systems, *Green Chem.*, **4** (2002) 319.
26. J.S. Beck, J.C. Vartuli, W.J. Roth, M.E. Leonowicz, C.T. Kresge, K.D. Schmitt, C.T.-W. Chu, D.H. Olson, E.W. Sheppard, S.B. McCullen, J.B. Higgins and J.L. Schlenkert, A new family of mesoporous molecular sieves prepared with liquid crystal templates, *J. Am. Chem. Soc.,* **114** (1992) 10834.

Chapter 2

Template-directed synthesis of mesoporous ceramic membranes: An overview

Facts are stubborn things

Abstract*

Surfactant templated silica materials become increasingly popular in the field of materials scientists due to its regular structure and easy preparation methods. Formation of surfactant templated materials (or in general liquid crystalline materials as template) is the combination of sol-gel science and surface science. Different characterization techniques like XRD, synchotron radiation, NMR, TEM, SEM are employed to get the insight of the formation process and structural properties. Apart from silica, the same synthetic strategies have been successfully applied to for alumina, titania and zirconia materials. These templated materials show promises in the field of catalysis, process engineering, environmental science and in electronics as low dielectric materials.
In this chapter we will discuss about the principles of formation of surfactant templated materials and its applications.

* Part of this chapter has been published in conference proceedings of 9th Aachen Membrane Colloquium, 18-20 March 2003.

1. Introduction

State of the art mesoporous inorganic membranes for liquid separation processes are normally made by sol-gel processing of inorganic precursors. Depending on the conditions during sol synthesis, film deposition, drying and thermal treatment, it is possible to obtain amorphous thin porous films with narrow pore size distributions in the meso- or microporous size range.

In the last decade a new sol-gel process has been developed (1,2) in which arrays of self-assembled surfactant molecules are used as structure directing templates for the pore structure, around which inorganic species can be polymerized. The method allows the creation of ordered pore geometries with tailored pore sizes in oxide matrials, which may lead to improved performance in terms of flux and selectivity when they are applied as mesoporous membranes.

In this chapter the main principles behind these so-called template-directed sol-gel synthesis methods are summarized, and the application of templated oxide materials in the form of thin films and membranes is discussed. As the application of templated silica and non-silica films as gas or liquid separation membranes has been reported to date in only few works, only a first impression of some of the possible future applications and the main challenges that lie ahead in research can be given.

2. Template-directed synthesis of mesoporous oxides and thin films

2.1 Surfactant/water phase diagram

A surfactant that is typically used in templated-assisted sol-gel synthesis is cetyl-trimethyl-ammonium-bromide (CTAB, $[C_{16}H_{33}\text{-}N(CH_3)_3]^+Br^-$). CTAB dissociates in water, and the quarternary ammonium cation (CTA^+) has typical surfactant characteristics. Figure 1 shows schematically the volume fraction vs. temperature phase diagram of a two-phase system like water/CTAB.

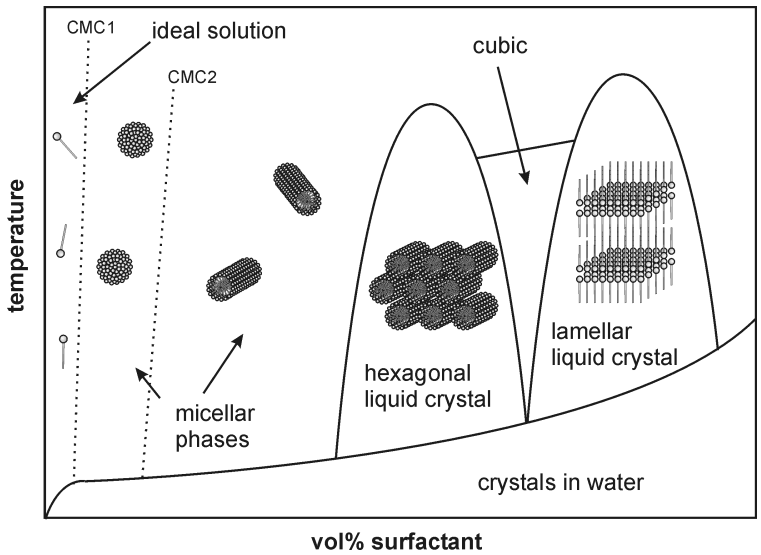

Figure 1. Schematic surfactant/water phase diagram.

Upon increasing the CTAB volume fraction in water from zero upwards at around room temperature, a number of phase transformations of the surfactant structure can be observed (3). CTA^+ ions are singularly dissolved in water only at very low concentrations. Beyond the so-called critical micelle concentration (CMC1 in Figure 1, <0.1 vol%) most CTA^+ molecules are assembled in the form of spherical aggregates (micelles), the apolar C_{16} tails directed towards the centre of the aggregate, and the hydrophilic NR_3^+ heads towards the surrounding water phase. At substantially higher CTAB volume fractions (CMC2) the spherical micelles transform into longer tubular structures that are randomly dispersed in the water phase. At even higher concentrations steric crowding occurs, causing the individual 'rods' to assemble into ordered 2D hexagonal arrays on a mesoscale (10^{-9}-10^{-6} m). Finally, at very high CTAB concentrations a lamellar structure can be identified that consists of sheets of ordered micelles, separated by thin layers of water. In between the 2D hexagonal and lamellar phases a third ordered region is found in which both the water and the surfactant phase are spatially (3D) continuous, and this region shows a cubic symmetry in x-ray diffraction (XRD) experiments. It is thought to consist of a 3D-continuous ordered network of tube-shaped micelles dispersed in a continuous water phase (4).

2.2 Surfactant-assisted sol-gel synthesis

The formation of liquid crystalline mesophases in water and alcohols as discussed above provides the basis for the possibility to make porous oxides with ordered pore geometries, since polymerisation of suitable oxide precursors such as metal alkoxides can be carried out in the water-containing phase. The most commonly known precursor for meso- and microporous silica is tetra-ethoxy-ortho-silicate (TEOS, $Si(OC_2H_5)_4$) (5). The initial silica sol is made by acid- or base-catalysed hydrolysis and condensation of TEOS at temperatures of 25-80°C:

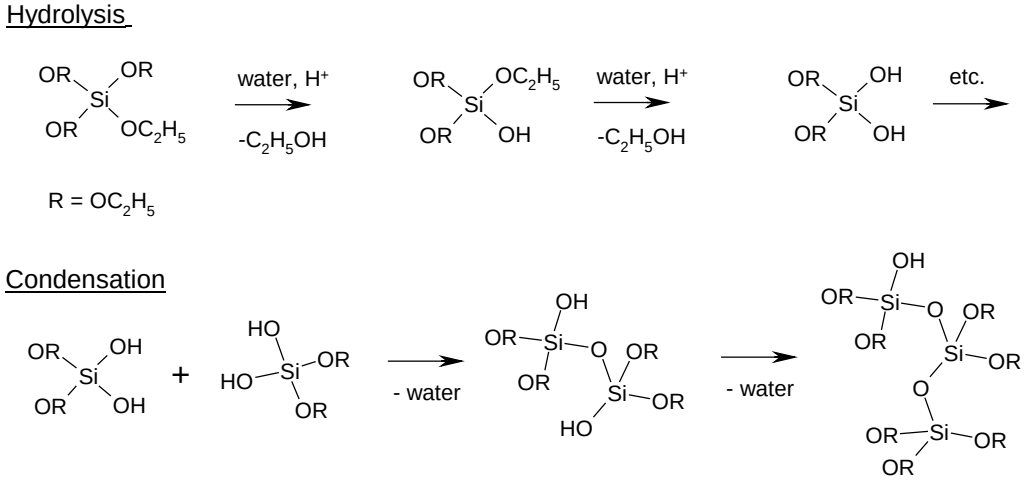

This finally results in polymer- or particulate-like sols of nanometer size that have a net *negative* charge above pH 2.5. Since a net *positive* charge is present on the surface of the cationic CTAB micelles, attractive coulombic interactions occur between the colloidal particles and the micelles.

There is substantial debate in literature about the details of the formation mechanism of long-range ordered micelle – silica hybrid phases. The presence of charged colloids has an inductive effect on the formation of micelle aggregates, since the formation of ordered phases in the presence of silica precursors has been observed even in dilute solutions, where the concentration of surfactant is far below the volume fractions at which ordering phenomena (which are induced in the 2-phase system by steric hindrance between surfactant assemblies) are expected (6). To explain this phenomenon it has therefore been suggested that the formation of a micelle-colloid complex in solution is the first step in the overall assembly formation mechanism, as illustrated below in Figure 2.

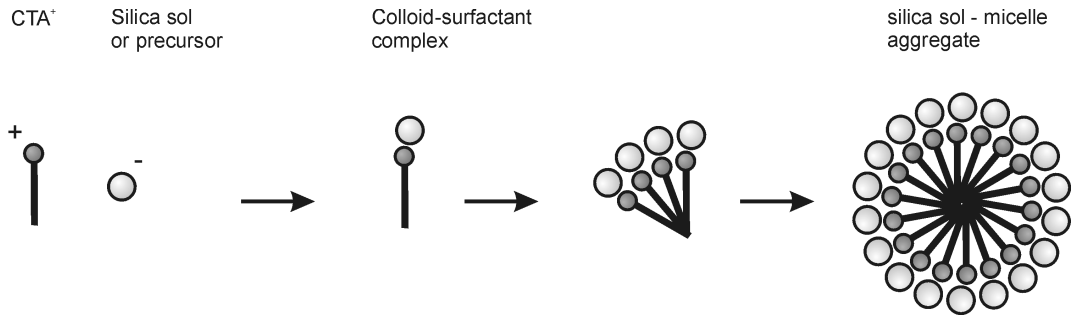

Figure 2. Possible reaction scheme for the formation of ordered surfactant-sol aggregates.

In subsequent steps, these complexes assemble into larger structures with lower solubility, finally resulting in regular micelles with 'adsorbed' sol monolayers. Alternative pathways for supramolecular association are also thought to exist and will depend on the exact conditions during the entire preparation process in practice (7).

After removal of the solvent, dry ordered micelle – silica hybrid phases are obtained. Composite structures with hexagonal symmetry are commonly known as MCM-41-type materials, while composite with cubic and lamellar symmetries are named MCM-48 and MCM-50, respectively. Heat treatment of the hybrid composites at 350-450°C in air leads to the removal of the organic template, and the formation of mesoporous oxide powders with very narrow pore size distributions and pore architectures defined by the spatial ordering of the supramolecular liquid crystalline templates. MCM-41 has straight parallel 1D channels with long range 2D hexagonal ordering, while MCM-48 is thought to have a slightly tortuous 3D network structure of pores of similar size (3). MCM-50 does not have a 3D oxidic network structure but rather consists of stacked isolated 2D layers. It is therefore not thermally stable: upon removal of the template at elevated temperature the lamellar structure collapses and no ordered mesophase can be identified afterwards.

The presence of long-range ordering and the symmetry of the pore structure can be easily checked by XRD at small diffraction angles (2θ typically 1-7°). As a typical example the XRD spectrum of calcined silica-CTAB powder with MCM-48 structure is shown in Figure 3.

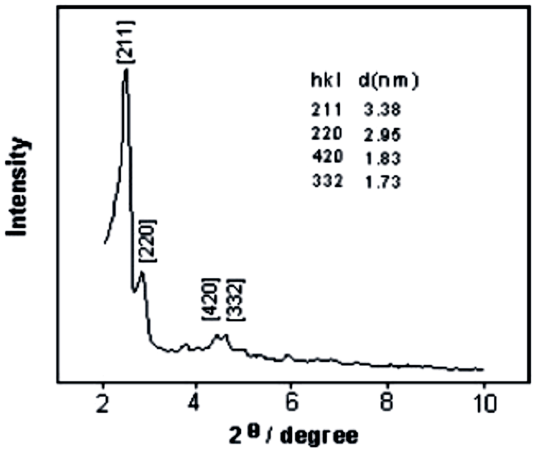

Figure 3. XRD diagram of calcined silica-CTAB powder (from W. Zhao and Q. Li, *Chem. Mater.*, **15** (2003) 4160.)

In addition to cationic surfactants like CTAB and related compounds, which give rise to oxides with pore sizes of 1.5–4.2 nm (3), many other suitable surfactants have been identified as well. An important class of surfactants are the non-ionic triblock copolymers that were first employed by Stucky and coworkers (8). These consist of ethylene oxide (EO) – propylene oxide (PO) – ethylene oxide (EO) segments with typically 100-300 EO/PO monomers. Mesoporous oxide powders of varying composition and controlled pore sizes up to 25 nm could be prepared using these block copolymers, which became later known as SBA-type materials. They exhibit essentially similar liquid crystalline mesophases as CTAB.
The porosity of surfactant-templated mesoporous oxides is often much higher than the porosity of conventional mesoporous selective membranes such as γ-alumina with 40-50 vol% porosity. MCM-type materials may exhibit porosities of 40-65%, while SBA-type silicas with uniform pore sizes have been made in the form of powders with porosities up to 1.2 cm^3/g, i.e., with ~75% total porosity (8).

2.3 Control of pore size and pore geometry

There are several ways to control the pore size and overall 3D pore structure on the mesoscale. The factors that were first identified were surfactant concentration and nature of the surfactant. In general, upon increasing the surfactant concentration during synthesis, the same sequence of occurring mesophases will be observed in hybrid composites as in the CTAB/water phase diagram, i.e., going from hexagonal to cubic to lamellar symmetry.
Systematic control over pore size was first demonstrated by Brinker (3) and Stucky (9) by variation of the surfactant tail length and nature of the ionic head group. Upon increasing the length of the hydrocarbon tail in a series of C_n-NR_3^+ (R=CH_3) surfactants from *n=6* to *n*=18, the average pore size in silica could be tuned from ~1.5 nm to 4.2 nm. By using auxiliary organic solvents that are known to move into the hydrophobic cores of the micelles, the pore diameter could be increased further

to 7-10 nm (3). A dimensionless factor *g* was defined that describes the main effect of the surfactant on the expected pore curvature in the oxide matrix:

$$g = \frac{V}{a_0 z} \qquad [1]$$

where *V* is the volume of the surfactant chain plus any organic solvents, *z* the surfactant tail length, and a_0 the effective head group area. Essentially, as illustrated below in Figure 4, *g* expresses the volume fraction of the hydrophobic chain (dark area) in the total volume of a surfactant molecule.

On purely geometrical grounds it can be calculated that spherical micelles should form preferentially when *g*=1/3, hexagonally ordered micelles when *g*=1/2, cubic symmetry is expected when *g*=1/2-2/3, and finally lamellar symmetry is obtained when *g* approaches 1 (3,9). Generally speaking, short hydrocarbon tails and small head groups favour the occurrence of strongly curved pore architectures.

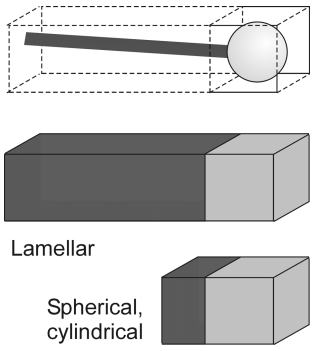

Figure 4. Influence of geometric features of the surfactant on the expected pore geometry.

Although the above-mentioned factors provide a rough estimate of the expected pore size and geometry, it has become evident that the conditions during synthesis also have a profound influence on the final mesoporous structure. In situ XRD investigations during sol condensation by Tolbert et al. (10) showed time-dependent structural rearrangements in ordered mesophases upon condensation of the sol. They attributed this effect to the decreasing space charge density of the silica sol upon condensation. The space charge of silica sols is due to hydroxyl groups (i.e., $-O^-$, -OH, $-OH_2^+$) present at the surface of the sol. As sol condensation proceeds through reaction of these hydroxyl groups, i.e., 2 ≡Si-OH → ≡Si–O–Si≡ + H_2O, the charge density of sols decreases gradually in the course of reaction, and since there is a continuous balance between the space charge density in the sol and the surface charge density of the micelles, micelles will respond to the changing counter-charge density by rearranging into structures with a higher degree of curvature (Figure 5).

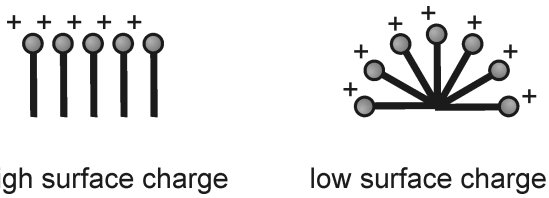

Figure 5. Dependence of surface charge density on curvature of self-assembled micelle.

This implies that although the surfactant concentration in the solution increases upon drying of the solution, the actual symmetry exhibited by liquid crystal phase templates tends to change from lamellar via cubic to hexagonal (10). The final pore geometry also depends on the moment that the mesophase structure becomes fixed due to lack of solvent that would facilitate further structural rearrangements.

2.4 Film formation of mesoporous thin layers

The first reports on film formation of templated mesoporous oxide films appeared in 1997 (11). In principle, the deposition of thin films can be done with the same techniques as employed for the deposition of amorphous mesoporous layers, like dip coating and spin coating. Previous works had shown that by exceeding the critical micelle concentration of a bulk silica-surfactant solution, hexagonal mesophase films with 1D pore channels were formed at the solid-liquid and liquid-vapour interfaces. However, this formation process was slow (~days) and the supported films were granular. Lu et al. (11) started with homogeneous water/ethanol solutions containing surfactant (CTAB) concentrations far below CMC1. The solutions were deposited on (100) silicon wafers by dip coating. Upon evaporation of the solvents, the surfactant concentration increased and exceeded CMC1 and CMC2, so that an ordered mesophase was formed within seconds upon drying. Micelles are known to be capable of self-assembling in time spans of milliseconds. A typical drying trajectory for the film formation process in the tri-phase diagram water-ethanol-silica/surfactant is shown in Figure 6 (12).

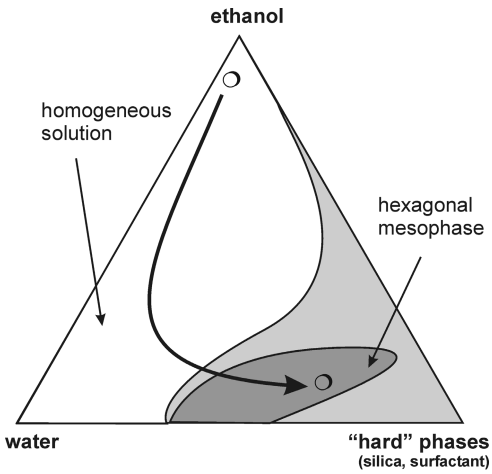

Figure 6. Drying trajectory in the tri-phase diagram water-ethanol-silica/surfactant.

The isotropic starting solution and the speed of drying and self-assembly assure a homogeneous distribution of the silica and surfactant phases in the final thin film. Brinker named this process EISA (evaporation-induced self-assembly) and it is now the standard technique for preparing mesostructured thin films. Thin films of both MCM- and SBA-type materials have been reported in literature (12,13), the majority of reports on film formation on dense substrates (14).
It was pointed out by several researchers that MCM-41 type thin films have a straight channel pore architecture with preferential *in-plane* porosity (12). Micelle assemblies tend to align themselves parallel to the liquid/substrate and liquid/air interfaces upon drying. Essentially, these interfaces act as the main nucleation planes for stacking of ordered micelle assemblies. Growth of the stacks proceeds from these two nucleation planes towards the "bulk" of the thin film. Under fast drying conditions, small ordering errors will occur during the stacking process. The degree of long-range ordering observed in the bulk of a thin film is therefore often substantially lower than near the interfaces (12). In the case of MCM-41, a mesoporous thin film with an in-plane ordered pore structure remains after thermal treatment. Such a layer is not expected to exhibit high permeability for liquids, as the real transport path through the film will be rather long (high tortuosity). Unfortunately, no effective method is yet known to control the orientation of the straight channel pore structure of MCM-41 relative to the substrate without destroying long-range ordering. The situation is different for MCM-48. As the pore structure of the latter is thought to consist of a periodic 3D network of similarly sized worm-like pores (4), transport paths will exist in all 3 principal directions.

3. Templated mesoporous oxides as membranes

The number of reports in which templated-assisted syntheses were used for the preparation and application of mesoporous ceramic membranes is still very limited. One of the first reports in which templated silica was utilized (15) showed that the flux and selectivity of a conventional tubular supported microporous silica membrane in gas separation could be improved substantially if an extra intermediate templated mesoporous silica layer with pore diameter of 10-23 Å was deposited between the mesoporous γ-alumina support layer (~50 Å pore diameter) and the separative microporous silica top layer (3-4 Å pore diameter). The extra interlayer was thought to improve the smoothness of the support for the final microporous silica layer, thereby reducing the chance of occurrence of defects. Moreover, the extra layer prevents the microporous silica sol to penetrate deep into the support, and this will effectively reduce the thickness of the final silica top layer. CTEABr [$C_{16}H_{33}N(C_2H_5)_3Br$, a (short-chain) C_6-analogue of CTAB, or a non-ionic di-block copolymer was used in the processing of templated interlayers. CO_2 permeances of up to $3 \cdot 10^{-7}$ mol m^{-2} s^{-1} Pa^{-1} with CO_2/CH_4 permselectivities of 15-50 were reported. The same stacked membrane system without interlayer showed CO_2 fluxes that were 3-4 times lower under identical conditions, and the

permselectivities were lower as well (~10). Hydrogen permeances were in the range of 3-6·10^{-7} mol m^{-2} s^{-1} Pa^{-1}.

Direct deposition of an MCM-48 silica layer on conventional α-alumina substrates using CTAB has also been reported (16,17). The permeances of H_2, He, CH_4, N_2 and CO_2 were measured at 2-3.7 bar feed pressure and atmospheric pressure at the permeate side. The permeance of hydrogen was found to be ~2.2·10^{-7} mol m^{-2} s^{-1} Pa^{-1} and was independent of the magnitude of the pressure gradient over the membrane, which indicates a Knudsen diffusion process. This was also reflected in the H_2/He and H_2/N_2 permselectivities, which were very close to the theoretical Knudsen separation factors (1.4 and 3.7, respectively). The same membranes were also employed in the separation of a 90/10 vol/vol ethanol/water mixture by vapour permeation at room temperature. A water flux of ~16 kg m^{-2} h^{-1} and a water/ethanol separation factor of ~3.3 were found.

MCM-41 silica layers of ~1 μm thickness and with ~1.8 nm pore size on α-alumina substrates were reported in a study with cetylpyridinium chloride as the template-forming precursor (18). The authors noted that direct deposition on the coarse-grained support led to a silica layer with poorly developed morphology. This could be improved by completely filling the alumina pores with a PVA solution prior to silica deposition. The improvement in surface morphology is thought to be due to the improved smoothness of the support upon filling the support layer pores. No data on gas or liquid transport were reported.

The synthesis of defect-free 0.3-0.5 μm thick supported hexagonal MCM-41 membranes using CTAB or its C_{12}-analogue was reported by Klotz et al. (19,20). The silica layers were deposited on ~3 μm thick γ-alumina mesoporous layers with ~5 nm pore size. The pore sizes in the templated layers were 2.2-3.1 nm depending on surfactant tail length, and the total porosity was 52-57%. Using small-angle XRD techniques it could be seen that mainly in-plane ordered straight-channel porosity was present in the film. As expected, the nitrogen permeance through these layers was rather low, but it could be increased substantially upon addition of 12 nm silica "nanoseeds" to the surfactant-containing sol, up to a total volume fraction of ~5.5 vol% in the final film. These seeds were shown to disturb long-range in-plane ordering of pores effectively, so that 2-5 times higher nitrogen permeances of up to 1.7·10^{-6} mol N_2 m^{-2} s^{-1} Pa^{-1} were achieved after seeding. McCool et al. reported preparation of mesoporous silica films on α-alumina supports. They carried out single gas permeation and multi-gas separations using these membranes. They found gas permeation behaviour strongly depend upon Knudsen diffusion behaviour (21).

A mesoporous silica film was synthesised from TEOS as silica source and ($CH_3(CH_2)_{14}(CH_2$-$CH_2O)_{12}$-OH) as surfactant source. NaF was used as catalyst and the film was deposited on a alumina tube. This membrane was used for ultrafiltration of water solution of poly ethylene glycol (PEO) (22).

4. Future applications and challenges

The two most interesting features of template-assisted mesoporous membranes are their regular pore geometry and the narrow and tunable pore size distribution. In principle, this may allow membrane developers to choose the desired pore architecture in a more rational way than is now common, and this may ultimately lead to much improved selectivities in different kinds of liquid filtration and nanofiltration processes.

To use these surfactant templated mesoporous silica materials as membrane materials in the pressure driven processes like nanofiltration, it is important to know the chemical and mechanical stability of the silica layer. It has been found that these materials can preserve the ordered structure at the pH < ~5. The mesoporous structure collapse at around pH 7 and it becomes microporous material in the alkaline medium (~pH 9) (23). To solve this problem silica has been doped with 3% zirconia. This zirconia doped silica shows excellent stability even at pH ~12 (24).

The improvement of flux and selectivity in CO_2/CH_4 separation upon application of an extra intermediate layer between the conventional γ-alumina layer and the microporous top layer described above (15) illustrates another promising feature of templated oxide layers: It is often believed that the resistance to transport in supported membranes occurs to a large extent at the interfaces between layers with different pore sizes. This effect becomes more pronounced when the difference in pore size between subsequent layers is large. By bridging the gap between such layers with one or more extra interlayers with intermediate pore sizes, the overall transport resistance may be reduced significantly.

The ultimate goal in template-assisted mesoporous membrane synthesis will be the controlled formation of straight channel open pore architectures with MCM-41 like structures, but with a pore orientation that is perpendicular to the underlying substrate. This will yield selective layers with the theoretically minimal tortuosity of 1, which should improve the permeability of the layer highly. As was discussed in the previous sections the natural tendency during the self-assembly process of MCM-41 films is to form in-plane ordered pore structures. No efficient strategic methods are yet known to achieve thin layers with perpendicular through pores, and no general strategies have been suggested in literature to achieve this goal.

Another important goal in templated membrane research will be to generalise the formation of thin films and membranes to oxide compositions other than the commonly used silica. The hydrothermal stability of silica is rather low, especially under alkaline conditions, and essentially the same pore geometries and pore sizes could be made in other oxides as well. The main difficulty of non-siliceous oxide materials compared with silica concerns their high tendency to crystallisation during drying and heat treatment. Most often this leads to a collapse of the mesostructure during or after calcination, so that the ordered pore architecture is lost. The formation of mesoporous titania and alumina films on dense supports has been reported to date (25-27). Mechano-chemical action may lead to structural collapse of the mesoporous silica materials. Decomposition of the material

structure occurs through Si-O-Si bond hydrolysis. Presence of ambient moisture is found to be responsible for structure collapse. The pore wall thickness and particle size also has a significant effect on structural stability of mesoporous silica materials under mechanical pressure (28). Besides these efforts substantial work is also done to improve the mechanical and hydrothermal stability of silica films (29).

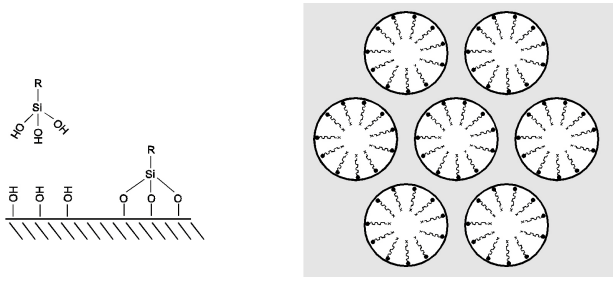

Figure 8. Left: covalent attachment of organosilane to surface. Right: Mesostructured 2D hexagonal (MCM-41) oxide with functionalised pore surface.

In addition to the use of templating techniques, post-synthesis modification of the the internal pore walls by covalently bonded monolayers with a specific chemical function is another topic that is receiving considerable attention lately (30). See Figure 8. Post-modification by grafting the internal pores with organo-functional silanes may for instance result in mesoporous layers with reduced hydrophilicity. Such modification was already demonstrated to alter the selectivity in an ethanol/water separation process (16). While unmodified silica layers showed a preferential selectivity towards water, similar membranes with internally methylated pore walls had a preferential selectivity towards ethanol.

5. Conclusions

In summary, template-assisted sol-gel methods have been explored widely over the past 10 years. The formation of thin films on dense substrates using conventional deposition techniques has also become feasible in the last 5-6 years. Currently the first works on the application of thin templated mesoporous oxide membranes in gas and liquid permeation are appearing in literature. The template method offers a cheap, fast and versatile technique for the formation of selective mesoporous ceramic membrane layers and allows a higher degree of control over the final pore architecture and pore size distribution than is common today.

References

1. J.S. Beck, J.C. Vartuli, W.J. Roth, M.E. Leonowicz, C.T. Kresge, K.D. Schmitt, C.T.-W. Chu, D.H. Olson, E.W. Sheppard, S.B. McCullen, J.B. Higgins, J.L. Schlenkert, A new family of mesoporous molecular sieves prepared with liquid crystal templates, *J. Am. Chem. Soc.* **114** (1992) 10834.
2. M.E. Raimondi, J.M. Seddon, Liquid crystal templating of porous materials, *Liq. Cryst.*, **26** (1999) 305.
3. N.K. Raman, M.T. Anderson, C.J. Brinker, Template-based approaches to the preparation of amorphous, nanoporous silicas, *Chem. Mater.*, **8** (1996)1682.
4. M.W. Anderson, Simplified description of MCM-48, *Zeolites*, **19** (1997) 220.
5. J. Livage, M. Henry, C. Sanchez, Sol-gel chemistry of transition metal oxides, *Prog. Solid St. Chem.*, **18** (1988) 259.
6. D.M. Antonelli, J.Y. Ying, Synthesis of a stable hexagonally packed mesoporous niobium oxide molecular sieve through a novel ligand-assisted templating mechanism, *Angew. Chem. Int. Ed.*, **35** (1996) 426.
7. J. Patarin, B. Lebeau, R. Zana, Recent advances in the formation mechanisms of organized mesoporous materials, *Curr. Opin. Colloid Interface Sci.*, **7** (2002) 107.
8. D. Zhao, J. Feng, Q. Huo, N. Melosh, G.H. Fredrickson, B.F. Chmelka, G.D. Stucky, Triblock copolymer syntheses of mesoporous silica with periodic 50 to 300 angstrom pores, *Science*, **279** (1998) 548.
9. Q. Huo, D.I. Margolese, G.D. Stucky, Surfactant control of phases in the synthesis of mesoporous silica-based materials, *Chem. Mater.*, **8** (1996) 1147.
10. S.H. Tolbert, C.C. Landry, G.D. Stucky, B.F. Chmelka, P. Norby, J.C. Hanson, A. Monnier, Phase transitions in mesostructured silica/surfactant composites: Surfactant packing and the role of charge density matching, *Chem. Mater.*, **13** (2001) 2247.
11. Y. Lu, R. Ganguli, C.A. Drewien, M.T. Anderson, C.J. Brinker, W. Gong, Y. Guo, H. Soyez, B. Dunn, M.H. Huang, J.I. Zink, Continuous formation of supported cubic and hexagonal mesoporous films by sol gel dip-coating, *Nature*, **389** (1997) 364.
12. C.J. Brinker, Y. Lu, A. Sellinger, H. Fan, Evaporation-induced self-assembly: Nanostructures made easy, *Adv. Mater.*, **11** (1999) 579.
13. D. Zhao, P. Yang, N. Melosh, J. Feng, B.F. Chmelka, G.D. Stucky, Continuous mesoporous silica films with highly ordered large pore structures, *Adv. Mater.*, **10** (1998)1380.
14. K.J. Edler, S.J. Roser, Growth and characterization of mesoporous silica films, *Int. Rev. Phys. Chem.*, **20** (2001) 387.
15. C.Y. Tsai, S.Y. Tam, Y. Lu, C.J. Brinker, Dual-layer asymmetric microporous silica membranes, *J. Membr. Sci.*, **169** (2000) 255.

16. D.H. Park, N. Nishiyama, Y. Egashira, K. Ueyama, Enhancement of hydrothermal stability and hydrophobicity of a silica MCM-48 membrane by silylation, *Ind. Eng. Chem. Res.*, **40** (2001) 6105.
17. N. Nishiyama, D.H. Park, A. Koide, Y. Egashira, K. Ueyama, A mesoporous silica (MCM-48) membrane: preparation and characterization, *J. Membr. Sci.*, **182** (2001) 235.
18. Y.S. Kim, S.M. Yang, Preparation of continuous mesoporous silica thin film on a porous tube, *Adv. Mater.*, **14** (2002) 1078.
19. M. Klotz, A. Ayral, C. Guizard, L. Cot ,Synthesis conditions for hexagonal mesoporous silica layers, *J. Mater. Chem.,* **10** (2000) 663.
20. M. Klotz, A. Ayral, C. Guizard, L. Cot, Synthesis and characterization of silica membranes exhibiting an ordered mesoporosity. Control of the porous texture and effect on the membrane permeability, *Sep. Purif. Tech.*, **25** (2001) 71.
21. B.A. McCool, N. Hill, J. DiCarlo, W.J. DeSisto, Synthesis and characterization of mesoporous silica membranes via dip-coating and hydrothermal deposition techniques, *J. Membr. Sci.*, **218** (2003) 55.
22. C. Boissiere, M.A.U. Martines, P.J. Kooyman, T.R. de Kruijff, A. Larbot, E. Prouzet, Ultrafiltration membrane made with mesoporous MSU-X silica, *Chem. Mater.,* **15** (2003) 460.
23. A. Doyle, B.K. Hodnett, Stability of MCM-48 in aqueous solution as a function of pH, *Micropor. Mesopor. Mater.,***63** (2003) 53.
24. D.H. Park, H. Saputra, N. Nishiyama, Y. Egashira, K. Ueyama, Synthesis of zirconium-containing mesoporous silica Zr-MCM-48 membranes with high alkaline resistance for nanofiltration, *Studies in surface science and catalysis*, **146** (2003) 327
25. D. Grosso, G.J.D.A.A. Soler-Ilia, F. Babonneau, C. Sanchez, P.A. Albouy, A. Brunet-Bruneau, A.R. Balkenende, Highly organized mesoporous titania thin films showing mono-oriented 2D hexagonal channels, *Adv. Mater.*, **13** (2001) 1085.
26. F. Bosc, A. Ayral, P.A. Albouy, L. Datas, C. Guizard, Mesostructure of anatase thin films prepared by mesophase templating, *Chem. Mater.,* **16** (2004) 2208.
27. L. Pidol, D. Grosso, G.J.A.A. Soler-Illia, E.L. Crepaldi, C. Sanchez, P.A. Albouy, H. Amenitsch, P. Euzen, Hexagonally organised mesoporous aluminium-oxo-hydroxide thin films prepared by the template approach. In situ study of the structural formation *J. Mater. Chem.,* **12** (2002) 557.
28. T. Tatsumi, K.A. Koyano, Y. Tanaka, S. Nakata, Mechanical stability of mesoporous materials, MCM-48 and MCM-41, *J. Porous Mat.,* **6** (1999) 13.
29. K. Cassiers, T. Linssen, M. Mathieu, M. Benjelloun, K. Schrijnemakers, P. Van Der Voort, P. Cool, E.F. Vansant, A detailed study of thermal, hydrothermal, and mechanical stabilities of a wide range of surfactant assembled mesoporous silicas, *Chem. Mater.*, **14** (2002) 2317.

30. R. Anwander, SOMC@PMS. Surface Organometallic Chemistry at Periodic Mesoporous Silica, *Chem. Mater.*, **13** (2001) 4419.

Chapter 3

Structural and liquid transport properties characterization of surfactant templated silica materials

I don't have a solution but I admire the problem

Abstract*

In this chapter two different synthesis routes to prepare surfactant-templated silica materials via sol-gel methods are described. The powders derived from the two sols have been characterized by nitrogen sorption and X-ray diffraction methods. The formation of silica films on dense, mesoporous and macroporous supports is described. These films are structurally characterised by TEM, XRD, XPS and permporometry. It has been found that the mesoporous silica layer does not grow directly on a mesoporous support. Instead it grows on a structurally disordered interface of ~20 nm thickness. This observation differs considerably from studies on film formation on dense supports as reported in the literature. Water transport experiments were carried out on the silica films deposited on porous supports. These experiments suggest that the intrinsic water permeability through films deposited on mesoporous supports is higher than through those deposited on macroporous supports. Solvent permeation experiments were carried out on several selected silica membranes.

* Part of this chapter has been presented in Materials Research Society spring meeting at San Francisco, U.S.A. 2003.

1. Introduction

Since the first development of surfactant templated MCM-type silica materials (1), ordered mesoporous silica systems achieved a lot of attention of scientists from different fields (2-4). In the 1990s the effort was mostly given to the preparation and characterization of surfactant templated silica powders and thin films (5-6). Powders were prepared from different silica sources, using different types of surfactants to achieve regular pore geometries (7-8). Thin films were made either in self-supported form or were supported by different dense substrates (6-13). A comprehensive review on surfactant templated silica films has been published by Edler et al. (14). In the last few years a considerable amount of work on the application of ordered mesoporous silica layers as membranes was reported (15-20). These dealt with the formation of mesoporous silica films on macroporous (19, 20) and mesoporous (15) supports. The preparation of defect-free mesoporous silica layers on macroporous supports by temporary modification of the support, or introduction of an extra intermediate layer on top of the support has been reported (18). These membranes have been used for gas separation (15,16), pervaporation (17) and ultrafiltration (19).

In this chapter the preparation of surfactant templated silica powders and silica layers on dense, mesoporous and macroporous supports from sols that were prepared by two different synthetic routes is reported. A detailed structural characterization of these layers has been carried out. The water permeability through the layers has been measured and the values are compared. Non-aqueous solvent permeability experiments through selected membranes are also presented.

2. Experimental

2.1 Silica sol preparation

Two different preparation methods have been employed to prepare mesoporous silicas.

In the first sol preparation (sol 1), the synthesis was carried out as described by Honma et al. (21). In this method, 8.0 ml of silica source Tetraethoxyorthosilicate (TEOS) (Aldrich, purity 99%) was mixed with 17.5 ml 1-propanol, and this mixture was stirred in a 100 ml flask at 600 rpm for 5 min. The TEOS was then hydrolysed by an HCl solution in deionised water (0.33 ml 36 (N) HCl solution in 2 ml water) and stirred for 60 min. Co-solvent 2-butanol (8.8 ml) was added and stirring was continued for another 30 min. In the last step, 1.75 g of CTAB was dissolved in 4.5 ml of de-ionized water. This surfactant solution was prepared separately and then poured into the silica solution. The final solution was stirred again for 60 min.

The second sol preparation (sol 2) procedure was described by McCool et al. (22). 22 ml TEOS was measured and added to 17.5 ml of ethanol and the mixture was stirred for an hour. The TEOS was then hydrolysed by an HCl solution in water (5 µl HCl in 1.8 ml water) and refluxed at 60°C for 60 minutes. After cooling to room temperature, more ethanol (99 ml) and aqueous HCl (395 µl in 7 ml water) was added. Finally ~ 5 g CTAB was added to the solution and stirred for 30 min.

2.2 Preparation of silica powder

The sols were dried in a glass petri dish under flowing air. The air flow rate was kept low and was directed parallel to the surface. It took eight hours or more to evaporate the solvents and form glassy materials. The aging time of the sols was varied from one day to several days. The glassy materials were calcined at 400°C for three hours with heating and cooling rates of 0.2°C/min.

2.3 Choice of supports

Three types of substrates with varying degree of porosity were used for deposition of silica films. Polished silicon wafers (004 type) with a native oxide surface layer were used as a dense support for thin film deposition. α-Alumina and γ-alumina disks were used as macroporous and mesoporous supports, respectively.

2.4 Preparation of α-alumina support

The α-alumina supports were made by colloidal filtration of well-dispersed 0.3 μm α-alumina particles (AKP-30, Sumitomo). The dispersion was stabilized by peptizing with nitric acid. After drying at room temperature, the filter compact was sintered at 1100°C. Flat disks of Ø 39 mm and 2.0 mm thickness were obtained after machining and polishing. The final porosity of these supports is ~30% and the average pore size is in the range of 80-120 nm.

2.5 Preparation of α-alumina supported mesoporous γ-alumina layer

The γ-alumina membrane consisted of a macroporous α-alumina support and a thin mesoporous γ-alumina layer. The α-alumina supports were coated with a γ-alumina layer by the dip coating technique. The dip sol was prepared by mixing 30 ml of boehmite sol with 20 ml of PVA (polyvinyl alcohol, Fluka, 98% purity) solution, which was made from 150 g of 0.05 M HNO_3 in water added to 4.5 g of PVA (MW=72000 g/mol) and stirred for 2 h at 80°C. The supports were dip-coated into the γ-alumina sol with a turning speed of approximately 23.9 cm s^{-1} and a dip-coating speed of approximately 1.1 cm s^{-1}. It was then put in a climate chamber for 3 h, followed by calcination at 900°C for 3 h, using a heating and cooling rate of 0.5°C min^{-1}. The dipping procedure and calcination were done again on the calcined membrane. This resulted in a flat γ-alumina layer with a pore diameter of 8-9 nm and a layer thickness of ~3 μm on α-alumina support.

2.6 Coating of silica sol on supports

The silica sols were coated twice on the α-alumina disks and the α-alumina supported γ-alumina layers using the dip coating technique as mentioned earlier. Coating on the silicon wafer was done with spin coating at 4000 rpm for 30 seconds with 3 ml of silica sol. Silica coated supports were calcined at 450°C for 90 min. in air with heating and cooling rates of 0.2°C min^{-1}.

2.7 Structural characterization of silica powder and supported silica layers

The silica powder was subjected to nitrogen adsorption and desorption experiments at 77K (Micrometrics) and X-Ray diffraction (XRD). The supported silica films were characterized by X-ray diffraction, Transmission Electron Microscopy (TEM), Electron Diffraction (ED), and permporometry. XRD was carried out using a Philips SR5056 with Cu Kα radiation. Transmission electron microscopy (TEM) and Electron Diffraction (ED) were carried out with a Philips CM30 Twin (S)TEM with a LaB_6 filament. A 300 kV electron beam was used for TEM. Pore size distributions of mesoporous layers on macroporous supports were determined by permporometry measurements using cyclohexane as condensable liquid (23). TEM analysis was carried out on selected films. X-Ray photoelectron spectroscopy (XPS) was carried out with a PHI Quantum 2000 Scanning ESCA Microprobe. XPS depth profiling of the α-alumina supported silica layer was carried out with a 3 keV argon ion beam with an etching rate of 7 nm min^{-1}.

.

2.8 Liquid transport property characterization of silica layer

Steady state water permeability measurements were carried out in a dead end filtration cell with different membranes. The membranes used for this experiments were an α-alumina support, a α-alumina supported γ-alumina membrane, an α-alumina supported double coated silica membrane, and α-alumina / γ-alumina supported double coated silica membranes from sol 1 and sol 2. Steady state ethanol, toluene and n-hexane permeation was carried out through α-alumina / γ-alumina supported double coated silica membranes from sol 2. The volume of the filtration cell was 1 dm^3 and liquid stirring was done with a mechanical stirrer at a constant stirring speed of 200 rpm throughout the permeation experiments.

3. Results and Discussion

3.1 Structural characterizations

3.1.1 The powders

3.1.1.1 Nitrogen adsorption and desorption experiment

Figure 1a shows the nitrogen adsorption and desorption isotherms for the powders derived from sol 1 with different aging time. In each case, Type I isotherms were observed, characteristic for microporous systems. Table 1a presents the BET surface areas and pore diameters calculated from the desorption data. The BET surface area is large, which indicates a very open structure. The isotherms and pore diameter and t-plot suggest that the powders from sol 1 are microporous in nature, almost independent of aging time.

Table 1a. Adsorption/desorption data for powders from sol 1

Ageing time	Isotherm	BET surface area [m^2/g]	Pore diameter[nm]	Porosity (%)
1 day	Microporous	1032	1.8	27.1
2 days	Microporous	916	1.35	28.3
24 days	Microporous	971	1.36	28.7

Figure 1b shows the nitrogen adsorption and desorption isotherms of the powders produced from sol 2 with different aging times. This figure shows that the pore architecture changes from microporous to mesoporous upon prolonged aging. The results suggest that the powders produced from sol 2 should be aged sufficiently to obtain a mesoporous structure. Table 1b presents the BET surface areas and pore diameters calculated from the desorption data of the powders derived from sol 2. This table shows that after a certain aging time there is not much variance in the data for the BET surface area (747-848 m^2/g), the pore diameter (2.3-2.5 nm) and the mesoporous porosity (21.3-27.3 %). The porosity (ε) of the materials can be calculated as

$$\varepsilon = V_v/(V_s + V_v) \qquad [1]$$

Where V_v is the total pore volume and V_s specific volume of the solid.. The mesoporous porosity can be calculated from the porosity in the mesoporous section of the curve and the total porosity of the system.

Table 1b. Adsorption/desorption data for the powders from sol 2.

Ageing time	Isotherm	BET surface area [m^2/g]	Pore diameter [nm]	Total porosity [%]	Mesoporous porosity [%]
7 days	Microporous	1038	1.68	33.9	-
14 days	Mesoporous	795	2.51	53.9	26.5
28 days	Mesoporous	848	2.36	49.2	21.3

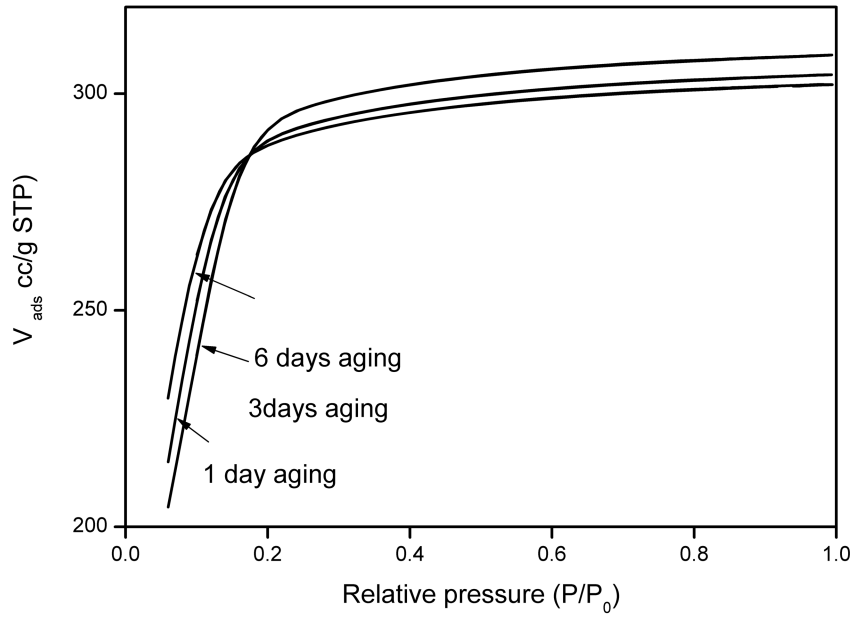

(a)

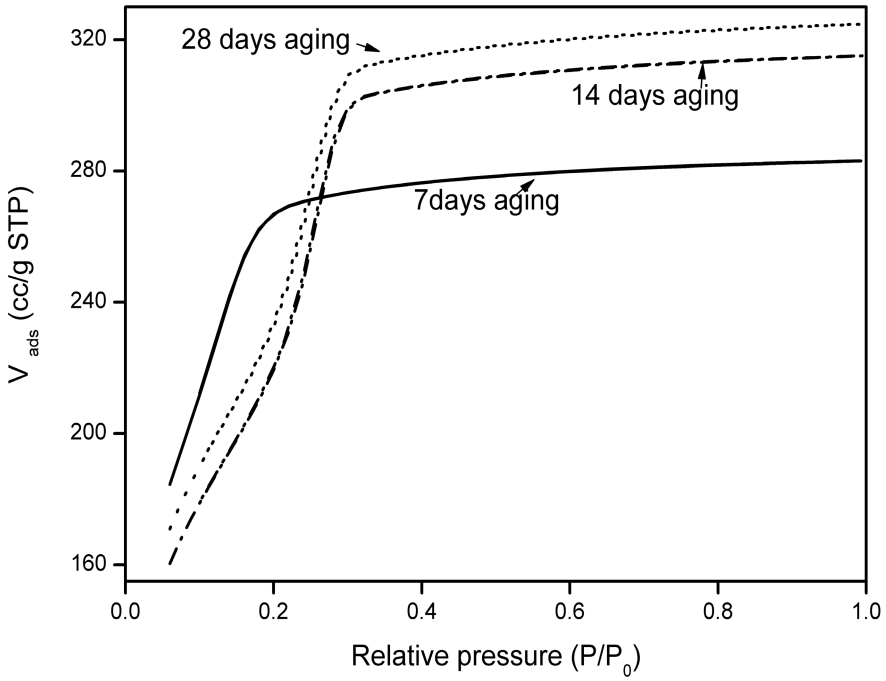

(b)

Figure 1. Nitrogen adsorption-desorption isotherm of silica powders; a) sol 1 and b) sol 2.

3.1.1.2 XRD measurements

Low angle X-ray diffraction measurements on the powders from sol 1 did not show any peak that is characteristic of an ordered mesoporous structure. On the other hand low angle X-ray diffraction measurements on the powders from sol 2 showed some peaks and some weak reflections at low 2θ values. Figure 2 presents a representative XRD spectrum of a calcined powder derived from sol 2 with an aging time of 14 days. The plot shows a clear peak at 2.5° with a shoulder at 2.8°. The corresponding d-spacings are 3.5 nm and 3.2 nm, respectively. Two more weak reflections can be observed at 4.8º and 5.8º, with corresponding d-spacings of 1.8 nm and 1.5 nm, respectively.

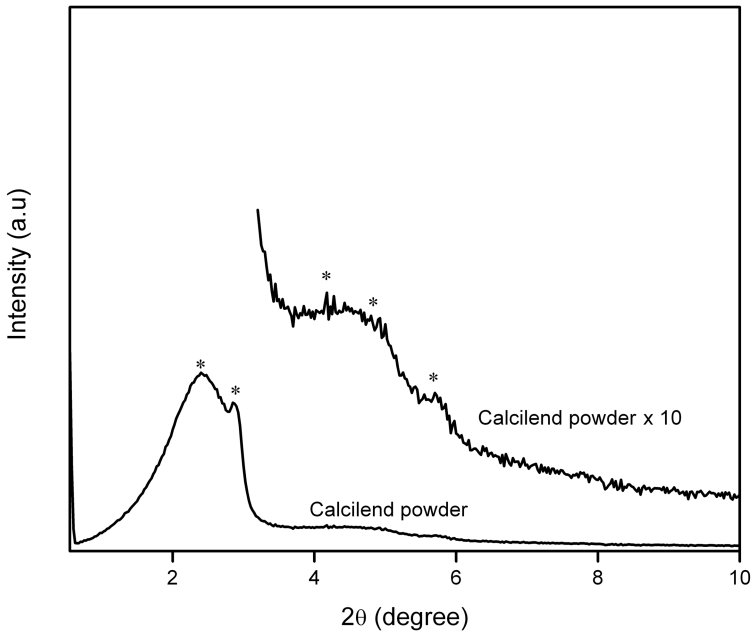

Figure 2. Representative XRD diagram of the calcined powder derived from sol 2 after 14 days aging.

3.1.2 Silica films on silicon wafer

3.1.2.1 XRD measurements

Figure 3a shows the X-ray diffraction peaks of a silica film (uncalcined and calcined) made from sol 1 with 1 day aging. Figure 3b shows the pattern of a film (uncalcined and calcined) made from sol 2 with 14 days aging. The peak positions of these films before and after calcination are listed in Table 2. From the figure it is clear that the number of peaks in either of the films is not sufficient to assign a space group to these mesoporous materials with certainty. However, the presence of peaks at low 2θ values suggests that ordered mesoporous domains are present in the films. The peak positions of the calcined silica films from sol 1 do not vary much from the uncalcined ones, but the number of visible peaks is different in the two cases. Uncalcined films of sol 2 show peak positions that could be assigned to

lamellar (MCM-50 type) or hexagonal structures with pores parallel to the surface (MCM-41 type). In either case these two reflections will come from (100) and (200) planes. But this cannot be stated with certainty. The calcined silica film from sol 2 shows peaks at different values of 2θ, which could not be interpreted in terms of a certain MCM-type symmetry. However, if the X-ray reflections from the film before calcinations would arise from MCM-50 type symmetry (a lamellar structure), the structure should have collapsed during calcination and no visible XRD peak, characteristic for ordered mesoporous structures, should be present after calcination. As these films do show indications of an ordered mesostructure after calcination, it is most likely that the uncalcined films contain a hexagonally ordered pore structure with pores parallel to the surface. It is noted that the powders from sol 1 did not show any characteristic peak of an ordered mesoporous structure at low 2θ values, but it did show the characteristic peaks in the silicon-supported thin film. The difference is probably related to differences in drying conditions during preparation of the powder and thin film. It has been reported that faster solvent evaporation leads to a higher degree of mesopore ordering in the film (24). As stated earlier, thin film formation on silicon wafers was done by the spin coating technique, which allows rapid evaporation of solvents, typically within one minute, while drying of unsupported powders took several hours.

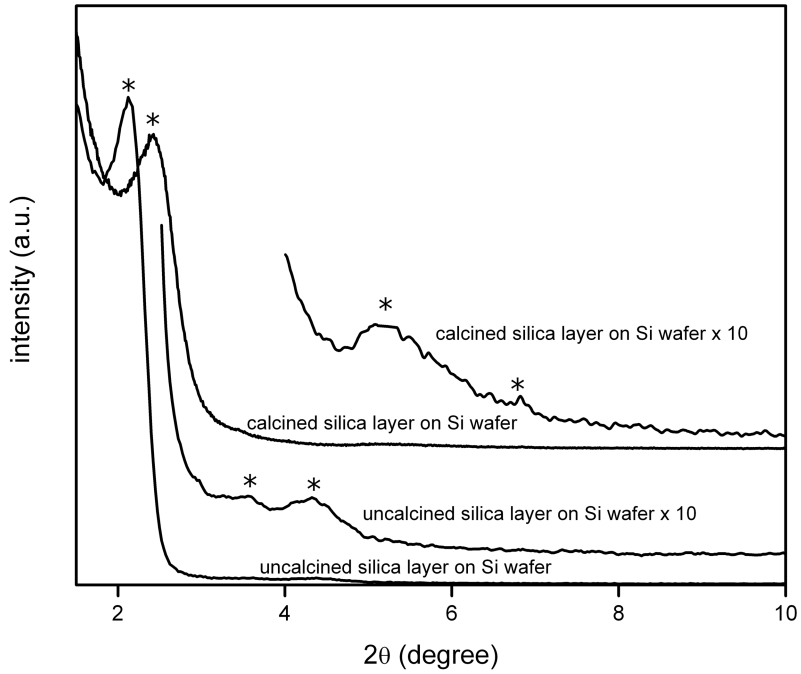

(a)

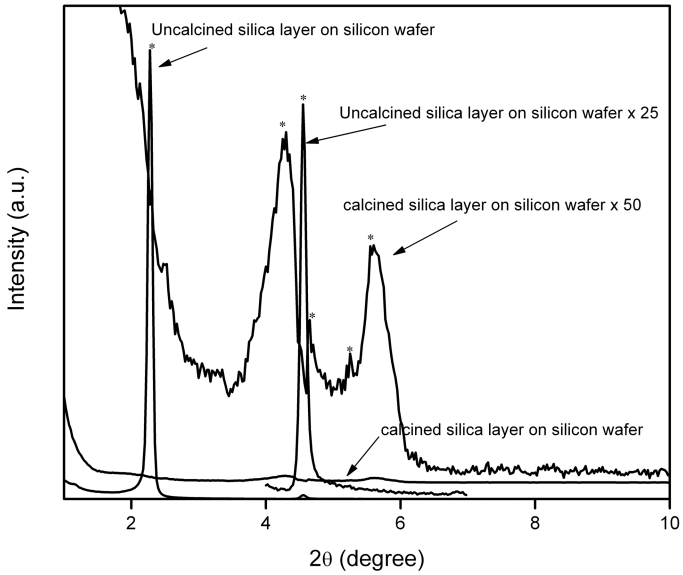

(b)

Figure 3. XRD diagram of uncalcined and calcined silica films on silicon wafer; a) sol 1 and b) sol 2.

Table 2. XRD data on silicon wafers

Coating sol		2θ angle [°]	d-spacing [Å]
Sol 1	Uncalcined	2.1	42
		3.6	25
		4.3	21
	Calcined	2.4	37
		5	18
		6.8	13
Sol 2	Uncalcined	2.2	40
		4.4	20
	Calcined	4.2	21
		4.6	19
		5.2	17
		5.6	15

3.1.2.2 TEM analysis

TEM analysis was unsuccessful as the samples suffered from charging under the electron beam.

3.1.3 γ-alumina supported silica layers

3.1.3.1 Permporometry

Figure 4 presents the pore size distributions of an α-alumina supported γ-alumina layer, and γ-alumina supported silica layers prepared from sol 1 and sol 2. The γ-alumina membrane has a quite broad distribution of pores with an average Kelvin radius of ~4 nm. On the other hand, the pore size distribution of the γ-alumina supported silica layer from sol 1 is bimodal. It has a narrow pore size distribution with a primary maximum at an average Kelvin radius of 1.7-1.8 nm, and a small fraction of pores with a slightly broader pore size distribution and an average Kelvin radius of ~2.5 nm. The pore size distribution around 1.7 nm probably arises from the micropores of the silica materials, as revealed by the nitrogen adsorption and desorption data. The sharp distribution is probably an artefact of the measurement technique, as these measurements are near the limits of what the method can probe. The silica layer formed by sol 2 showed an average Kelvin radius of ~2.1 nm. It was found that the pore sizes of the supported silica layers obtained from both sols are larger than those of the corresponding silica powders. This is probably due to the fact that the supported films have less possibility to shrink during calcination, as they are adhered to a support and can therefore not shrink freely. There are no such restrictions for unsupported materials, so that smaller pore sizes are obtained in powders compared to thin films when they are heat treated at the same temperature (25).

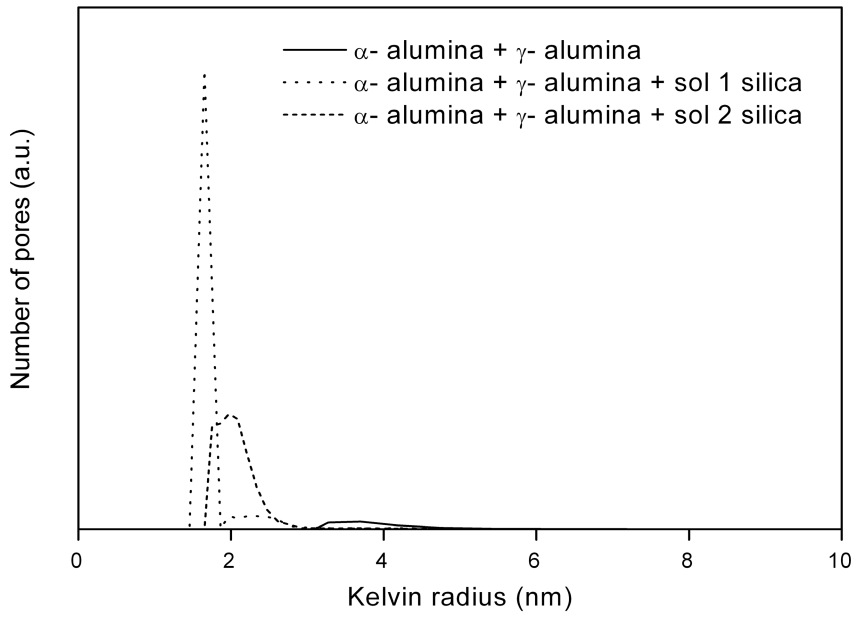

Figure 4. Pore size distribution of α-alumina supported γ-alumina membrane, α- + γ-alumina supported silica membrane from sol 1, and α- + γ-alumina supported silica membrane from sol 2, determined by permporometry.

3.1.3.2 XRD measurements

The silica layers from sol 1 and sol 2 supported by γ-alumina were subjected to XRD analysis. The layer from sol 2 did not show any indications of an ordered mesoporous layer, i.e., no visible peaks were present within the 2θ range of 0-10º. However, the layer derived from sol 1 showed peaks around 1.6º, 3.2º, and 3.4º, and a shoulder around 4º, which are characteristic of an ordered mesoporous structure. The d-spacing calculated from these peaks and shoulder positions are 5.5 nm, 2.7 nm, 2.6 nm and 2.2 nm, respectively.

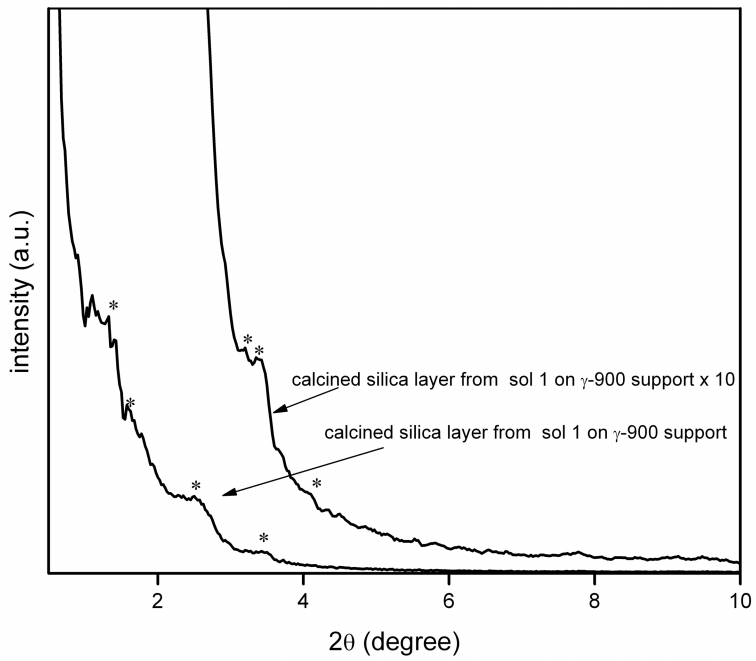

Figure 5. XRD diagram for silica layer (after calcination) from sol 1 deposited on γ-alumina layer.

3.1.3.3 TEM analysis

TEM micrographs of the γ-alumina supported silica layer from sol 1 are shown in Figure 6. The superstructure in the silica layer is clearly visible in this figure. It is clear that the ordered silica layer does not grow directly on the γ-alumina layer outwards starting from the γ-alumina/silica interface. The figure instead shows that there is a structurally disordered interfacial region between the silica and γ-alumina layers. A possible explanation for this phenomenon may be as follows. At the time of dip coating the silica sol comes into contact with the mesoporous γ-alumina substrate. The γ-alumina pores of ~8 nm diameter may exert a large capillary suction force on the sol liquid. This large suction force may prevent the surfactant micelles from ordering, i.e., the ordered micellar domains may collapsed, resulting in no ordered mesostructure near the interface. As soon as the γ-alumina

capillaries near the surface are saturated by the sol liquid, the sol may grow an ordered structure on the top of the interface (figure 2b). The structurally disordered interfacial region between the ordered silica and γ-alumina layer has a thickness of around 20 nm. In general, it has been reported in literature that ordered silica layers grow directly on the dense substrate, the growth starting at the interface (26). The experiment presented here suggests that the situation is different for porous substrates. Dark Field imaging (not shown here) indicated an amorphous microstructure for the interface layer. EDX point analyses in the centre of the Si film, the γ-alumina film, and the α-alumina substrate yielded atomic concentrations that are listed in Table 3. The electron beam diameter in this experiment was approximately 6 nm. From the EDX line scans it could be concluded that the interfacial layer is silica rich. Together with the results from TEM contrast imaging and morphology, however, it is reasonable to assume that the interfacial region has a similar chemical composition as the ordered mesoporous SiO_2 film.

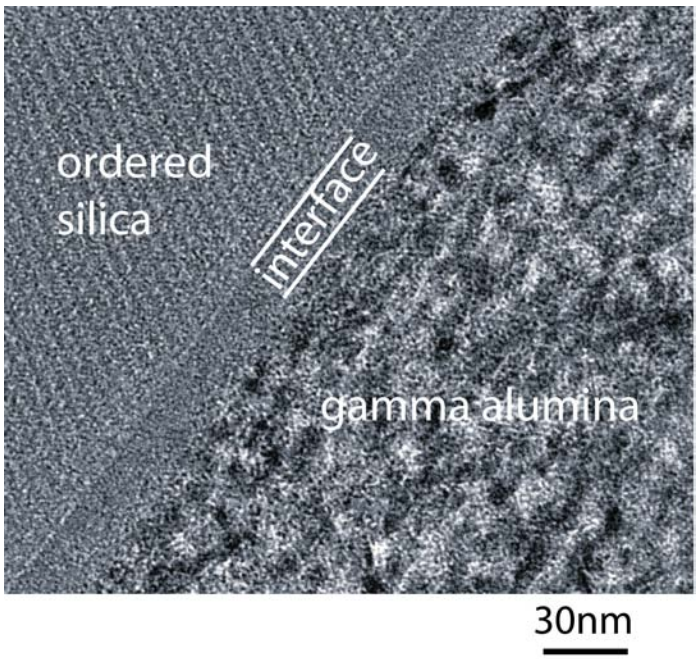

Figure 6. TEM image showing an ordered silica layer on a mesoporous γ-alumina layer with a structurally disordered silica-rich interface of thickness ~20 nm.

Table 3. Atomic compositions of different layers of a supported silica membrane deposited on a γ-alumina layer. Data extracted from EDX point analysis.

	O (atomic %)	Al (atomic %)	Si (atomic %)
Ordered Si film	66.4	1.7	31.9
Interfacial layer	66.1	1.4	32.5
γ-alumina	61.1	33.2	5.7
α-alumina	60.0	39.8	0.2

3.1.4 α-Alumina supported silica layers

3.1.4.1 Permporometry

Permporometry experiments were carried out on silica layers made from sol 1 and sol 2 supported on α-alumina discs. Figure 7 shows the oxygen flux through open pores versus the relative vapour pressure of cyclohexane. In the absence of cracks or large defects in the layer, the oxygen flux should be zero at relative cyclohexane pressures close to unity. The figure clearly shows that the layer derived from sol 1 was crack free, but the layer from sol 2 was not. It is also noted that this plot also illustrates the microporous nature of the silica layer obtained from sol 1. As the Kelvin equation is no longer valid for microporous systems, no pore size distribution can be calculated from the permporometry measurements on this system. The cyclohexane saturation point at a relative pressure of ~0.3 corresponds with an average pore radius of ~0.9 nm, which is in close agreement with the nitrogen sorption data of the powders made from sol 1. For the sake of comparison, Figure 7 also includes the oxygen flux through an α-alumina supported γ-alumina membrane, calcined at 600ºC. This system has average pore diameter of ~4.4 nm. Nitrogen sorption data of this system showed that it is mainly mesoporous system (see chapter 4 of this thesis). From the figure it can be seen that this plot has three different regions. When the relative pressure is higher than 0.8, all pores are blocked by condensed cyclohexane and no oxygen flux is observed. Reduction of the relative pressure from 0.8 to 0.3 leads to a drastic increase of the oxygen flux, due to desorption of cyclohexane from the pores in the capillary condensation regime. A further decrease in relative pressure leads to a slight further increase of the oxygen flux. This is thought to be mainly due to a change in the t-layer thickness inside the pores.

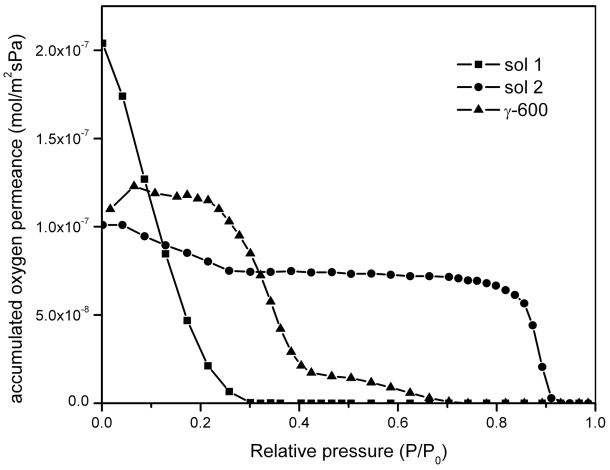

Figure 7. Oxygen flux versus relative vapour pressure of cyclohexane through silica layers prepared from sol 1 and sol 2 directly deposited on α-alumina. Data of an α-

alumina supported mesoporous γ-alumina membrane calcined at 600°C are shown for the sake of comparison.

3.1.4.2 XRD analysis

None of the silica layers derived from sol 1 and sol 2 that were deposited on an α-alumina support showed no indications of ordered mesoporosity by XRD. For silica from sol 1, this is likely due to the microporous nature of the silica layer as revealed by permporometry and nitrogen sorption. For silica from sol 2, it is probably due to an insufficient amount of material deposited on the α-alumina surface.

3.2 Liquid transport through the silica layers

3.2.1 Water transport property through the silica membranes

The steady state water fluxes through an α-alumina support, an α-alumina supported γ-alumina membrane (calcined at 900°C), γ-alumina supported silica membranes from sol 1 and sol 2, and a α-alumina supported silica layer from sol 1 are shown in Figure 8. According to Darcy's law, when the transport mechanism obeys the viscous flow model, the liquid flux is proportional to the applied pressure, irrespective of the type of liquid. The mathematical formulation of Darcy's law is

$$J = (-1/\eta)\, K_m\, \Delta P \qquad (2)$$

where J is the volumetric flux, η the bulk liquid viscosity, ΔP the applied pressure difference across the membrane and K_m the overall liquid permeability of the membrane.

The overall transport resistance of liquids through a stacked α-alumina/γ-alumina or α-alumina/γ-alumina/silica membrane can be regarded as two (or three, depending upon the number of layers) resistances in series. The overall membrane permeability coefficient K_m can be therefore be deconvoluted into the permeabilities of the individual layers according to

$$\frac{1}{K_m} = \frac{1}{K_\alpha} + \frac{1}{K_\gamma} + \frac{1}{K_{Si}} \text{ or } \frac{1}{K_m} = \frac{1}{K_\alpha} + \frac{1}{K_\gamma}, \qquad (3)$$

where K_α, K_γ and K_{Si} are the permeability coefficients of the α-alumina support, the mesoporous γ-alumina layer, and the silica top layer, respectively. Table 4 summarizes the permeability coefficients (K values) of the individual layers for water.

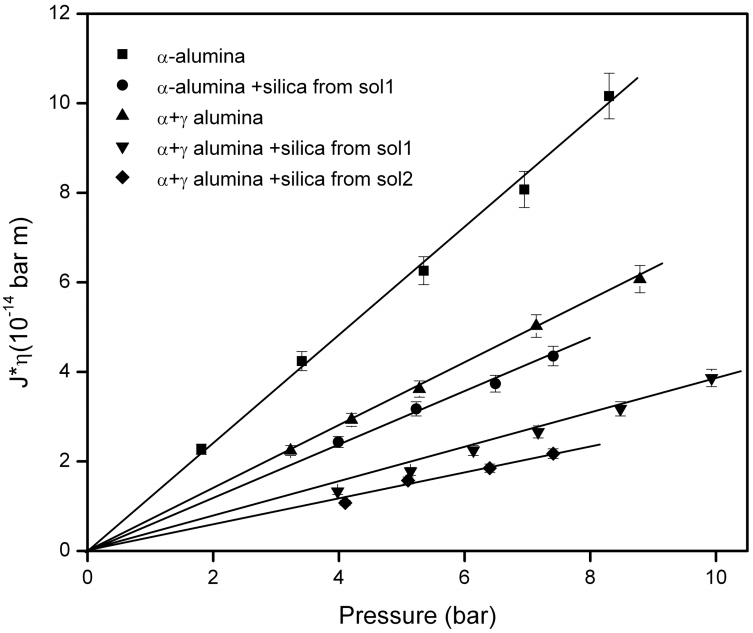

Figure 8. Water flux through different membranes.

Table 4. Permeability coefficient of water in individual layers from different stacked membranes.

Layer	Permeability (10^{-14}m)
α-alumina support	1.17 ± 0.06
(α-alumina supported) γ-alumina	0.69 ± 0.03
(α/γ-alumina supported) silica from sol 1	0.37 ± 0.03
(α-alumina supported) silica from sol 1	0.59 ± 0.10
(γ-alumina supported) silica from sol 2	0.29 ± 0.02
γ-alumina	1.68 ± 0.01
(γ-alumina supported) silica from sol 1	0.79 ± 0.05
(γ-alumina supported) silica from sol 2	0.52 ± 0.03
(α-alumina supported) silica from sol 1	1.19 ± 0.07

From table 4 it can be seen that the γ-alumina layer has the highest permeability coefficient. This is due to the high porosity (55%) and very large average pore diameter of this layer. The silica layer derived from sol 1 coated directly on an α-alumina support has a larger permeability coefficient for water than the other silica layers. This is probably due to the smaller film thickness, though this layer has

lowest average pore diameter. The silica layer from sol 1 deposited on γ-alumina shows a higher water permeability than the silica layer derived from sol 2 deposited on γ-alumina. This could be due to the manifestation of ordered pore architecture in the layer derived from sol 1.

3.2.2 Comparison of water transport through silica and alumina layers based on their thickness

Figure 9 shows an XPS depth profile indicating the thickness of an α-alumina supported silica layer derived from sol 1, and a TEM image of a γ-alumina supported silica layer derived from sol 1. The figure shows that the γ-alumina supported film has a thickness of ~600 nm, while the α-alumina supported film has a thickness of ~240 nm. A measure for the intrinsic permeability of the mesoporous structure is given by the product $k_\beta L_\beta$, where L_β is the thickness of the mesoporous layer. The $k_\beta L_\beta$ values of the α-alumina supported silica layer and the γ-alumina supported silica layer are listed in Table 5. From this table it is clear that the γ-alumina supported layer has a higher intrinsic water permeability than the α-alumina supported layer. This is probably due to the fact that the γ-alumina supported film has a significant amount of mesopores with an average Kelvin radius of ~2.5 nm. The presence of these pores and their ordered nature probably increases the permeability of this layer.

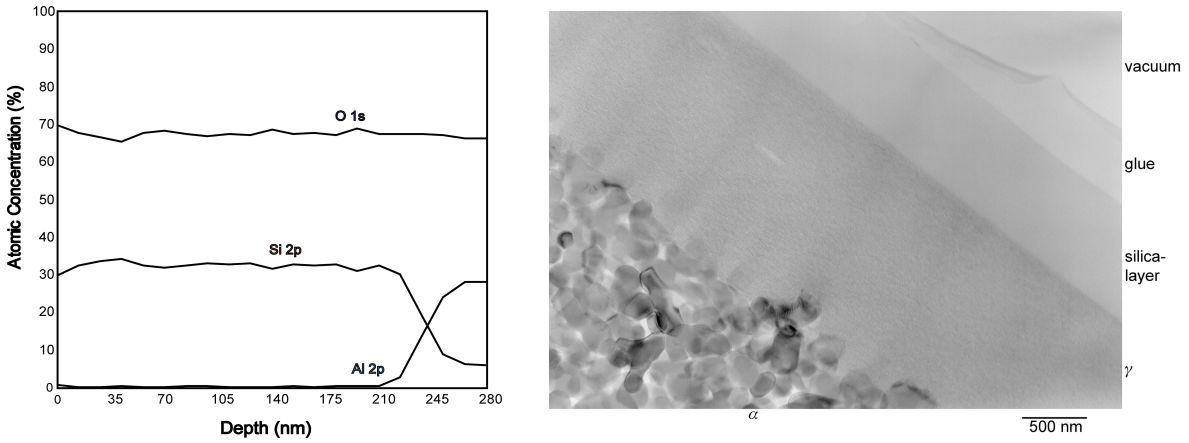

(a) (b)

Figure 9. Thickness of the supported silica layers derived from sol 1;
a) XPS depth profile of an α-alumina supported silica layer, b) γ-alumina supported silica layer.

Table 5. Permeability coefficients of water through individual membrane layers, before and after correction for differences in membrane layer thickness.

Membrane	Thickness L_β (μm)	Permeability coefficient k_β (10^{-14} m)	Intrinsic water permeability $k_\beta L_\beta$ (10^{-20} m^2)
(α-alumina supported) silica	0.24	1.19 ± 0.07	0.28
(γ-alumina supported) silica	0.6	0.79 ± 0.05	0.47
(α-alumina supported) γ-alumina	3.0	1.68 ± 0.01	5.4

It is also interesting to compare these values with that of an α-alumina supported γ-alumina layer calcined at 900ºC, which has an average pore radius of ~4 nm. The permeability coefficients of this layer before and after thickness correction are also listed in table 5. It is clear that the γ-alumina membrane layer has a higher intrinsic water permeability compared with the γ-alumina supported silica layer and the α-alumina supported silica layer. This difference can be explained by considering that γ-alumina has a much larger pore diameter, a large porosity and absence of any microporosity (cf. γ-800, chapter 4 of this thesis). The smaller average pore diameter and the presence of a considerable fraction of micropores in the supported silica layers probably make them intrinsically less permeable to water.

3.2.3 Liquid transport through γ-alumina supported silica layers

Figure 10 a presents the ethanol, toluene and n-hexane flux through γ-alumina supported silica membranes derived from sol 2. This figure shows that solvents with lower viscosity show a higher flux at similar pressure. Figure 10 b shows the fluxes after correction for viscosity differences. It can be seen that the solvent permeability decreases with an increase of the hydrophobicity of the solvents. A similar type of observation has also been made for γ-alumina membranes and the reasons for these permeability differences of different types of solvents are explored in detail in chapter 4 and chapter 5 of this thesis. Table 6 presents the numerical values of the permeability of the ethanol, toluene and n-hexane through the γ-alumina supported silica layer derived from sol 2.

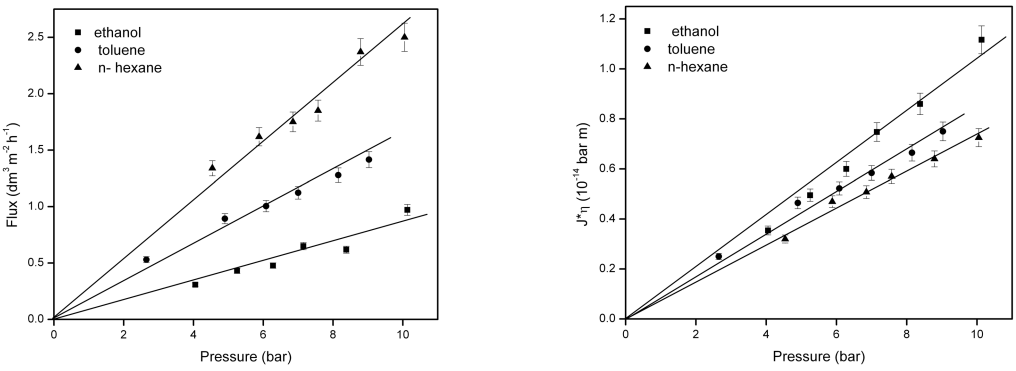

(a) (b)

Figure 10. Solvent fluxes through γ-alumina supported silica membrane derived from sol 2; (a) volumetric fluxes and (b) volumetric fluxes after correction for viscosity differences.

Table 6. Solvent permeability coefficients of γ-alumina supported silica membrane derived from sol 2.

Solvent	Overall permeability K_{ov} (10^{-14} m)	Layer permeability K_L (10^{-14} m)
Ethanol	0.09 ± 0.03	0.11 ± 0.06
Toluene	0.08 ± 0.01	0.09 ± 0.02
n-hexane	0.06 ±0.02	0.07 ± 0.02

4. Conclusions

In this chapter two different synthesis routes of surfactant templated silica materials have been presented. Powders derived from sol 1 did not show any sign of an ordered mesoporous structure, however films derived from sol 1 on different supports did contain ordered mesoporous domains. It has also been shown that the ordered silica layer does not grow directly on the mesoporous substrate. Instead it grows on a structurally disordered silica-rich interface of thickness ~20 nm. Defect-free layers could be formed from sol 1 both on macroporous and mesoporous supports. Powders and thin films grown on dense support, derived from sol 2, showed indications of an ordered mesoporous structure, but there was no sign of an ordered porous structure on porous substrates. Defect-free silica layers could be formed on mesoporous supports but not on macroporous supports. Water transport experiments showed that a silica layer deposited on an α-alumina support has the highest water permeability among all the silica layers, but the intrinsic permeability of the silica layer deposited on α-alumina support shows the lowest value. This is probably due to the microporous nature of the silica layer. Non-aqueous solvent permeation through the γ-alumina supported silica layer from sol 2 shows that hydrophilic liquids have a higher permeability coefficient than hydrophobic solvents.

References

1. J.S. Beck, J.C. Vartuli, W.J. Roth, M.E. Leonowicz, C.T. Kresge, K.D. Schmitt, C.T.-W. Chu, D.H. Olson, E.W. Sheppard, S.B. McCullen, J.B. Higgins, J.L. Schlenkert, A new family of mesoporous molecular sieves prepared with liquid crystal templates, *J. Am. Chem. Soc.*, **114** (1992) 10834.
2. M. Grun, A.A. Kurganov, S. Schacht, F. Schuth, K.K. Unger, Comparison of an ordered mesoporous aluminosilicate, silica, alumina, titania and zirconia in normal-phase high-performance liquid chromatography, *J. Chromatogr. A*, **740** (1996) 1.
3. P.D. Yang, G. Wirnsberger, H.C. Huang, S.R. Cordero, M.D. McGehee, B. Scott, T. Deng, G.M. Whitesides, B.F. Chmelka, S.K. Buratto, G.D. Stucky, Mirrorless lasing from mesostructured waveguides patterned by soft lithography, *Science*, **287** (2000) 465.
4. K. Kageyama, J. Tamazawa, T. Aida, Extrusion polymerization: Catalyzed synthesis of crystalline linear polyethylene nanofibers within a mesoporous silica, *Science*, **285** (1999) 2113.
5. K. Schumacher, P.I. Ravikovitch, A. Du Chesne, A.V. Neimark, K.K. Unger, Characterization of MCM-48 materials, *Langmuir*, **16** (2000) 4648.
6. V. Alfredsson, M.W. Anderson, Structure of MCM-48 revealed by transmission electron microscopy, *Chem. Mater.*, **8** (1996) 1141.
7. Q.S. Huo, R. Leon, P.M. Petroff, G.D. Stucky, Mesostructure design with gemini surfactants - supercage formation in a 3-dimensional hexagonal array, *Science*, **268** (1995) 1324.
8. F.X. Chen, L.M. Huang, Q.Z. Li, Synthesis of MCM-48 using mixed cationic-anionic surfactants as templates, *Chem. Mater.*, **9** (1997) 2685.
9. D. Zhao, P. Yang, N. Melosh, J. Feng, B.F. Chmelka, G.D. Stucky, Continuous mesoporous silica films with highly ordered large pore structures, *Adv. Mater.,* **10** (1998) 1380.
10. H. Yang, N. Coombs, I. Sokolov, G.A. Ozin, Registered growth of mesoporous silica films on graphite, *J. Mater. Chem.*, **7** (1997) 1285.
11. H. Miyata, K. Kuroda, Formation of a continuous mesoporous silica film with fully aligned mesochannels on a glass substrate, Chem. Mater. 12 (2000) 49.
12. N. Nishiyama, A. Koide, Y. Egashira, K. Ueyama, Mesoporous MCM-48 membrane synthesized on a porous stainless steel support, *Chem. Comm.,* (1998) 2147.
13. R. Schmuhl, J. Sekulic, S.Roy Chowdhury, C.J.M. van Rijn, K. Keizer, A. van den Berg, J.E. ten Elshof, D.H.A. Blank, Si-compatible ion selective oxide interconnects with high tenability, *Adv. Mater.,* **16** (2004) 900.
14. K.J. Edler, S.J. Roser, Growth and characterization of mesoporous silica films, *Int. Rev. Phys. Chem.*, **20** (2001) 387.
15. C.Y. Tsai, S.Y. Tam, Y.F. Lu, C.J. Brinker, Dual-layer asymmetric microporous silica membranes, *J. Membrane Sci.*, **169** (2000) 255.
16. M. Klotz, A. Ayral, C. Guizard, L. Cot, Synthesis and characterization of silica membranes exhibiting an ordered mesoporosity. Control of the porous

texture and effect on the membrane permeability, *Sep. Purif. Tech.,* **25** (2001) 71.
17. D.H. Park, N. Nishiyama, Y. Egashira, K. Ueyama, Enhancement of hydrothermal stability and hydrophobicity of a silica MCM-48 membrane by silylation, *Ind. Eng. Chem. Res.,* **40** (2001) 6105.
18. Y.S. Kim, S.-M. Yang, Preparation of continuous mesoporous silica thin film on a porous tube, *Adv. Mater.,* **14** (2002)1078.
19. C. Boissiere, M.A.U. Martines, P.J. Kooyman, T.R. de Kruijff, A. Larbot, E Prouzet, Ultrafiltration membrane made with mesoporous MSU-X silica, *Chem. Mater.,* **15** (2003) 460.
20. S. Roy Chowdhury, R. Schmuhl, K. Keizer, J.E. ten Elshof, D.H.A Blank, Pore size and surface chemistry effects on the transport of hydrophobic and hydrophilic solvents through mesoporous γ-alumina and silica MCM-48, *J. Membrane Sci.*, **225** (2003) 177.
21. I. Honma, H.S. Zhou, D. Kundu, A. Endo, Structural control of surfactant-templated hexagonal, cubic, and lamellar mesoporous silicate thin films prepared by spin-casting, *Adv. Mater.*, **12** (2000) 1529.
22. B.A. McCool, N. Hill, J. DiCarlo, W.J. DeSisto, Synthesis and characterization of mesoporous silica membranes via dip-coating and hydrothermal deposition techniques, *J. Membr. Sci.*, **218** (2003) 55.
23. G.Z. Cao, J. Meijerink, H.W. Brinkman, A.J. Burggraaf, Permporometry study on the size distribution of active pores in porous ceramic membranes, *J. Membrane Sci.,* **83** (1993) 221.
24. A. Shimojima, Y. Sugahara, K. Kuroda, Synthesis of Oriented Inorganic-Organic Nanocomposite Films from Alkyltrialkoxysilane-Tetraalkoxysilane Mixtures, *J. Am. Chem. Soc.,* **120** (1998) 4528.
25. K.N.P. Kumar, Nanostructured ceramic membranes; layer and texture formation, Ph.D. Thesis, University of Twente, Enschede, The Netherlands, 1993, p. 113.
26. Y.F. Lu, R. Ganguli, C.A. Drewien, M.T. Anderson, C.J. Brinker, W.L. Gong, Y.X. Guo, H. Soyez, B. Dunn, M.H. Huang, J.I. Zink, Continuous formation of supported cubic and hexagonal mesoporous films by sol gel dip-coating, *Nature*, **389** (1997) 364.

Chapter 4

Liquid transport through γ-alumina membranes

Part 1. Hydrophilic liquids

You don't have to agree with me, but it's quicker

Abstract*

In this chapter the transport of water and short chain alcohols through supported γ-alumina membranes with different pore diameters is described. It was found that water and alcohols have similar permeabilities when they are transported through membranes with pore diameters down to ~ 4.5 nm. However, the transport behaviour of alcohols and water differs considerably when they pass through membrane pores with an average diameter of ~3.4 nm. Here water still behaves as a classical Darcy type liquid during transport, irrespective of pore diameter, while the permeability of (water-containing) alcohols is smaller. The permeability of alcohols increases slightly with reduction of water content. At higher water concentrations the alcohols require a minimum threshold pressure to be exceeded before transport occurs, but this threshold pressure vanishes with the reduction of the water content in the alcohols. The water permeability through membranes with the smallest pore size is always larger than that of alcohols, irrespective of experimental conditions. These observations are interpreted in terms of viscosity increase in nanosized pores, and/or capillary condensation of water inside narrow pores.

* Part of this chapter has been published in *Journal of Membrane Science*, 225 (2003) 177.

1. Introduction

Sandwich-type ceramic composite membranes with NF characteristics typically have pore radii in the range of 0.5–3.5 nm (1,2). The surface charge of the pore walls depends upon pH and can be either positive or negative, depending on the pH relative to the iso-electric point (IEP) of the oxide surface. Under moderate process conditions the pore size and structure of ceramic membranes is fixed. Inorganic NF membranes have been prepared from γ-alumina (1,3), titania (4,5), and silica–zirconia (6,7), and were employed for the rejection of large organic molecules (7), and the retention of small (5,6) and complex ions (7).

Although solvent permeation through polymeric NF membranes has been demonstrated successfully in many cases (8-12), one of the advantages of inorganic membranes is their resistance to virtually all solvents. The permeation of pure alcohols as non-aqueous solvents through inorganic membranes has been discussed in detail for the silica-zirconia membrane system (13), but only very few papers to date have reported on the application of inorganic nanofiltration membranes for separations of non-aqueous solutions, one exception being a separation process in a supercritical medium.

In this chapter we report on the effect of systematic variation of the γ-alumina membrane pore size on the liquid permeation behaviour of water, ethanol and 1-propanol. We demonstrate that the short straight chain alcohols behave differently compared to water below a certain critical pore diameter. Following the literature available in different related fields we propose an explanation for the observed phenomena.

2. Experimental

2.1. Preparation of α-alumina supported mesoporous γ-alumina membranes

The γ-alumina membrane consisted of a macroporous α-alumina support and a thin mesoporous γ-alumina layer. The α-alumina supports were made by colloidal filtration of well-dispersed 0.3 μm α-alumina particles (AKP-30, Sumitomo). The dispersion was stabilized by peptizing with nitric acid. After drying at room temperature, the filter compact was sintered at 1100°C. Flat disks of Ø 39 mm and 2.0 mm thickness were obtained after machining and polishing. The final porosity of these supports is ~30% and the average pore diameter is in the range of 80-120 nm. Three different mesoporous γ-alumina membranes of ~3 μm thickness were prepared by dip-coating the above-mentioned porous α-alumina supports in a boehmite sol, followed by drying and calcining at 450°C, 600°C or 800°C (heating/cooling rates 0.5°C/min), respectively, for 1 h. These membranes are designated hereafter as γ-450, γ-600 and γ-800, respectively. The deposition/calcination cycle was carried out twice.

2.2. Preparation of γ-alumina powder

Three different γ-alumina powders were prepared by drying the boehmite sol in air, followed by calcination at 450º C, 600ºC or 800º C (heating/cooling rates 0.5°C/min), respectively, for 1 h. These powders were subjected to nitrogen adsorption/desorption experiments (Micromiretics) at 77 K.

2.3 Solvent permeation experiments

Steady state liquid flux measurements were carried out on α-alumina supports using water, ethanol and n-hexane in a dead-end nanofiltration cell. Water, ethanol and 1-propanol were used on supported γ-alumina composite membranes. Alcohol permeation through γ-450 membranes was carried out using alcohols with different water contents. The natural water content (i.e. water content of the as received alcohols) of ethanol is 0.03 mol/l and that for 1-propanol is 0.025 mol/l. The water content of the alcohols was varied by drying them using molecular sieve (Type 3A) and anhydrous $CaCl_2$ as drying agents, for different periods of time. Higher water contents in the alcohols were established by addition of water. The water content of the alcohols was measured using Karl Fischer titration (Metrohm KFT 756). The volume of the cell is 1000 ml and the operating pressure range was kept in the range of 2-14 bar. The stirring speed in the cell was kept constant at 200 rpm throughout all experiments.

3. Results and discussions

Figure 1 presents nitrogen adsorption / desorption isotherms of γ-450, γ-600 and γ-800 powders. The shape of the isotherm becomes more elongated with increasing calcination temperature. The shape of the isotherm clearly indicates the change of pore shape/geometry in the different powders. This figure shows the transition of adsorption-desorption hysteresis loop from type H2 to type H1, as the calcination temperature is increased (14). Alumina powders calcined at 800ºC show both steep adsorption and desorption branches (Type H1). This is characteristic of tubular shaped capillaries with both ends open. Alumina powder calcined at 450ºC shows a delayed adsorption branch and a steep desorption branch (Type H2). This may arise from the same type of open capillary as in Type H1, but the effective radii of the bodies of the pores are heterogeneously distributed and the narrow entrances are of equal size. Alumina powder calcined at 600ºC shows the intermediate behaviour of Type H1 and Type H2, which reflects the transition from H2 to H1 when we increase the calcination temperature.

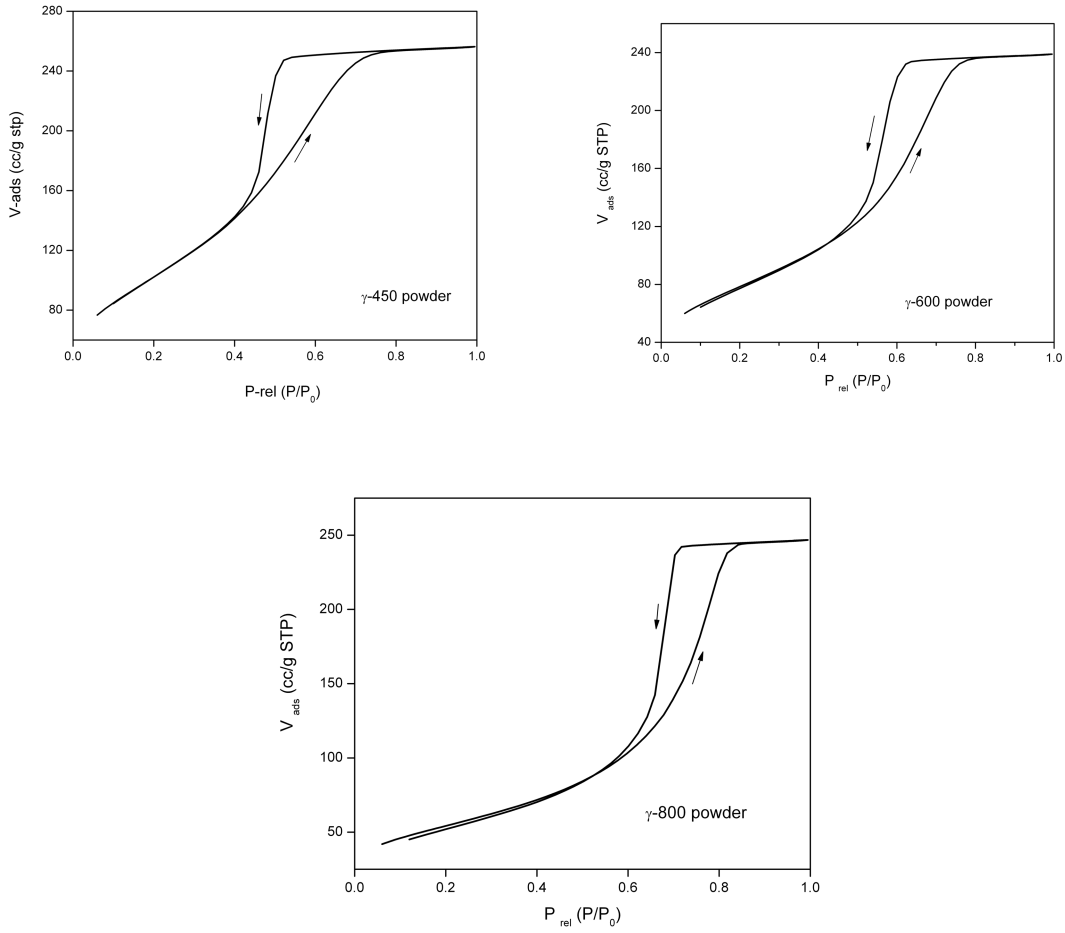

Figure 1. Nitrogen adsorption/desorption isotherms of γ-alumina powders calcined at 450º, 600º and 800º C, respectively.

The pore size distributions of the γ-450, γ-600 and γ-800 powders were calculated from the desorption isotherms. In Figure 2 it can be seen that the pore size increases and the pore size distribution becomes broader with increasing calcination temperature. Table 1 describes the physical properties of γ-alumina powders calcined at different temperatures.

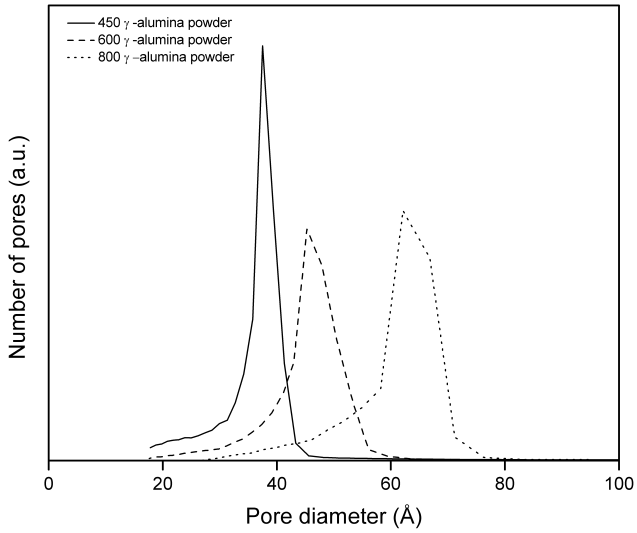

Figure 2. Pore size distribution of γ-alumina powders calcined at 450°, 600° and 800°C, respectively.

Table 1. Physical properties of γ-alumina powders.

Calcination temperature (°C)	BET area (m^2/g)	Pore diameter (nm)	Avarage pore diameter (nm)	Porosity (%)
450	373	1.8-4.2	3.2	55
600	285	2-6	4.4	55
800	196	3-8	6	55

It is known that the crystallite shape of the primary oxide particles change with calcination temperature. The morphology of the γ-alumina crystallites changes from platelet-like into spherical with increasing calcination temperature (15). This change of shape also changes the shape of the space between two crystallites. At lower calcination temperatures the pores are more or less slit shaped but with increasing calcination temperature it changes into more spherical.

Figure 3 shows the volume liquid flux as a function of pressure through a macroporous α-alumina support. The volume flux at steady state is proportional to the applied pressure, which indicates that pressure difference is the only driving force for the permeation of solvents. When the transport mechanism obeys the viscous flow model, the flux versus pressure plot can be expressed as a straight line that goes through the origin, irrespective of the type of liquid (Darcy's law). In

Figure 3 it can be seen that the liquid flux through the support decreases with increasing viscosity of the solvent according to

$$J = -\frac{1}{\eta} k_{\mathrm{m}} \Delta P \qquad [1]$$

where J is the volumetric flux, η the bulk liquid viscosity, ΔP the applied pressure difference across the membrane, and k_{m} the overall membrane permeability.

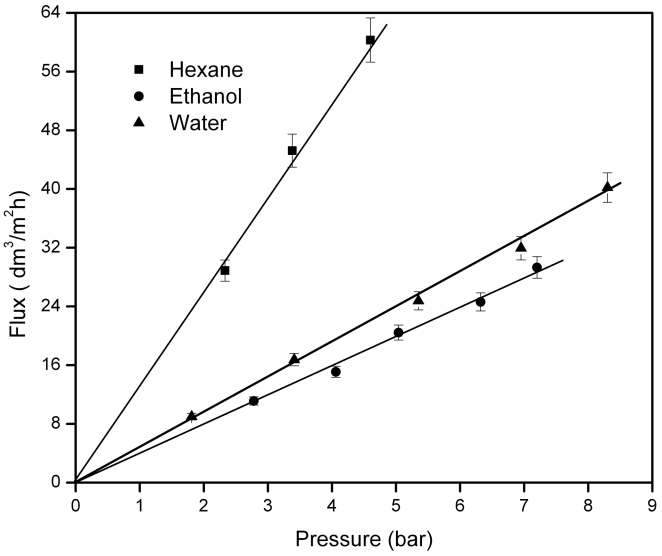

Figure 3. Solvent fluxes through α-alumina support.

Under conditions where Darcy's Law is valid, the membrane permeability coefficient k_{m} of a single membrane layer with pore radius r is defined as (16)

$$k_{\mathrm{m}} = \frac{\varepsilon r^2}{8\tau L}, \qquad [2]$$

where ε is the porosity of the membrane material, τ the tortuosity of the membrane layer, and L the membrane layer thickness. From Eq. (2) it is clear that k_m is a constant that depends only on the structural properties of the membrane material, not on the physical properties of the permeating liquid.

This is further illustrated in Figure 4, which shows the product of flux and solvent viscosity as a function of applied pressure. It is clear from this figure that the flux through α-alumina membranes with a pore diameter of ~100 nm follows Darcy' law and is only influenced by the applied pressure and solvent viscosity, as is expected for macroporous systems. A linear fit to the data of Figure 4 yields a value k_α=(1.17±0.08)·10^{-14} m for the permeability of the α-alumina layer.

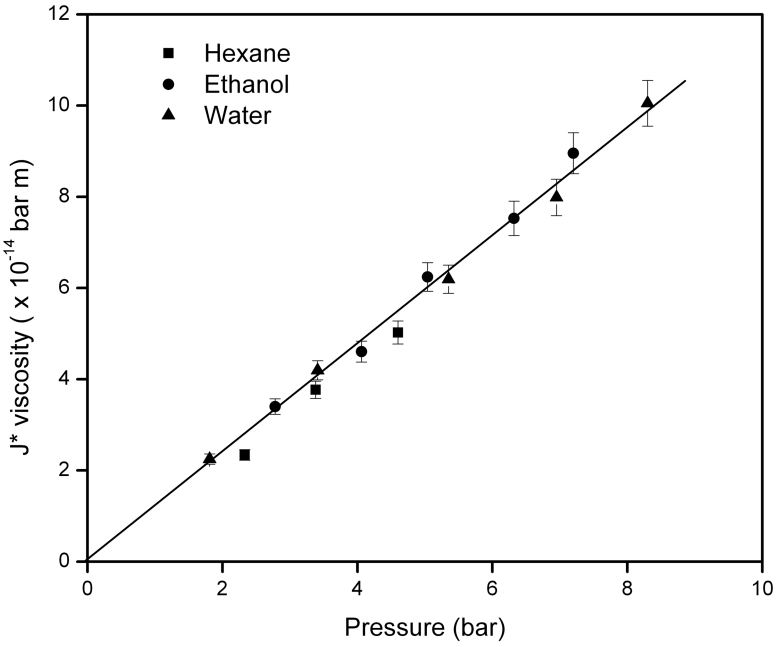

Figure 4. Viscosity-corrected fluxes through α-alumina support.

Figure 5 shows viscosity-corrected fluxes of water, ethanol and 1-propanol through γ-800 and γ-600 membranes. The slope of the fitted straight line is the overall permeability coefficient k_{ov} of the membrane for a given solvent. It is clear that the permeability through γ-800 and γ-600 membranes with an average pore diameter of 4-8 nm is not influenced by the nature of the solvent.

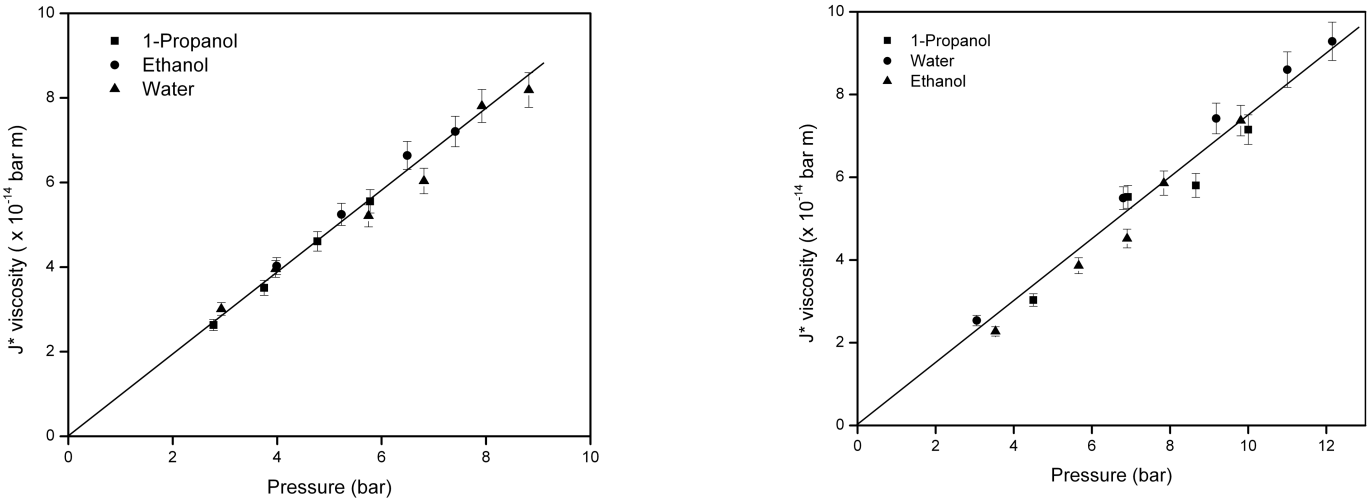

(a) (b)

Figure 5. Viscosity corrected fluxes through supported γ-alumina membranes; a) γ-800 and b) γ-600.

Figure 6 presents the plot of the product of volumetric flux through γ-450 membranes and solvent viscosity against applied pressure difference. This figure shows considerably different trends than figure 5. Here water has a considerably higher permeability than the alcohols. It also shows that a threshold pressure of ~0.7 bar has to be exceeded before volumetric flow of alcohols through the membrane starts. Table 2 summarizes the overall liquid permeabilities k_{ov} of different membrane – solvent combinations, and the permeability coefficients k_L of the individual γ-alumina layers, which were calculated using the relationship $1/k_{ov} = 1/k_L + 1/k_\alpha$ (12) .

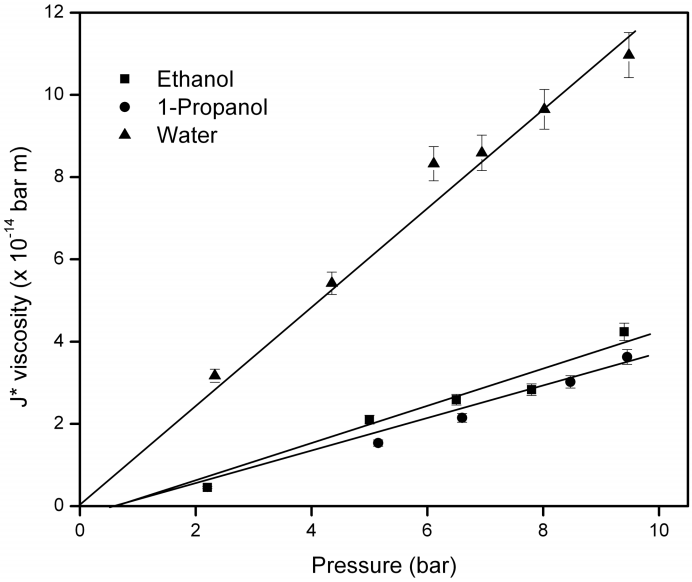

Figure 6. Product of flux and viscosity of ethanol, 1-propanol (as received) and water through supported γ-450 membrane.

Table 2a. Overall permeability coefficients of ethanol, 1-propanol (both before drying) and water through α-alumina supported mesoporous γ-alumina membranes.

Solvent	Permeability coefficient k_{ov} (10^{-14} m)		
	γ-800	γ-600	γ-450
Water	0.97 ± 0.05	0.82 ± 0.002	0.75 ± 0.08
Ethanol	0.97 ± 0.02	0.8 ± 0.07	0.5 ± 0.05
1-propanol	0.97 ± 0.06	0.8 ± 0.03	0.49 ± 0.03

Table 2b. Permeability coefficients of ethanol, 1-propanol (both before drying) and water through mesoporous γ-alumina layers.

Solvent	Permeability coefficient k_L (10^{-14} m)		
	γ-800	γ-600	γ-450
Water	5.7 ± 0.2	2.8 ± 0.3	2.2 ± 0.9
Ethanol	5.6 ± 0.1	2.6 ± 0.4	0.89 ± 0.06
1-propanol	5.6± 0.4	2.6 ± 0.6	0.86 ± 0.09

Figure 7 presents the permabilities of alcohols at different water contents through the γ-450 layer. The numerical values of the permeabilities and cut-off pressures are presented in table 3.

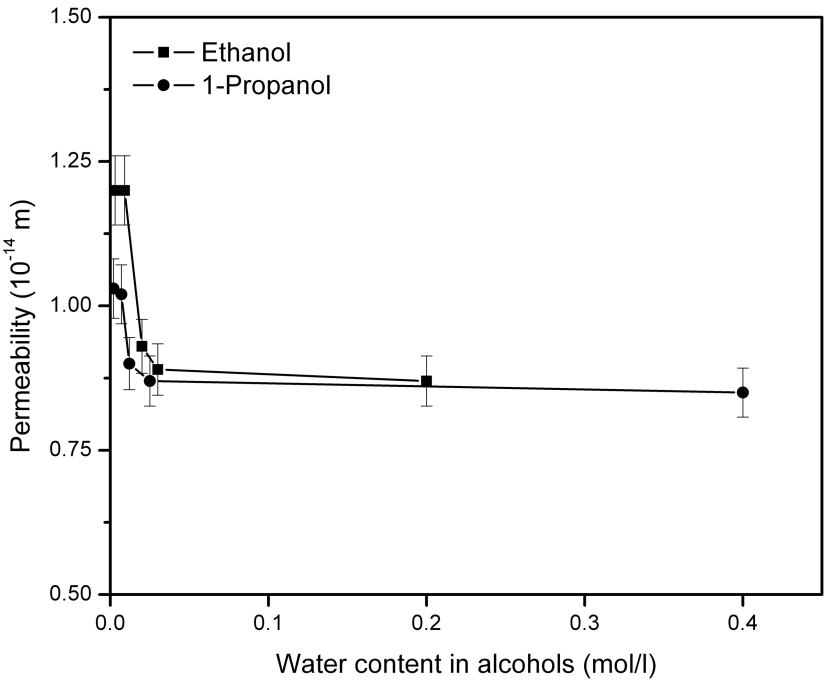

Figure 7. Permeability coefficients of alcohols with different water contents through γ-450 layer.

Table 3. Permeability coefficient and cut-off pressures for ethanol and 1-propanol with different water contents, when passing through γ-450 membrane.

Alcohol	Water content (mol/l)	Permeability coefficient k_L (10^{-14} m)	Cut-off pressure (bar)
Ethanol	0.003	1.2 ± 0.05	0
	0.009	1. 2 ± 0.07	0
	0.02	0. 94 ± 0.04	0.3 ± 0.28
	0.03	0. 89 ± 0.06	0.63 ± 0.45
	0.2	0.87 ± 0.04	0.37± 0.1
1-propanol	0.002	1.03 ± 0.03	0
	0.007	1.02 ± 0.04	0
	0.012	0.9 ± 0.05	0.43 ± 0.31
	0.025	0.86 ± 0.09	0.67 ± 0.52
	0.4	0.85 ± 0.04	0.61 ± 0.37

From figure 7 and table 3 it is clear that alcohol permeability through γ-450 increases with decreasing water content. The cut-off pressure also decreases with reduction of water content. Figure 7 shows some interesting features. As the water concentration in the alcohols is decreased, the difference in permeability between ethanol and 1-propanol increases. On the other hand, the difference in alcohol permeability almost vanishes at higher water concentration in the alcohols.

Figure 8 presents a logarithmic plot of membrane permeability coefficient k_L versus pore radius. This plot shows that a straight line fit with slope ~2 can be drawn through the data points. This observation shows that the permeability coefficient of water through mesoporous γ-alumina is proportional to the second power of pore radius. This is in accordance with equation (2), provided that all other parameters are more or less constant. It indicates that water behaves as a classical Darcy type liquid even when it is passing through a space as small as ~3.5 nm. On the other hand, the alcohols deviate considerably from classical Darcy type liquid behaviour when they pass through a very narrow pore.

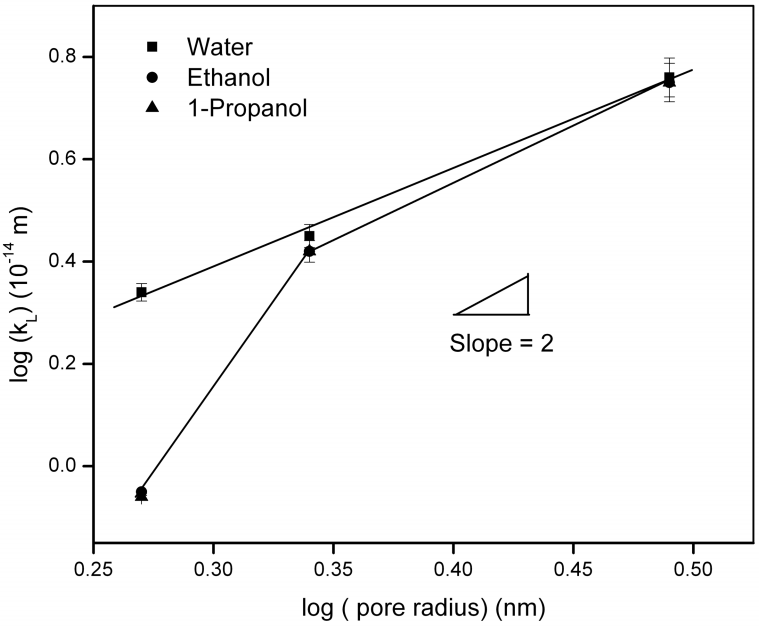

Figure 8. Logarithmic plot of the permeability coefficient of γ-alumina k_L as a function of membrane pore radius. The permeability values of the alcohols presented here are for alcohols prior to removal of water.

A number of factors may contribute to the difference of permeation behaviour of water and alcohols through γ-450 membranes and each should be considered in order to give a possible interpretation of the permeability differences between different solvent-membrane combinations. The first factor to consider is the extent to which the use of bulk liquid viscosities in Eq. (1) is still allowed at nanometer dimensions. It has been reported that the density and viscosity of *non*-hydrogen bonded liquids that are confined between two smooth surfaces can be strongly influenced by the close proximity of these surfaces (18,19). On the other hand, a Surface Force Apparatus (SFA) study showed that water remains in a fluid state even in very narrow confinements (21). However, from a study of alcohols on hydrophilic substrates using atomic force microscopy (AFM) it has been found that ordering of alcohols between flat surfaces and the AFM tip occurs only when the surface-tip distance is less than 4 nm (18), though this effect is strictly valid only for atomically smooth surfaces. There are no reports of ordering of short chain alcohols on rough hydrophilic surfaces. The pores of γ-450 alumina membranes can be considered as two rough surfaces facing each other at an average distance of ~3.5 nm. However, as Figure 2 shows, a small but substantial fraction of pores in γ-450 has a pore size < 2 nm, unlike γ-600 and γ-800. It is therefore plausible that at some locations inside the γ-450 membrane where necks in the pore structure occur, the real pore size will be in the range of ~0.5 nm to 1 nm, which is the typical surface roughness in SFA or AFM experiments where ordering of alcohol molecules has been reported (20). In this situation it is possible that some sort of

local ordering of alcohol molecules inside the membrane pores occurs. This local ordering of molecules will increase the viscosity of the liquid locally. The confinement effect may lead to local configurations in which the alcohol molecules are tilted with respect to the surface normal and interact with hydroxyl groups of the surfaces through hydrogen bonds. Provided that sufficient space is available to allow monolayer coverage on the whole pore wall, such an arrangement will lead to a bilayer structure of the alcohol molecules. The bilayer thickness can be roughly estimated with $2L \cos \theta$, where L is the length of the alcohol molecules and θ is the tilting angle (~47°) (20) with the surface normal. The length of the alcohol molecule can be estimated with $L = 1.23n + 2.98$ Å, where n is the number of carbon atoms in the straight chain alcohols. For 1-propanol the bilayer thickness is estimated to be ~1 nm. The model thus proposes a kind of molecular ordering happening within pores through hydrogen bonding, irrespective of surface roughness. The experiments presented here suggest that water retains its bulk viscosity in each type of membrane, but the viscosity of the alcohols differs locally from the bulk viscosity values, especially in pores with a diameter of less than 2 nm (microporous region), where the relative effect of the bilayer is more pronounced.

An alternative explanation for the observed phenomena is that alcohol molecules may react with the hydroxyl groups of metal oxide surfaces and that this reaction makes the oxide surface partly hydrophobic (22). On the molecular level simple alcohols like methanol, ethanol, etc., are not miscible with water in any proportion (23). The alkyl chains of the alcohol molecules are pointed towards the center of the pore and create a hydrophobic environment within the very narrow space. Under these conditions, phase separation of water that was dissolved in alcohol may occur, and a water bridge may form (22). This water bridge blocks the transport path for the alcohol molecules, in other words the effective porosity of the alumina layer available for alcohol transport decreases, and the length of the transport path for the alcohol molecules increases (i.e. the effective tortuosity increases). To induce transport of alcohols through some of the smallest pores this water bridge has to be broken. The extra work that has to be done to open up the pores is revealed in the threshold pressure for alcohols when they permeate through γ-450 membranes. The above-mentioned physical model of water condensation can also explain the increase of alcohol permeability and reduction in cut-off pressure through the γ-450 layer when the water content is reduced. It is generally assumed that a time period π is required to condense a water bridge in an interstitial volume (24), i.e.,

$$\pi = \pi_0 \exp\left(\frac{\Delta E}{k_B T}\right) \qquad [3]$$

π_0 is the time required to condense one liquid monolayer on the solid surface; k_B is the Boltzman constant, ΔE is the activation energy of the process and T is the absolute temperature. On nanometer length scales π is very small and the process is almost instantaneous. Any decrease of ΔE leads to a reduction of the value ot π. The activation energy can be approximated by $\Delta E \approx [A \ln (C_s/C)]$, where A is a constant at a fixed surface separation and C_s is the saturation concentration of

water in the fluid, while C is the actual concentration of water in the fluid. As the water content in the alcohols increases, ln (C_s/C) is reduced, consequently ΔE also becomes smaller and hence π reduces (24).

At higher water content in the alcohols, it seems that the rate of capillary condensation of water is fast enough to block some transport paths before the actual experimental data could be recorded. This is reflected in the almost same permeability values for ethanol and 1-propanol through γ-450 membranes.

At lower water contents, the value of π is larger than in the case mentioned above. In this case it is probable that separation of water from 1-propanol is faster than from ethanol as it is more hydrophobic due to the presence of an extra (-CH2-) segment. Then pore blocking by water is faster when 1-propanol is used, than when ethanol is used. This effect leads to a smaller permeability of 1-propanol, at least in the first few hours of the experiments (usually 4-6 h).

The water condensation effect and threshold pressure will be discussed in more detail in the next chapter, where the transport of hydrophobic solvents through γ-alumina membranes is described.

It can be noted from figure 7 and table 3 that when the alcohols are passing through the γ-450 membranes, even under water-free conditions, they do not have the same permeability coefficient as pure water. This indicates that together with water condensation, viscosity increase seems to play a significant role in the permeability of alcohols as discussed earlier. Another explanation for the differences between the alcohol and water permeabilities could be the difference in molecular size between water and alcohols. Alcohols have a molecular diameter of ~1.6 times that of water, which means that water molecules may enter some pores which are not available for alcohols. A molecular size dependence on alcohol permeability has also been reported in literature (7). The permeability difference between water-free ethanol and 1-propanol can be due to the differences in molecular size as well as the degree of ordering of the alcohol molecules inside the membrane pores. It has been reported that ordering of 1-propanol in a narrow channel is more pronounced than of ethanol (20). However, it is difficult to indicate the exact reason or reasons for the permeability differences between water and water-free alcohols through γ-450 membranes.

4.Conclusions

In this chapter it has been shown that water behaves as a classical Darcy type liquid down to average membrane pore sizes of ~3.5 nm. Short chain alcohols and water have similar permeability coefficients in membranes with pores down to ~4 nm. However, the permeability of alcohols deviates considerably from water when they pass through pores of less than ~4 nm diameter. The alcohol permeability through γ-450 membrane increases with reduction of water content. But under all conditions the water permeability is higher than that of alcohols through γ-450 membranes. We could explain this behavior in terms of molecular ordering

phenomena that have been observed by SFA and AFM studies on atomically flat surfaces. It appears that the transport of alcohols through small mesopores (<4 nm) is affected by the pore size and pore shape of the porous medium, local ordering of alcohols via hydrogen bonding with surface hydroxyl groups or alcohol hydroxyl groups, and possibly to phase separation of water from the alcohols, which may form water bridges, leading to hindered transport of alcohols.

References

1. A. Larbot, S. Alami-Younissi, M. Persin, J. Sarrazin, L. Cot, Preparation of γ-alumina nanofiltration membrane, *J. Membrane Sci.*, **97** (1994) 167.
2. W.B.S. de Lint, Transport of electrolytes through ceramic nanofiltration membranes, PhD thesis, University of Twente. The Netherlands, 2003.
3. S. Roy Chowdhury, J.E. ten Elshof, N.E. Benes, K. Keizer, Development and comparative study of different nanofiltration membranes for highly charged large ion recovery, *Desalination*, **144** (2002) 41.
4. S. Sarrade, G.M. Rios, M. Carles, Nanofiltration membrane behavior in a supercritical medium, *J. Membrane Sci.,* **114** (1996) 81.
5. G.M. Rios, R. Joulie, S.J. Sarrade, M. Carles, Investigation of ion separation by microporous nanofiltration membranes, *AIChE J.*, **42** (1996) 2521.
6. T. Tsuru, H. Takezoe, M. Asaeda, Ion separation by porous silica-zirconia nanofiltration membranes, *AIChE J.*, **44** (1998) 765.
7. T. Tsuru, S. Wada, S. Izumi, M. Asaeda, Silica–zirconia membranes for nanofiltration, *J. Membrane Sci.,* **149** (1998) 127.
8. D.R. Machado, D. Hasson, R. Semiat, Effect of solvent properties on permeate flow through nanofiltration membranes. Part I: investigation of parameters affecting solvent flux, *J. Membrane Sci.*, **163** (1999) 93.
9. X.J. Yang, A.J. Livingston, L. Freitas dos Santos, Experimental observations of nanofiltration with organic solvents, *J. Membrane Sci.,* **190** (2001) 45.
10. D. Banushali, S. Kloos, C. Kurth, D. Bhattacharyya, Performance of solvent-resistant membranes for non-aqueous systems: solvent permeation results and modeling, *J. Membrane Sci.*, **189** (2001) 1.
11. D.R. Machado, D. Hasson, R. Semiat, Effect of solvent properties on permeate flow through nanofiltration membranes, *J. Membrane Sci.,* **166** (2000) 63.
12. S. Roy Chowdhury, R. Schmuhl, K. Keizer, J.E. ten Elshof, D.H.A Blank, Pore size and surface chemistry effects on the transport of hydrophobic and hydrophilic solvents through mesoporous γ-alumina and silica MCM-48, *J. Membrane Sci.*, **225** (2003) 177.
13. T. Tsuru, T. Sudou, S. Kawahara, T. Yoshioka and M. Asaeda, Permeation of liquids through inorganic nanofiltration membranes, *J. Colloid Interf. Sci.*, **228** (2000) 292.
14. K.S.W. Sing, D.H. Everett, R.A. W. Haul, L. Moscou, R.A. Pierotti, J. Rouquerol, Reporting physisorption data for gas / solid systems, with special reference to the determination of surface area and porosity, *Pure & Appl. Chem.*, **57** (1985) 603.
15. A.F.M. Leenaars, A.J. Burggraaf, The preparation and characterization of alumina membranes with ultra-fine pores. Part 3. The permeability for pure liquids, *J. Membrane Sci.***, 24** (1985) 245.
16. M. Mulder, Basic principles of membrane technology, Kluwer Academic Press; Dordrecht, the Netherlands, (1996); Chapter 5.

17. S. Liu, J. Masliyah, Single fluid flow in porous media, *Chem. Eng. Comm.* **148-150** (1996) 653.
18. H.K.Christenson, Interactions between hydrocarbon surfaces in a nonpolar liquid - effect of surface-properties on solvation forces, *J. Phys. Chem.,* **90** (1986) 4.
19. S.Granick, Motions and relaxations of confined liquids, *Science*, **253** (1991) 1374.
20. V. Franz, H.J. Butt, Confined liquids: Solvation forces in liquid alcohols between solid surfaces, *J. Phys. Chem. B*, **106** (2002) 1703.
21. U. Raviv, J. Klein, Fluidity of bound hydration layers, *Science*, **297** (2002) 1540.
22. Y. Kanda, T. Nakamura, K. Higashitani, AFM studies of interaction forces between surfaces in alcohol-water solutions, *Colloid and surface-A,* **139** (1998) 55.
23. S. Dixit, J. Crain, W.C.K. Poon, J.L. Finney, A.K. Soper, Molecular segregation observed in a concentrated alcohol-water solution, *Nature*, **446** (2002) 829.
24. L. Bocquet, E. Charlaix, S. Ciliberto, J. Crassous, Moisture-induced ageing in granular media and the kinetics of capillary condensation, *Nature*, **396** (1998) 735.

Chapter 5

Liquid transport through γ-alumina membranes

Part 2. Hydrophobic liquids

If you're not confused, you're not paying attention

Abstract*

The transport behavior of toluene and n-hexane in γ-alumina membranes with different pore diameters was studied. It was shown that the permeability of water-lean hexane and toluene is in agreement with Darcy's law down to membrane pore diameters of 3.5 nm. The presence of molar water fractions of $5\text{-}8\cdot10^{-4}$ in these solvents led to a permeability decrease of the γ-alumina layer by a factor of 2-4 depending on pore size. In general a lower permeability was found for hexane than for toluene. Moreover, in the presence of water a minimum applied pressure of 0.5-1.5 bar was required to induce net liquid flow through the membrane. These phenomena were interpreted in terms of capillary condensation of water in membrane pores with a size below a certain critical diameter. This is thought to lead to substantial blocking of these pores for transport, so that the effective tortuosity of the membrane for transport of hydrophobic solvents increases.

* Part of this chapter has been published in *Langmuir*, 20 (2004) 4548.

1. Introduction

Nanofiltration (NF) membranes are used to separate solvents from multivalent ions and small organic molecules using pressure as driving force. Two parameters are of crucial importance in membrane separation processes, namely the level of molecule or ion retention, and the solvent permeability. The permeability of liquids depends to a large extent on the interactions between solvent and membrane pore surface. This will be a dominant factor especially when narrow pores of a few molecular diameters wide are considered. It has been demonstrated for polymeric membrane how solvent/membrane interactions influence solvent transport (1-4). The permeation of pure alcohols as non-aqueous solvents through inorganic membranes has also been discussed in detail (5). However, to date only few papers (6-12) have reported on the application of inorganic nanofiltration membranes to separations of non-aqueous solutions (10).

In this article we report on the effect of systematic variation of the γ-alumina membrane pore size on the liquid permeation behavior of toluene and n-hexane. We demonstrate how the presence of low concentrations of water affects the liquid permeability of these hydrocarbons considerably. We propose a hypothesis to explain the permeability change of hydrocarbon liquids through γ-alumina membranes in the presence of small amounts of water in the hydrocarbon liquid feed. These phenomena are also of practical importance for industrial liquid separation processes involving mesoporous membranes, since industrial organic solvents usually contain small amounts of water that are not considered explicitly.

2. Experimental

2.1. Preparation of α-alumina supported mesoporous γ-alumina membranes

The γ-alumina membrane consisted of a macroporous α-alumina support and a thin mesoporous γ-alumina layer. The α-alumina supports were made by colloidal filtration of well-dispersed 0.4 μm α-alumina particles (AKP-30, Sumitomo). The dispersion was stabilized by peptizing with nitric acid. After drying at room temperature, the filter compact was sintered at 1100ºC. Flat disks of Ø 39 mm and 2.0 mm thickness were obtained after machining and polishing. The final porosity of these supports is ~30% and the average pore diameter is in the range of 80-120 nm. Three different mesoporous γ-alumina membranes of ~3 μm thickness were prepared by dip-coating twice the above-mentioned porous α-alumina supports in a boehmite sol, followed by drying and calcining at 450ºC, 600ºC or 800ºC for 1 h (heating/cooling rates 0.5°C/min), respectively. These membranes are designated hereafter as γ-450, γ-600 and γ-800, respectively.

2.2. Preparation of γ-alumina powder

Three different γ-alumina powders were prepared by drying the boehmite sol in air, followed by calcination at 450ºC, 600ºC or 800ºC for 1 h (heating/cooling rates 0.5°C/min), respectively. These powders were subjected to nitrogen adsorption/desorption experiments (Micromiretics) at 77 K.

2.3. Solvent permeation experiments

Steady state liquid flux measurements were carried out in a dead-end nanofiltration cell at room temperature on α-alumina supported γ-alumina composite membranes using water-rich toluene (0.005 mol H_2O/l), water-rich hexane (0.006 mol H_2O/l), water-lean toluene (< 0.001 mol H_2O/l) (Aldrich) and water-lean hexane (< 0.001 mol H_2O/l) (Aldrich). The water concentrations were determined using a Metrohm KFT 756 Karl Fischer coulometer. The volume of the permeation cell is 1000 ml and the operating pressure range was kept in the range 2-14 bar. The stirring speed in the cell was kept constant at 200 rpm throughout all experiments. Liquid permeation experiments were done on fresh membranes for each run. Liquid permeation tests with water-lean solvents were carried out in the presence of 1 nm pore sized dry molecular sieves (2 mm bead diameter, Merck) inside the permeation vessel to remove trace amounts of moisture from the vessel. Fluxes were measured with increasing and decreasing pressure steps after reaching (pseudo-) steady state conditions, and all measurements were usually done within the first three hours of operation of the membrane. Permeation tests with water-rich and water-lean hexane for longer times to observe the effect of operation time on membrane permeability were carried out on γ-450 membranes at a constant pressure of 8.6 bar.

3. Results

The γ-450, γ-600 and γ-800 powders were subjected to nitrogen adsorption/desorption experiments. From Figure 1 it can be seen that the pore size increases and the pore size distribution becomes broader with increasing calcination temperature. The main physical properties of the powders are listed in Table 1.

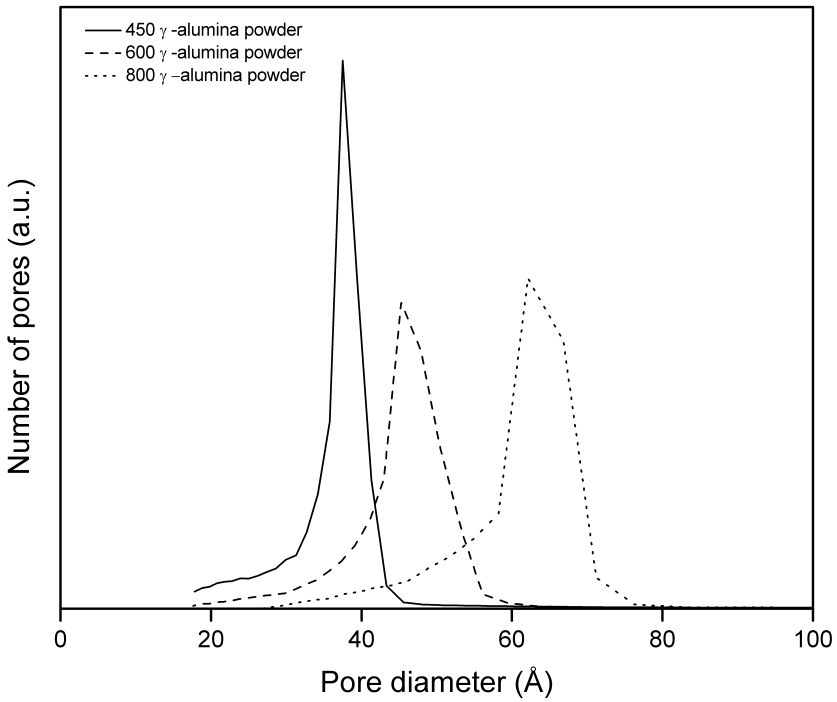

Figure 1. Pore size distribution of γ-alumina powders calcined at 450º, 600º and 800°C.

Table 1. Physical properties of γ-alumina powders.

Calcination temperature (ºC)	BET area (m^2/g)	Pore diameter (nm)	Porosity (%)
450	373	3.5	55
600	285	4.4	55
800	196	5.9	55

Figure 2 shows the volumetric solvent fluxes versus applied pressure through γ-800 membranes with water-rich hydrocarbons.

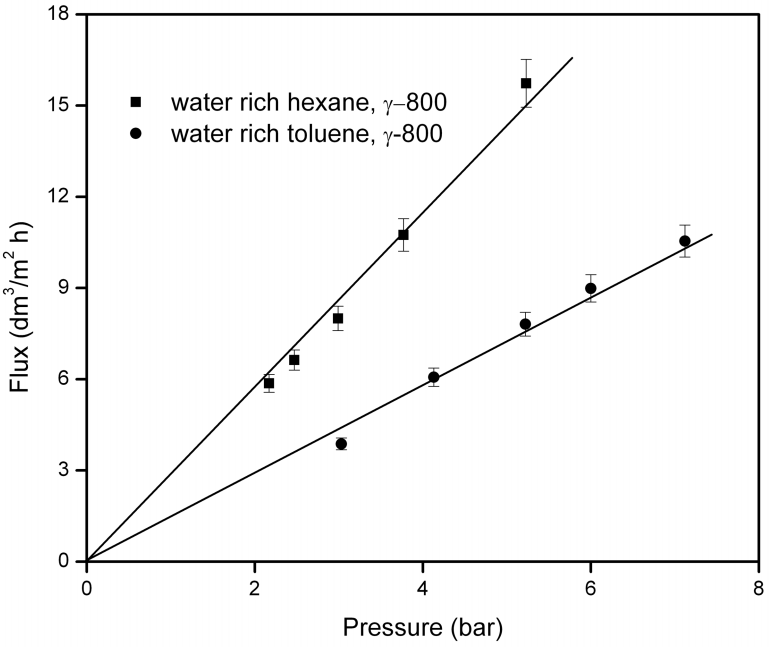

Figure 2. Volumetric liquid fluxes versus applied pressure through γ-800 membranes.

According to Darcy's law, when the transport mechanism obeys the viscous flow model, the flux is proportional to the applied pressure, irrespective of the type of liquid. The mathematical formulation of Darcy's law is (13)

$$J = -\frac{1}{\eta} k_{\mathrm{p}} \Delta P \,, \qquad [1]$$

where J is the volumetric flux, η the bulk liquid viscosity, and ΔP the applied pressure difference across the membrane. The membrane permeability coefficient k_{p} of a single membrane layer with pore radius r is defined as (14)

$$k_{\mathrm{p}} = \frac{\varepsilon r^2}{8\tau L} \,, \qquad [2]$$

where ε is the porosity of the membrane material, τ the tortuosity of the membrane layer, and L the membrane layer thickness. From Eq. (2) it is clear that k_{p} is a constant that depends only on the structural properties of the membrane material, not on the physical properties of the permeating liquid. This is illustrated in Figure 3, which shows the product of flux and solvent viscosity as a function of applied pressure. The slope of the fitted straight line is the overall permeability coefficient k_{m} of the membrane for a given solvent. It is clear that the permeability through γ–800 membranes with a pore diameter of 6-8 nm is not influenced by the nature of the solvent.

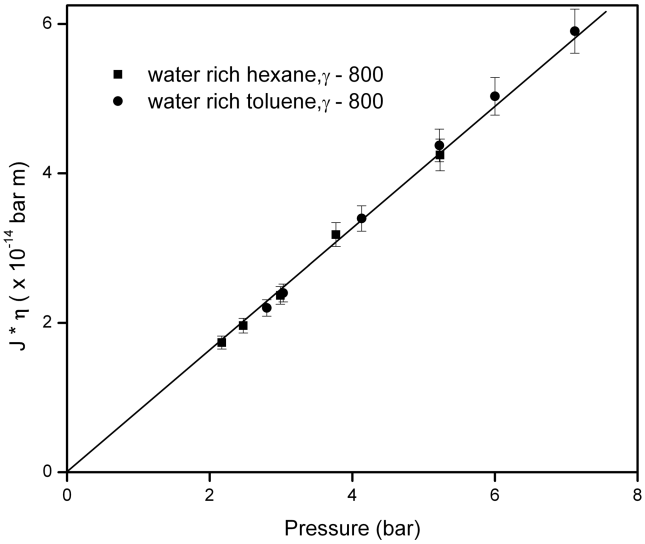

Figure 3. Product of volumetric liquid flux and liquid viscosity versus applied pressure through γ-800 membranes.

Figure 4 shows similar viscosity-corrected fluxes of water-rich hydrocarbons through γ-600 and γ-450 membranes. In comparison with Figure 3, some remarkable features are observed. Both toluene and hexane require a certain threshold pressure to be exceeded before transport through the γ-alumina membranes is observed. These two liquids also have different permeability coefficients, and it appears that the permeability of hexane through γ-alumina is smaller than that of toluene.

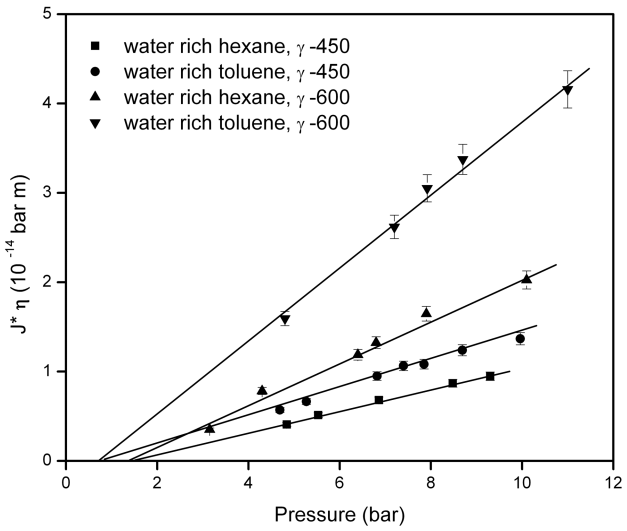

Figure 4. Product of volumetric liquid flux and liquid viscosity versus applied pressure through γ-600 and γ-450 membranes.

Figure 5 shows viscosity-corrected fluxes of water-lean liquids through γ-800, γ-600 and γ-450 membranes. Comparison with the data in Figures 3 and 4 shows that the permeabilities of these liquids through γ-450 and γ-600 are 2-4 times higher than the permeabilities of the corresponding water-rich liquids through the same membranes. Moreover, in contrast to water-rich liquids, no threshold pressure for liquid transport with water-lean liquids was observed within experimental error.

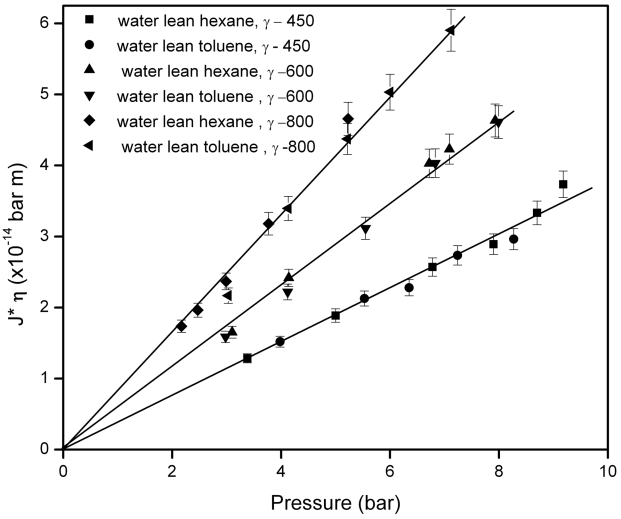

Figure 5. Product of volumetric liquid flux and liquid viscosity versus applied pressure of water-lean solvents.

Figure 6 shows the time dependence of water-lean and water-rich hexane fluxes at constant pressure through γ-450 membranes. The figure shows that both liquid fluxes decrease with time, but the permeability decrease of water-rich hexane occurs slightly faster.

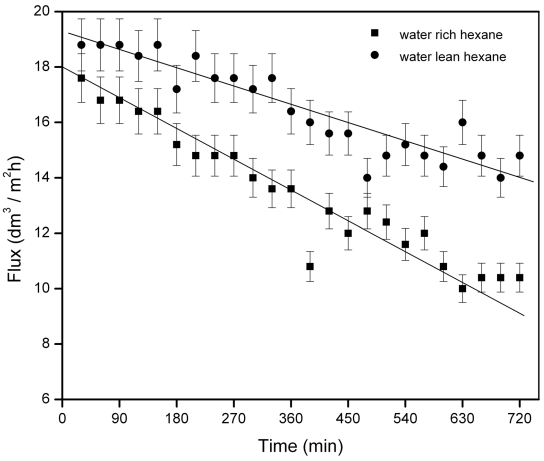

Figure 6. Volumetric fluxes of water-lean and water-rich hexane through a γ-450 membrane at constant applied pressure of 8.6 bar. Drawn lines serve as guide to the eye.

4. Discussion

The experiments showed that when water-lean or water-rich hexane or toluene pass through membranes with relatively large pores, e.g. the γ–800 membrane with ~6 nm pores, the permeability coefficients of all liquids are the same, and the liquid behavior appears to obey Darcy's law, Eq. (1).

The overall transport resistance of liquids through a stacked α-alumina/γ-alumina membrane can be regarded as a series of two transport resistances in series. The overall membrane permeability coefficient k_m can be therefore be deconvoluted into the permeabilities of the individual layers according to (6)

$$1/k_m = 1/k_\alpha + 1/k_\gamma, \qquad [3]$$

where k_α and k_γ are the permeability coefficients of the α-alumina support (k_α = $1.17 \cdot 10^{-14}$ m) and the mesoporous γ-alumina top layer, respectively. Table 2 summarizes the k_γ values of different γ-alumina top layers for different liquids.

Table 2. Permeability coefficients k_γ of water-lean and water-rich organic liquids through mesoporous γ-alumina membrane, calculated from Eq. (3).

Solvent	Permeability coefficient k_γ (10^{-14} m)		
	γ-800	γ-600	γ-450
Water-rich hexane	3.1 ± 0.22	0.30 ± 0.063	0.13 ± 0.011
Water-rich toluene	3.1 ± 0.26	0.66 ± 0.13	0.19 ± 0.034
Water-lean hexane	3.1 ± 0.29	1.32 ± 0.15	0.54 ± 0.059
Water-lean toluene	3.1 ± 0.15	1.32 ± 0.085	0.54 ± 0.044

The permeabilities of water-lean toluene and hexane in all three membranes appear to follow Darcy's law, i.e., the permeability coefficients are independent of the nature of the solvent. With these k_γ values and the values of pore size and porosity as presented in Table 1, the effective τ values of the mesoporous top layers were calculated from Eq. (2). Table 3 lists these τ values. The tortuosities of the γ-800 and γ-600 membranes fall in the range of tortuosities of 5–13 reported in literature for γ-800 (15), while a slightly larger τ value is found for γ-450. It is known that the crystallite shape of the primary oxide particles is one of the main parameters that control the tortuosity τ of a porous material (15). For spherical particles τ has a value close to 5, but for platelet-shaped crystallites its value will be larger. Since the morphology of γ-alumina crystallites changes from platelet-like into spherical with increasing calcination temperature (15), the τ-values listed in Table 3 reflect the change of crystallite shape with increasing calcination temperature (15).

Table 3. Tortuosities of mesoporous top layers calculated from Eq. (2).

Mesoporous top layer	Tortuosity τ
γ-800	6.4 ± 1.2
γ-600	8.2 ± 1.6
γ-450	16 ± 1.8

According to the data in Figure 4 and Table 2, the permeability coefficients appear to depend on the nature of the permeating liquid when the pore size is smaller than in γ–800 and water-rich hydrocarbons are employed. Moreover, the permeabilities of the water-rich hydrocarbons are substantially smaller than those of the corresponding water-lean equivalents, while the transport of water-rich liquids through γ-600 and γ-450 also requires a non-zero threshold pressure to be exceeded before net transport occurs. These phenomena are in disagreement with Darcy's law. The threshold pressures of the different liquids through γ-450 and γ-600 membranes, calculated from the intercepts of the extrapolated flux versus pressure plots, are listed in Table 4.

Table 4. Threshold pressure for water-rich solvent transport through mesoporous alumina membrane.

Solvent	Threshold pressure (bar)	
	γ-600	γ-450
Water-rich hexane	0.86 ± 0.34	1.36 ± 0.20
Water-rich toluene	0.85 ± 0.37	1.34 ± 0.28

A number of factors may possibly contribute to these effects and they should be considered in order to interpret the permeability differences between different solvent-membrane combinations. The first factor to consider is the extent to which the use of bulk liquid viscosities in Eq. (1) is still allowed. It has been reported that the density and viscosity of *non*-hydrogen bonded liquids that are confined between two smooth surfaces can be strongly influenced by the close presence of these surfaces (16,17). However, the roughness of the internal γ-alumina membrane surfaces that are considered in the present study will probably smear out the solvation forces (18) that are responsible for the density gradient in a liquid in narrow confinement (16). This suggests that mostly Van der Waals type of interactions occur between liquid molecules and pore wall, and that the liquid viscosities in these 4-7 nm wide pores will therefore be similar to the viscosities of the corresponding bulk liquids.

The second factor is the possibility of phase separation of water from hydrocarbon-water binary liquids. This process can be regarded as a conventional capillary condensation process occurring in systems of poorly miscible liquids, and was described experimentally by Christenson (18-21), and theoretically by Evans (22). A phase-separated water phase may form capillary water bridges in narrow pores, effectively leading to complete blocking of these pores for transport (19). In thermodynamic equilibrium phase separation and subsequent capillary condensation of the water phase in a pore with an effective Kelvin radius r_K will occur spontaneously when

$$r_K < \frac{-\gamma_{sw} V_m}{RT \ln(x_w \chi_w)}, \qquad [4]$$

where x_w and χ_w are the molar fraction of water and the activity coefficient of water in the solvent, respectively, γ_{sw} is the surface tension between water and hydrocarbon, V_m is the molar volume of water, and R and T are the gas constant and temperature, respectively. The surface tensions γ_{sw} of water-hexane and water-toluene can be estimated to be ~50 mN/m (23). For very dilute solutions the product $x_w\chi_w$ can be replaced by the ratio of water concentration c_w and saturation concentration c_w^0 (20). Since the solubility limit of water in toluene and hexane are ~0.015 mol/l and ~0.0067 mol/l (24), respectively, the relative activities $x_w\chi_w$ of water in toluene and in hexane are ~0.35 and ~0.9, respectively. Hence, the critical pore sizes at which capillary condensation will occur in thermodynamic equilibrium fall in the 1-10 nm range, and the critical pore size is substantially larger for hexane than for toluene. It is noted that the critical pore size may be different from the predictions of Eq. (4) under non-equilibrium transport conditions.

Pores that are wider than the critical size predicted by Eq. (4) will not become completely filled with water, but their effective pore radius (for hydrocarbon transport) may be reduced due to the formation of an annulus water phase that is adsorbed on the pore walls. This phenomenon is more or less similar to the well-known t-layer adsorption of condensable gases on surfaces (25). In the present case, the formation of a water film will be driven by hydrogen bonding-type interactions between water and the OH-functional γ-alumina pore walls, which are energetically more favorable than the Van der Waals-type interactions between hydrocarbon and pore wall.

The physical significance of water bridge formation on hydrocarbon liquid transport is that it decreases the effective porosity ε of the membrane medium. But more importantly, it also increases the effective tortuosity τ of the membrane medium, because several transport paths become blocked for hydrocarbon transport, and alternative (longer) paths have to be taken by the liquid. Hence, the reduction of permeability of water-rich liquids in γ-600 and γ-450 membranes can be understood in terms of a collective effect of porosity and tortuosity changes. The ratio ε/τ in Eq. (2) decreases in the presence of water, and therefore the permeability coefficient of water-containing liquids is smaller. This effect is most pronounced in the γ-450 membrane, which has the largest fraction of small pores.

Due to the higher solubility of water in toluene, the critical pore size r_K for phase separation is larger in the water-hexane system. The fraction of pores that is blocked by water will therefore be smaller when toluene is used than when hexane is used. This could explain why the permeability differences between water-lean and water-rich hydrocarbons are larger in the γ-450 membrane than in the γ-600 membrane, and why toluene is transported more easily than hexane. Since no substantial differences were observed between the permeabilities of water-lean and water-rich hydrocarbons in the γ-800 membrane, it seems that the pores in that membrane are wide enough to prevent spontaneous capillary condensation of water.

As was shown in Figure 4 and Table 4, water-rich hexane and toluene both need a certain threshold pressure to be exceeded before liquid flow through the membrane commences. This phenomenon may be understood by considering the occurrence of two different types of flow under the experimental conditions, namely spontaneous imbibition (displacement of a less wetting fluid by a more wetting fluid) and pressure-driven drainage (displacement of a more wetting fluid by a less wetting fluid) (26). These two competitive processes make the permeation process complicated to describe. The threshold pressure is most likely required to open up some of the water-blocked membrane pores by drainage working against the capillary pressure (or Laplace pressure) of the condensed water phase inside the largest blocked membrane pores (27). Under completely water-free conditions, the flux versus pressure plot should follow Darcy's law once the pores have opened. However, since we are dealing with water-rich hydrocarbon feeds, spontaneous re-condensation of water (21) may occur as soon as a sufficiently large volume of water-rich hydrocarbon has entered and passed the membrane pores. This would ultimately lead to pore blocking again if no sufficient pressure is applied to keep these pores open.

The spreading coefficients of toluene and hexane on water should also be considered in this discussion. Although the alumina surface is a high-energy surface on which any type of liquid can spread spontaneously, it is reasonable to assume that at least a very thin layer of physisorbed water has formed on the inner and outer alumina surface, over which the hydrocarbon liquid has to pass in order to be transported. It has been found that the equilibrium-spreading coefficient of toluene on water is zero, whereas the same coefficient for hexane is negative (-0.5) (28). A value of zero is a sufficient condition for spontaneous spreading, but a negative value suggests that only partial wetting will occur. It is therefore possible that full wetting of the membrane pores by hydrocarbons, and net hydrocarbon transport will occur only when a certain minimum pressure is applied on the liquid.

Figure 6 illustrates how the liquid fluxes tend to decrease slowly with time for both water-lean and water-rich hexane. The decline of permeability of the water-rich liquid seems to occur slightly faster than with the water-lean liquid. The permeability decrease of both liquids may be attributed at least partly to ongoing capillary condensation of water from the hydrocarbon feeds that are constantly being supplied during the experiment. As the amount of water that is supplied per

unit time is small, the blocking of pores that are small enough for capillary condensation may continue for a considerable period of time during which the permeability decreases gradually. This explanation may also hold for the water-lean system as it also does contain some water (<0.001 mol/l).

Alternatively, it is also possible that the gradual flux decrease is somehow related to phenomena occurring in the hydrocarbon phase. It has been reported (8)that solvent molecules may become strongly adsorbed and immobilized on γ-alumina surfaces during organic liquid transport. Such an adsorption process would lead to a gradual reduction of the effective pore size available for transport, and thereby to a reduction of solvent permeability. In the case that traces of water are also present, phase separation of water and adsorption of organic molecules may work synergistically in reducing the permeability with time.

5. Conclusions

We have shown that the permeability of liquids is affected by the membrane pore size and the water content of organic liquids. A very low molar fraction (~$5 \cdot 10^{-4}$) of dissolved water in hydrophobic solvents was shown to decrease the permeability of toluene and hexane through γ-alumina membranes with pore diameters < 6 nm considerably. This effect was explained by the occurrence of phase separation and capillary condensation of water from the hydrocarbon phase, which leads to pore blocking of small pores. The presence of water as a trace component was also shown to lead to phenomena like a non-zero cutoff pressure for liquid flow, which was not observed with water-lean solvents. Water-lean hexane and toluene had similar permeability coefficients for a given membrane, but different permeabilities were observed when water was present. In the latter cases the less polar solvent hexane exhibited a lower permeability than toluene. This is probably related to the higher relative activity of water in hexane than in toluene, which leads to blocking of larger pores, and possibly to more physisorption of water on non-blocked pore walls.

References

1. D.R. Machado, D. Hasson and R. Semiat, Effect of solvent properties on permeate flow through nanofiltration membranes. Part I: investigation of parameters affecting solvent flux, *J. Membrane Sci.*, **163** (1999) 93.
2. X.J. Yang, A.J. Livingston and L. Freitas dos Santos, Experimental observations ofnanofiltration with organic solvents, *J. Membrane Sci.*, **190** (2001) 45.
3. D.R. Machado, D. Hasson, R. Semiat, Effect of solvent properties on permeate flow through nanofiltration membranes, *J. Membrane Sci.*, **166** (2000) 63.
4. D. Banushali, S. Kloos, C. Kurth, D. Bhattacharyya, Performance of solvent-resistant membranes for non-aqueous systems: solvent permeation results and modeling, *J. Membrane Sci.* , **189** (2001) 1.
5. T. Tsuru, T. Sudou S. Kawahara T. Yoshioka and M. Asaeda, Permeation of liquids through inorganic nanofiltration membranes, *J. Colloid Interf. Sci.*, **228** (2000) 292.
6. S. Roy Chowdhury, R. Schmuhl, K. Keizer., J. E. ten Elshof and D. H. A. Blank "Pore size and surface chemistry effects on the transport of hydrophobic and hydrophilic solvents through mesoporous g-alumina and silica MCM-48", *J. Membrane Sci.*, **225** (2003) 177.
7. T.G. Knudstrup, I.A. Bitsanis, G.B. Westermannclark,"Pressure driven flow experiments in molecularly narrow straight pores of molecular dimension in mica" *Langmuir*, **11** (1995) 893.
8. J. Font, R.P. Castro, Y. Cohen, "On the loss of hydraulic permeability in ceramic membranes" *J. Colloid Interf. Sci*, **181** (1996) 347.
9. Tsuru T, Miyawaki M, Kondo H, Yoshioka T, Asaeda M, "Inorganic porous membranes for nanofiltration of nonaqueous solutions" *Separation and purification technology*, **32** (2003) 105.
10. S. Sarrade, G.M. Rios and M. Carles, Nanofiltration membrane behavior in a supercritical medium, *J. Membrane Sci.*, **114** (1996) 81.
11. T. Van Gestel, B. Van der Bruggen, A. Buekenhoudt, C. Dotremont, J. Luyten, R. Leysen, C. Vandecasteele, G. Maes, Surface modification of □-Al_2O_3/TiO_2 multilayer membranes for applications in non-polar organic solvents, *J. Membrane Sci.,* **224** (2003) 3.
12. C. Guizard, A. Ayral, A. Julbe, Potentiality of organic solvents filtration with ceramic membranes. A comparison with polymer membranes, *Desalination*, **147** (2002) 275.
13. M.J. Gieselmann, Permeabilities of unsupported ceramic membranes of alumina, *Langmuir* **1992**, *8*, 1342.
14. M. Mulder, "Basic principles of membrane technology", Kluwer Academic Press, Dodrecht, The Netherlands (1996)
15. A.F.M. Leenaars, A.J. Burggraaf, The preparation and characterization of alumina membranes with ultra-fine pores. Part 3. The permeability for pure liquids, *J. Membr. Sci.*, **24** (1985) 245.

16. H.K. Christenson, Interaction between hydrocarbon surfaces in a nonpolar liquid effect of surface properties on solvation forces, *J. Phys. Chem.*,**90** (1986) 4.
17. S. Granick, Motions and relaxations of confined liquids, *Science,* **253** (1991) 1374.
18. H.K. Christenson, R.G. Horn, J.N. Israelachvili, Measurement of forces due to structure in hydrocarbon liquids, *J. Colloid Interf. Sci.*, **88** (1982) 79.
19. H.K. Christenson, C.E. Blom, Solvation forces and phase separation of water in thin film of nonpolar liquids between mica surfaces, *J. Chem. Phys.*, **86** (1987) 419.
20. H.K. Christenson, Capillary condensation in systems of immisible liquids, *J. Colloid Interf. Sci*, **104** (1985) 234.
21. H.K. Christenson, J, Fang, J.N. Israelachvili, Experimental-study of phase-separation in films of molecular dimensions, *Physical Rev. B,* **39**, (1989) 11750.
22. R. Evans and U. M. B. Marconi, Phase equilibra and solvation forces for fluids confined between parallel walls, *J. Chem. Phys.,* **86** (1987) 7138
23. F.M. Fowkes, Attractive forces at interfaces, *Ind. Eng. Chem.* **1964**, *56*, 40.
24. J.A.Riddik, E.E. Toops Jr. *Organic Solvents, Physical properties and methods of purification.* Interscience Publishers, Inc.; New York, USA, 1955, Chapter III.
25. B.C Lippens, B.G. Linsen, J.H. De Boer, Studies on pore systems in catalysts .1. the adsorption of nitrogen - apparatus and calculation *J. Catal.* **1964**, *3*, 32.
26. M. Hashemi, B. Dabir, M. Sahimi, Dynamics of two-phase flow in porous media: Simultaneous invasion of two fluids, *AIChE J.*, **45** (1999) 1365.
27. P.Schneider, P. Uchytil, Liquid expulsion permporometry for characterization of porous membranes, *Membrane Sci.* **1994**, *95*, 29.
28. H. Dobbs, D.Bonn, Predicting wetting behaviour from initial spreading coefficient, *Langmuir*, **17** (2001) 4674.

Chapter 6

Recycling of a sandwich type polyoxometalate oxidation catalyst using solvent resistant nanofiltration

If at first you don't succeed, redefine success

Abstract*

In this chapter the preparation of homogeneous polyoxometalate (POM) catalyst for the conversion of cyclooctene to cyclooctene oxide is described. The recycling of this homogeneous catalyst from aqueous and organic solution using γ-alumina membranes is also reported. It has been found that the catalyst retention through this membrane is almost quantitative. The catalytic activity of toluene-soluble POM increases with the number of recycling step through the membrane. This observation can be attributed to the partial removal of some catalyst precursors, which have a negative influence on the reaction. The water-soluble catalyst solution behaves as a Darcy type fluid and has almost the same permeability as pure water. The organic soluble catalyst solution deviates from Darcy's law. This behaviour can be explained by a combination of concentration polarization of POM, leading to high viscosity near the membrane surface, and/or capillary condensation of dissolved water inside the membrane pores from toluene.

* Part of this chapter has been published in *Chemical Communications* (2005) 1206.

1. Introduction

Catalyst recycling is often indispensable in order to arrive at economically acceptable catalyst costs per product unit. In the area of homogeneous catalyst recycling, much attention has been paid to catalyst immobilization, arriving at either heterogeneous (1) or enlarged homogeneous (2) catalysts. However, this method is not attractive since additional synthetic steps are required to obtain these modified catalysts, which usually display other catalytic properties compared to their homogeneous analogues. Nanofiltration allows for the recycling of non-enlarged homogeneous catalysts, but often low retentions are obtained (2,3-6). Polyoxometalate (POM) catalysts have all features necessary for successful recycling by nanofiltration; they are large, they have a rigid structure (7), which is charged (8), and the lack of organic ligands makes them stable towards many different reaction conditions (9).

In this chapter the preparation of a water soluble sodium salt of a polyoxometalate (POM) catalyst will be described and will be shown how this sodium salt of POM has been made soluble in organic solvents like toluene by exchange of Na^+ ions with $[MeN(n\text{-}C_8H_{17})]^+$ moieties. It will also be demonstrate that how an inorganic, "sandwich" type polyoxometalate oxidation catalyst can be recycled very efficiently with near-quantitative retentions using nanofiltration. The recycling of a "sandwich" type polyoxometalate catalyst in a model alkene epoxidation with aqueous hydrogen peroxide will be demonstrated. The successful recycling (6 runs) without loss of activity confirms the high stability of the "sandwich" type polyoxometalate catalyst towards strongly oxidizing conditions.

2. Experimental

2.1 Membrane preparation and structural analysis

γ-Alumina membranes calcined at 600°C (further denoted as γ-600) or at 900°C (denoted as γ-900) were prepared and analysed according to the procedures described in chapters 4 and 5. The average pore diameters of these two membranes are ~ 4.4 nm and ~8 nm, respectively.

2.2 Catalyst generation

Aqueous $Na_{12}POM$ was prepared in near-quantitative yield via self-assembly according to (10,11,12)

$$19\ Na_2WO_4 + 5\ ZnCl_2 + 16\ HCl = Na_{12}[WZn_3(ZnW_9O_{34})_2] + 26\ NaCl + 8\ H_2O.$$

$Na_2WO_4{\cdot}2H_2O$ (62.5 g, 0.19 mol) was dissolved in water (175 mL) at 85°C. At this temperature, aqueous 37 % HCl (13.3 mL, 0.16 mol) was added. The yellow solid that was formed dissolved almost immediately, and the reaction mixture was heated to 95°C. A solution of $ZnCl_2$ (6.81 g, 50 mmol) in water (75 mL) was added dropwise in 4 h to the well-stirred solution. This turbid solution was divided into two parts. One part was used for generation of pure water-soluble POM catalyst

(sodium salt of POM, $Na_{12}POM$) and the other part was used to generate toluene soluble POM catalyst.

Toluene solutions of $Q_{12}POM$ ($Q=MeNOc_3^+$) ($Oc = C_8H_{17}$) were prepared by addition of QCl (Aliquat 336) to aqueous $Na_{12}POM$. $[MeNOc_3]Cl$ (Aliquat 336) (40 g, 0.10 mol) was added in toluene, and the mixture was stirred for 6 h. The layers were separated and the aqueous layer was washed with pure toluene. The combined toluene layers were dried on Na_2SO_4 and the Zn-content was measured by ICP-AES. A POM-concentration of 6.4 mM $Q_{12}POM$ in toluene was calculated.

Elemental analysis of the toluene solution showed that 60% of the POM^{12-} anions present in the aqueous layer were extracted into toluene by addition of 12 equivalents QCl; i.e., the $Q_{12}POM$ toluene solution contains an excess of QCl relative to the POM.

2.3 Epoxidation

5 mL 6.4 mM $Q_{12}POM$ in toluene (32 μmol), 10 mL toluene, 0.5 mL dodecane (internal standard) and 2.6 mL cyclooctene (20 mmol) were mixed and heated to 60°C. 1.5 mL 50% H_2O_2 in H_2O (27 mmol) was added in 5 portions during a 2 h period (300 μL per half hour) and the biphasic mixture was stirred at 60°C. After 5 h the stirring was stopped, the mixture was cooled to room temperature and the water layer was removed.

2.4 Nanofiltration

Dead-end nanofiltration experiments were performed in a cell equipped with an α-alumina supported mesoporous γ-600 membrane. Both water-soluble and organic-soluble POM catalysts were recycled. A α-alumina supported mesoporous γ-900 membrane was also used for recovery of toluene soluble $Q_{12}POM$ catalyst. The retention of a given membrane is charactersed by the retention coefficient which is defined by $R_{obs} = 1- C_p/C_b$, with C_p the solute concentration in the permeate and C_b the solute concentration in the bulk of the feed.

For nanofiltration experiments with water-soluble POM, 10 mmol of pure and isolated $Na_{12}POM$ was dissolved in a liter of deionized water to make the stock solution. 50 ml of feed solution was used as feed and ~ 8mL of the permeate solution was collected. Permeation experiments were carried out over a range of 3-12 bar applied pressure.

We also carried out nanofiltration experiments with water soluble POM in the presence of 4M NaCl to obtain a solution with very high ionic strength.

For nanofiltration experiments with the epoxidation reaction mixture, the nanofiltration cell was charged with the organic layer separated after the epoxidation reaction and pressurized. This feed mixture will further be referred to as CM liquid. After ~15 mL of permeate solution was collected, the cell was depressurized, which stopped the permeation process. The retentate (~1 mL) plus 4 mL extra toluene was used for a subsequent epoxidation, instead of fresh 5 mL $Q_{12}POM$ stock solution.

The level of retention of Aliquat 336 in toluene-d8 (deuterated toluene) through a γ-600 membrane was also determined. The concentration of Aliquat 336 in the permeate was determined by a Bruker DRX 500 spectrometer.

2.5 GC-analysis

GC samples (30 μL of the organic layer in 0.6 mL toluene) were taken at t = 0, 2, 3, 5 hours. GC spectra were measured on a HP6890 spectrometer, using a cross-linked 5% PH ME siloxane column. Conversions of run 2-6 were corrected for residual cyclooctene oxide in the retentates.

2.6 Catalyst analysis:

Catalyst concentrations were calculated from the Zn-content, measured by ICP-AES techniques after acidic destruction of the catalyst. Measurements of stock solutions of Na_2WO_4 and $Zn(NO_3)_2$ in H_2O proved inaccurate in W-content (+/- 20%), but accurate in Zn-content. ICP-AES measurements were performed on a Perkin Elmer Optima 3000, using a rhodium standard.

2.7 XPS measurements

X-ray Photoelectron Spectroscopy (PHI Quantera Scanning ESCA Microprobe, USA) on the membrane after the use for POM recovery with Ar^+ sputtering was carried out to identify the atomic concentrations of O, Al, Zn, and W by measuring the O *1s*, Al *2p*, Zn *2p*, and W *4f* spectra as a function of depth inside the layer at a sputter rate of 17.9 nm/min.

3. Results and discussion:

3.1 Retention of POM catalyst:

Figure 1 shows the percentage of retention of POM molecules from different solutions. Toluene soluble Q_{12}POM was retained nearly quantitatively (>99.9%) by a γ-600 membrane. Pure water-soluble Na_{12}POM has ~97% retention by the same membrane. This figure also includes the retention level of ~ 93% of toluene soluble POM through a γ-900 membrane and the retention level of water soluble pure Na_{12}POM in presence of 4M NaCl through γ-600 membrane (~90%).

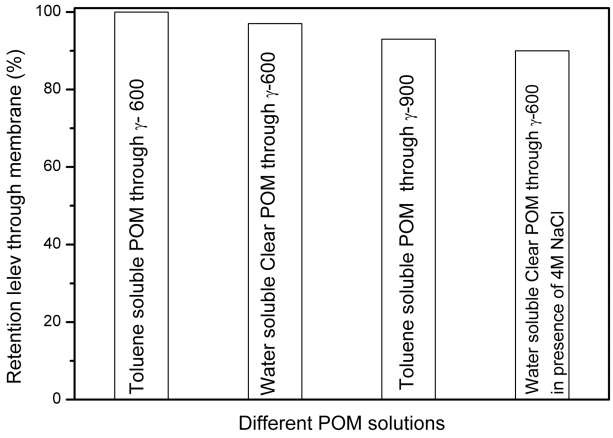

Figure 1. Percentage retention of different POM solutions through different γ-alumina membranes.

Figure 2 shows the results of XPS depth profiling measurements on a γ-600 membrane after repeated nanofiltration experiments with CM liquids. The results indicate that the catalyst did not enter the pores of the membrane substantially. Only very low atomic concentrations of W and Zn of 0.6 at% and 0.3 at%, respectively, were observed. If we consider the specific surface area of γ-600 to be 285 m^2/g (16) and W and Zn to be residing on the internal pore surface, the surface concentrations of W and Zn atoms per nm^2 internal pore area are 0.6 nm^{-2} and 0.3 nm^{-2}, respectively. Since one POM molecule contains 19 W atoms and 5 Zn atoms, a W/Zn ratio of 3.8 would be expected if POM were the only molecular species present inside the membrane pores. The experimentally observed W/Zn ratio of ~2 can be rationalized if we assume that chemical species other than POM are also present. These species could be the starting compounds like Na_2WO_4 or $ZnCl_2$ or derivatives thereof. In view of the large size of the POM anion, its complete retention within experimental error, and the fact that W atoms in $[WZn_3(ZnW_9O_{34})_2]^{12-}$ are present in two oxidation states, while XPS detected W in the layer in only one oxidation state, it is unlikely that POM is present at all.

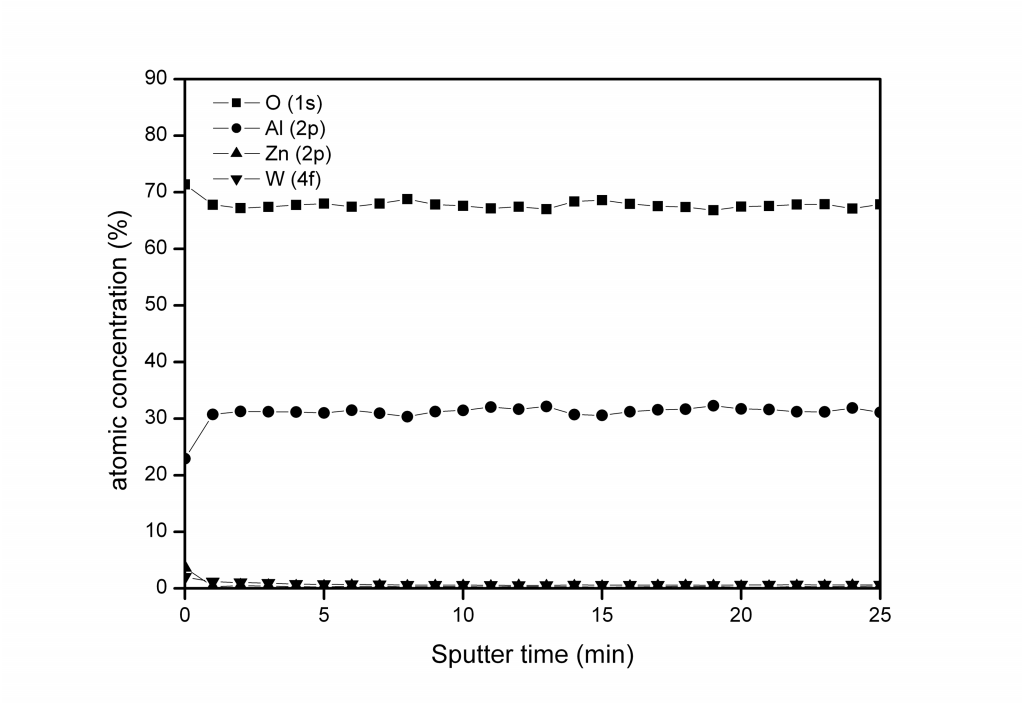

Figure 2. XPS depth profile of a γ-600 membrane after retention experiments with CM liquids containing Q_{12}POM.

Since the POM catalyst was used as an *in situ* prepared mixture, it is well possible that small amounts of unreacted Zn- and W-containing starting materials were still present in the CM feed, and adsorbed on γ-alumina. Although no retention measurements were performed on the starting compounds, it is expected that these much smaller molecules will pass through the membrane more easily than the large POM.

The retention behaviour of POM ions can be predicted qualitatively by the electrical double layer theory. This theory says that as the electrolyte strength increases the double layer thickness decreases. The thickness of the diffuse double layer can be estimated from the Debye screening length κ^{-1} (13)

$$\kappa^{-1} = \sqrt{\frac{\varepsilon_0 \varepsilon_r k_B T}{e^2 \sum_i z_i^2 n_i^0}}, \qquad [1]$$

where n_i^0 the number density of ionic species i in the bulk of the electrolyte solution, and $\frac{1}{2}\sum z_i^2 n_i^0$ is the electrolyte strength (13). ε_0 and ε_r are the dielectric constant of vacuum and the relative dielectric constant of the liquid medium, respectively, k_B is the Boltzman constant, T is the absolute temperature and e is the elementary electron charge. The double layer thickness is not constant but decreases with electrolyte strength and increases with surface charge density (13), i.e., with species having different degrees of ionization, the double layer thickness will vary according to the number of ions present in the solution, and the charge of these ions. When $\kappa r_p < 1$, where r_p is the pore radius, the dimensions of narrow-sized pores approach the length of the double layers and double layer overlap

occurs from opposite sides of the pore. Under these conditions the channel becomes less permeable to ions with the same charge as the surface charge, thus making it a selective barrier for transport of either cationic or anionic species (14). Alternatively, under conditions at which $\kappa r_p > 1$, the double layer is confined to a small region near the channel wall, and the centre of the channel is electrically uncharged, i.e., the fluid in the center of the pore contains both anions and cations, the total amounts of positive and negative charge being the same. Under these conditions both cationic and anionic species can be transported through the centre of the channel.

For a 10 mM $Na_{12}POM$ solution in water ($\varepsilon_r = 80$) and a 6.4 mM solution of $Q_{12}POM$ in toluene ($\varepsilon_r \sim 2.4$), we estimated the thickness of the double layer. The double layer thicknesses for different degrees of ionization of the $Na_{12}POM$ or $Q_{12}POM$ molecule are shown in Table 1.

Table 1a. Electrical double layer thickness as a function of degree of $Na_{12}POM$ ionisation.

Degree of ionization (%)	Double layer thickness κ^{-1} (nm)
100 *(12 Na^+ + POM^{12-})*	0.35
50 *(6Na^+ + $[Na_6(POM)]^{6-}$)*	0.66
25 *(3Na^+ + $[Na_9\ (POM)]^{3-}$)*	1.24
16.6 (2Na^+ + $(Na_{10}\ (POM)^{-2}$)	*1.8*
8.3 *(Na^+ + $[Na_{11}\ (POM)]^{1-}$)*	*3*
100 *(12 Na^+ + POM^{12-})*+ 4M *NaCl*	0.14

Table 1b. Electrical double layer thickness as a function of degree of $Q_{12}POM$ ionisation

Degree of ionization (%)	Double layer thickness (nm)
50 *(6Q^+ + $[Q_6(POM)]^{6-}$)*	0.14
25 *(3Q^+ + $[Q_9\ (POM)]^{3-}$)*	0.27
8.3 *(Q^+ + $[Q_{11}\ (POM)]^{1-}$)*	0.66

From this table we can see that only at very low degree of of ionization of $Na_{12}POM$, the pores at the lower end of the pore size distribution (i.e. smaller than 3 nm) can be completely spanned by the electrical double layer. Sodium salts are usually highly dissociated in aqueous solutions, so a low degree of dissociation is unlikely for the water-soluble sodium salt of POM. In that case the POM retention is mainly

due to size exclusion. But when we carried out the experiment in the presence of 4M NaCl solutions, the retention level of POM dropped slightly (from 97% to 90%). In this case, due to presence of an extra electrolyte like NaCl, the double layer was collapsed almost completely in all types of pores present in the membrane. This may have favoured partially the transport of POM with lower degrees of dissociation through pores that would have been blocked otherwise. The experiment with an extra electrolyte shows that electrical charge exclusion plays a minor role in the POM retention mechanism.

For toluene soluble POM catalysts our molecular dynamics (MD) calculations showed that the POM molecules are present in the organic medium in associated form, i.e., POM anions and Q-ammonium ions form loosely bounds complexes of ~3 nm size in toluene. The hydrocarbon tails of the Q-ammonium ion have a favourable interaction with toluene molecules due to their organic character, and as the POM anion has a highly negative charge and inorganic (polar) character, the anion itself is unable to dissolve in toluene. It is thus expected that the POM anion will form the core, and the Q-ammonium cations form a shell layer, thus forming a large associated complex with the hydrophobic end groups of the Q-ammonium cation exposed to the surrounding toluene phase. The larger effective size of these associated POM molecules is essentially of the same size as the pores of the γ-600 membrane. In this case the catalyst molecules do not enter the membrane at all and this gives an even slightly higher retention level than Na_{12}POM in water. In the case of γ-900 membranes with an average pore size of ~8 nm, 93% retention was obtained. This drop of the retention value is probably due to the larger pore size of the membranes, which negatively affects the retention level.

3.2 Solvent permeability through the membranes

Figure 3 shows that the volumetric flux of CM liquid containing Q_{12}POM is considerably lower than that of pure toluene through γ-600 membrane at any given pressure. This may be caused by capillary condensation of water in the pores of the membrane, leading to partial pore blocking (15,16), and/or by the higher viscosity of the Q_{12}POM solution. In chapter 5 we saw that even a trace amount of water present in the organic liquid phase can affect the permeability behaviour through the membrane significantly. In the CM liquid, there may be additional water present in the reaction mixture that was formed due to the decomposition of H_2O_2. H_2O_2 has been used as an oxidizing agent in the epoxidation process. Since the solubility of water in pure toluene is limited, the gross water concentration in the reaction mixture could be well above the saturation level of toluene, and be present in the form of 2nd phase droplets emulsified by Q^+ ions. Although the Q_{12}POM concentration is too low to significantly influence the viscosity of the bulk solution, a local high concentration (concentration polarization) can occur at the membrane surface, leading to a strongly increased viscosity. This so-called cake formation is a problem that has often been observed in dead-end filtrations. For larger scale applications, it can easily be overcome by using a loop reactor. The permeability,

which is defined as the volumetric flux per unit of pressure difference, of the Q_{12}POM containing organic layer that was separated after the epoxidation reaction by a γ-900 membrane was higher than that of pure toluene through a γ-600 membrane. This can be explained by the larger pore diameter of γ-900 membranes, as it is known that the liquid permeability is proportional to the second power of the membrane pore radius.

Figure 3 shows that a minimum threshold pressure needs to be exceeded before pure toluene and the Q_{12}POM containing CM mixture starts permeating through the γ-600 membrane. The occurrence of a threshold pressure is explained in detail in Chapter 5 and may be explained as follows. Condensation of dissolved water from liquids with a limited solubility of water can occur when the liquid is confined to a narrow space. The thermodynamics of capillary condensation of water can be described using the modified Kelvin equation

$$r_K < \frac{-\gamma_{sw} V_m}{RT \ln(x_w \chi_w)} \qquad [2]$$

where x_w and χ_w are the molar fraction of water and the activity coefficient of water in the solvent, respectively, γ_{sw} is the surface tension between water and hydrocarbon, V_m is the molar volume of water, and R and T are the gas constant and temperature, respectively. Condensation occurs when Eq. (2) is satisfied, i.e., when the pore radius is below a certain critical diameter. The phase-separated water capillaries block individual pores for transport of the non-aqueous phase. A minimum threshold pressure for organic liquid transport through the ~3-6 nm pores of γ-600 membranes is thus required to open up some of the water-blocked membrane pores by drainage working against the capillary pressure (or Laplace pressure) of the condensed water phase inside the largest blocked membrane pores. Figure 3 allows us to give a very rough estimate of the cut off pressure for toluene (~ 0.7 bar) and the Q_{12}POM solution (~ 0.9 bar) when they are filtered by a γ-600 membrane.

In contrast, Q_{12}POM solution does not show any cut-off pressure when it is passing through a γ-900 membrane. This is in agreement with the results presented in Chapter 5 of this thesis, where it is shown that capillary condensation does not occur in γ-800 membranes, most likely because the pores are too wide for Eq. (2) to be satisfied.

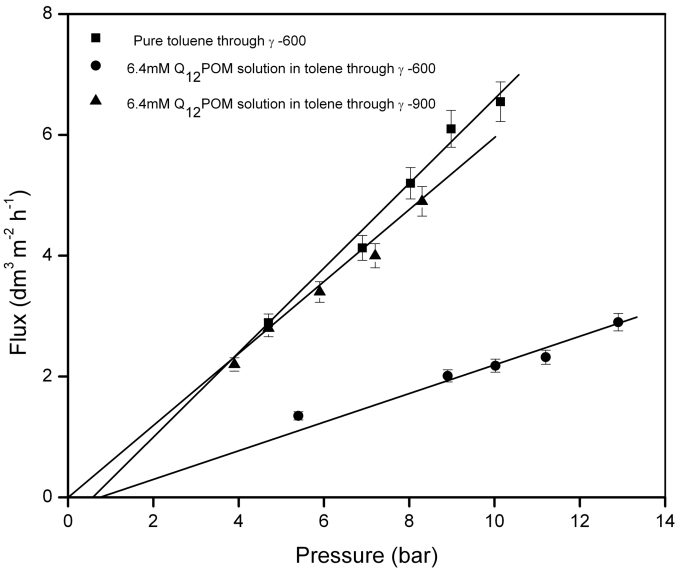

Figure 3. Volumetric flux versus applied pressure of pure toluene and a toluene solution of Q_{12}POM through γ-alumina membranes calcined at 600°C and 900°C.

Figure 4 shows the volumetric flux versus applied pressure for pure water and a POM solution through the membrane calcined at 600°C. In contrast to the results displayed in Figure 3, here we observe that pure water and the clear Na_{12}POM solution (water solution) have a very similar permeability through the membrane calcined at 600°C. This agrees with the fact that the viscosities of pure water and the Na_{12}POM solution in water are the same, and capillary condensation effects as observed in non-aqueous nanofiltration will not occur in water.

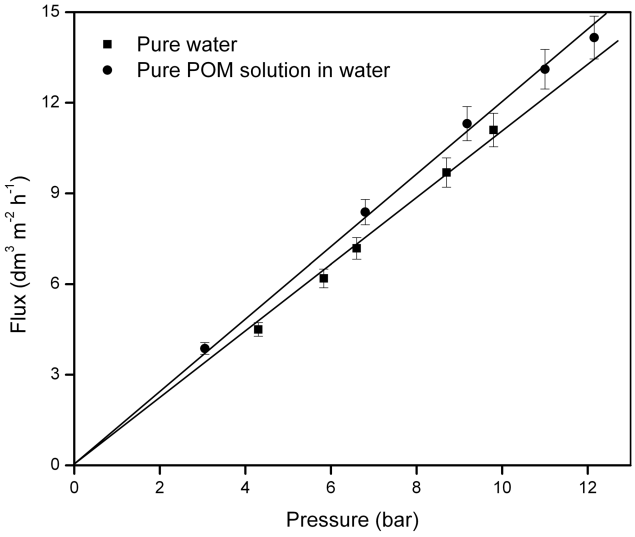

Figure 4. Volumetric flux versus applied pressure for pure water and Na_{12}POM solution in water through the membrane calcined at 600°C.

Table 2 presents the permeability of the different solvents and solutions through γ-600 and γ-900. It is noted that the γ-900 membrane could more interesting for industrial use if quantitative recovery of POM is not required. The membrane has a 3 times higher liquid permeability than γ-600 and a relatively high retention level of ~ 93% for Q_{12}POM.

Table 2: Permeability of different solvents and solutions through the γ-alumina membranes

Membrane	Solvent / solution	Permeability ($dm^3m^{-2}\,h^{-1}\,bar^{-1}$)
γ-600	Water	1.2 ± 0.02
γ-600	Na_{12}POM solution in water	1.1 ± 0.01
γ-600	Toluene	0.7 ± 0.05
γ-600	Q_{12} POM solution in toluene	0.2 ± 0.02
γ-900	Q_{12} POM solution in toluene	0.57 ± 0.01

3.3 Reuse of catalyst

For catalyst recycling, the epoxidation of cyclooctene as shown in the following scheme was investigated. This r eaction has the advantage that it forms one

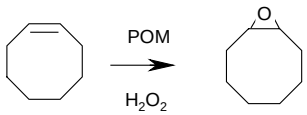

well-defined product, with little change of unwanted side-reactions like allylic oxidation or epoxide ring opening. In order to make an accurate comparison of the different reaction cycles, reaction conditions were chosen that did not lead to full conversion. Although cyclooctene can easily be epoxidized with 100% conversion and selectivity, the main issues dealing with nanofiltration of large anions will not be influenced by the choice of substrate or reaction conditions.

Figure 5 shows the results for the recycled Q_{12}POM in cyclooctene epoxidation after different numbers of recycles. Surprisingly, the activity of the catalyst increased after each round of recycling. This was most probably caused by removal of the small excess of Aliquat 336 from the *in situ* generated Q_{12}POM catalyst solution. Previously, it has been reported that an excess of QCl (Aliquat 336) has a negative effect on the epoxidation of cyclooctene (10). We also carried out the nanofiltration of QCl (Aliquat 336) dissolved in toluene-d8 separately using a γ-600 membrane. The retention of Aliquat 336 in toluene-d8 was found to be 65%, as determined by ^{1}H NMR.

Elemental analysis of the permeates, presented in Table 3, showed nearly quantitative catalyst retentions for every recycling step, except for recycle #3. The relatively high amount of Zn found in permeate #3 was probably caused by an impurity, since permeates #4 and #5 show again very high retentions with out any drop of catalyst activity in run 4 of the epoxidation reaction.

Table 3. Elemental analysis of the permeates after each run

	Amount permeate	Zn	W	Retention based on	
	g	mg/kg	mg/kg	Zn	W
Permeate 1	9.04	0.5	272	>99.9%	97.8%
Permeate 2	8.14	<0.2	133	>99.9%	99.0%
Permeate 3	10.75	13	685	98.6%	93.4%
Permeate 4	10.54	0.8	335	>99.9%	96.9%
Permeate 5	10.68	0.3	143	>99.9%	98.7%

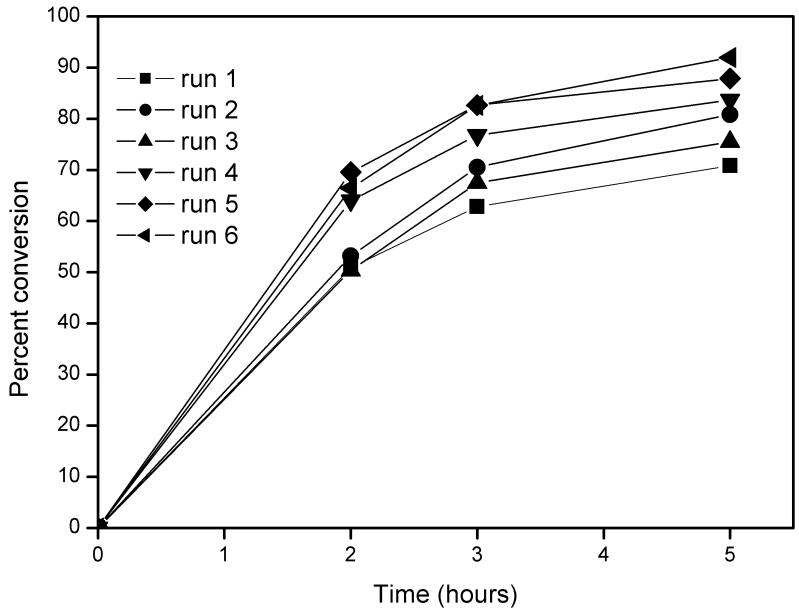

Figure 5. Q_{12}POM catalyzed epoxidation of cyclooctene after 0 – 5 recycles of the catalyst.

Analysis of the reaction mixture obtained after run #6 by ^{189}W NMR and IR spectroscopy showed that the POM moiety of the catalyst was still intact. The high stability of the large POM moiety is the key step to enable successful recycling. Decomposition of the POM into smaller W-based compounds would surely have lead to lower retentions.

4. Conclusions

In this chapter we discussed the recovery of an industrially important catalyst using two types of γ-alumina membranes. We carried out nanofiltration experiments on aqueous solutions of Na_{12}POM and an organic liquid mixture containing Q_{12}POM. The γ-alumina membrane calcined at 600ºC showed > 96% retention of POM ions, regardless of the nature of their counter ions and the nature of the solvent. γ-Alumina membranes calcined at 900ºC showed a lower level of retention for toluene soluble Q_{12}POM. The analysis shows that the retention of the catalyst is mainly due to size exclusion for both water-soluble Na_{12}POM and toluene-soluble Q_{12}POM. Liquid permeability studies showed that aqueous POM solutions obey Darcy flow behaviour, while a non-zero threshold pressure needs to be exceeded before (non-aqueous) hydrophobic liquid transport takes place. This threshold pressure was absent for γ-alumina membranes calcined at 900ºC, and this is most likely due to the larger pore size in the latter system. NMR and IR investigations on the final reaction mixture showed that the POM catalyst is stable under the used reaction and permeation conditions. XPS measurements together with experimental data showed that the POM did not enter the pores of the membrane, and thus it could be recovered easily. It has also been shown that the catalytic activity of the POM moiety increased with the number of membrane recycles, which was probably caused by removal of the excess of Aliquat 336 that was present in the catalyst stock solution.

References:

1. For a recent review, see: I. Tóth , P. van Geem, *Encyclopedia of Catalysis (on-line)*, Wiley Interscience, 2002.
2. For a recent review, see: H.P. Dijkstra, G.P.M. van Klink, G. van Koten, The use of ultra- and nanofiltration techniques in homogeneous catalyst recycling, *Acc. Chem. Res.*, **35**(2002) 798.
3. D. Nair, J.T. Scarpello, I.F.J. Vankelecom, L.M. Freitas dos Santos, L.S. White, R.J. Kloetzing, T. Welton, A.G. Livingston, Increased catalytic productivity for nanofiltration-coupled Heck reactions using highly stable catalyst systems, *Green Chem.*, **4** (2002) 319.
4. J.T. Scarpello, D. Nair, L.M. Freitas dos Santos, L.S. White, A.G. Livingston, The separation of homogeneous organometallic catalysts using solvent resistant nanofiltration, *J. Membr. Sci.*, **203** (2002) 71.
5. D. Nair, S. Singh Luthra, J.T. Scarpello, L.S. White, L.M. Freitas dos Santos, A.G. Livingston, Homogeneous catalyst separation and re-use through nanofiltration of organic solvents, *Desalination*, **147** (2002) 301.
6. K. de Smet, S. Aerts, E. Ceulemans, I.F.J. Vankelcom, P.A. Jacobs, Nanofiltration-coupled catalysis to combine the advantages of homogeneous and heterogeneous catalysis , *Chem. Comm.*, (2001) 597.
7. H.P. Dijkstra, C.A. Kruithof, N. Ronde, R. van de Coevering, D.J. Ramón, D. Vogt, G.P.M. van Klink, G. van Koten, Shape-persistent nanosize organometallic complexes: Synthesis and application in a nanofiltration membrane reactor, *J. Org. Chem.*, **68** (2003) 675.
8. W.B.S. de Lint, *Transport of electrolytes through ceramic nanofiltration membranes*, PhD thesis, University of Twente, (2003).
9. W. Adam, P.L. Alsters, R. Neumann, C.R. Saha-Möller, D. Sloboda-Rozner, R. Zhang, A highly chemoselective, diastereoselective, and regioselective epoxidation of chiral allylic alcohols with hydrogen peroxide, catalyzed by sandwich-type polyoxometalates: Enhancement of reactivity and control of selectivity by the hydroxy group through metal-alcoholate bonding, *J. Org. Chem.*, **68** (2003) 1721.
10. P.T. Witte, P.L. Alsters, W. Jary, R. Müllner, P. Pöchlauer, D. Sloboda-Rozner, R. Neumann, Self-Assembled $Na_{12}[WZn_3(ZnW_9O_{34})_2]$ as an Industrially Attractive Multi-Purpose Catalyst for Oxidations with Aqueous Hydrogen Peroxide , *Org. Proc. Res. Dev.*, **8** (2004) 524.
11. D. Sloboda-Rozner, P.T. Witte, P.L. Alsters, R. Neumann, Aqueous biphasic oxidation: A water-soluble polyoxometalate catalyst for selective oxidation of various functional groups with hydrogen peroxide, *Adv. Synth. Cat.*, **346** (2004) 339.

12. D. Sloboda-Rozner, P.L. Alsters, R. Neumann, A water-soluble and "Self-Assembled" polyoxometalate as a recyclable catalyst for oxidation of alcohols in water with hydrogen peroxide, *J. Am. Chem. Soc.*, **125** (2003) 5280.

13. R.J. Hunter, Foundations of Modern Colloid Science, 2nd ed.; Oxford University Press, Oxford (2001).

14. M. Mulder, Basic Principles of Membrane Technology, 2nd ed.; Kluwer, Dordrecht (1996).

15. H.K. Christenson, Capillary condensation in systems of immiscible liquids, J. *Colloid Interf. Sci.*, **104** (1985) 234.

16. S. Roy Chowdhury, K. Keizer, J.E. ten Elshof, D.H.A. Blank, Effect of trace amounts of water on organic solvent transport through gamma-alumina membranes with varying pore sizes, *Langmuir*, **20** (2004) 4548.

Chapter 7
Discussion and Recommendations

Take my advice, I don't use it anyway

In this chapter I will discuss the research results presented in chapters 1-6 from a broader scientific point of view. The main theme of this thesis is how to use porous materials successfully in fluid separation technology. During the study, several interesting things have been explored, which are broadly associated with colloid science, surface science and fluid mechanics. I will elaborate on these features in the rest of this chapter.

Fluid flow through porous media receives considerable attention in this thesis (Chapter 3-6). In these chapters fluid flow through porous media has been described in a very simple manner with Darcy's law. It has been found that the behaviour of all liquids (hydrophilic or hydrophobic) except water deviates from Darcy's law below some critical average diameter of the porous medium. The critical pore diameter is not the same for each and every liquid. To understand this behaviour we took into account two structural factors, namely porosity and tortuosity of the porous medium, which can affect the permeability of the liquids, and a physical parameter, namely the viscosity of the liquids. In chapter 4 it is discussed that for short chain alcohols one may expect an increase of alcohol viscosity below a pore diameter of 4 nm. This viscosity increase is possible through ordering of alcohols via hydrogen bonding with the pore surface, as well as through bilayer formation between alcohol molecules. However, this cannot the case for hydrophobic liquids (chapter 5), as they cannot interact with pore surfaces via hydrogen bonding. Their viscosity in narrow pores is expected to increase only by ordered layer formation on the pore surface. However, as the pore surfaces are not atomically flat on microscopic level, it is unlikely that an ordered packing of hydrophobic molecules, leading to an increase in viscosity, will occur. Therefore we see that there may be a fundamental difference between the transport mechanism of hydrophilic liquids and hydrophobic liquids when they are passing through a hydrophilic mesoporous medium.

When I investigated membrane permeability during the permeation process, I found that the presence of water as a secondary minority species in the liquid can play an important role. It is known that for a given binary fluid mixture (completely miscible or partially miscible) confined in a narrow space, preferential adsorption of one species on the surface may lead to phase separation (1). Phase separated water (or capillary condensate) may locally block the transport path of the non-aqueous liquids, leading to lowering of the porosity of the medium. This pore blockage also leads to a longer average travel path for the transporting liquids (higher effective tortuosity). Capillary condensation of water inside the narrow pore will thus have a negative influence on the liquid permeability. Obviously, this is a hypothesis, but it can be verified in various ways as I did by varying the water content in the liquid. Another effective verification could be carrying out liquid permeability tests at different temperatures. As the temperature of the system is increased, the solubility of water in the liquid will increase. Under such conditions capillary condensation of water inside the narrow pores will be less probable. This phenomenon should lead to less blocking of the transport paths for the permeating liquid. We also should

take into account that an increase of temperature leads to a reduction of liquid viscosity. So, the permeability increase will not only be due to less pore blocking by water, but also to reduction of viscosity in accordance with Darcy's law. I did not carry out any temperature programmed permeation experiments because of experimental limitations. But there is a report, which describes that at higher temperatures the hydrophobic solvent permeability in porous media increases (2). This is in line with what we expect but does not validate my hypothesis. However, the hypothesis can be validated by the statement in the same article that "solvent permeability for the unmodified membranes (i.e. hydrophilic membrane) increased drastically with temperature, especially in the case of high concentrations of water". This experiment was carried out with a silica-zirconia membrane with an average pore diameter of ~3.5 nm. This also suggests capillary condensation of water from another liquid; inside narrow pores it presumably does not depend on the chemical composition of the porous medium. It only depends upon hydrophilic/hydrophobic nature of the porous medium. In general capillary condensation of water is a very common phenomenon that is observed in sand dunes (3), and in precipitation of colloidal particles in the presence of trace amounts of water, which would otherwise remain suspended in an organic medium (4). In inorganic membrane development, different workers have anticipated this water condensation effect but no effort to quantify this phenomenon has been reported.

This thesis also dealt with the successful recycling of a homogeneous oxidation catalyst from a reaction mixture using a nanofiltration process (chapter 6). The chemical reaction was carried out in a highly oxidising environment. Under such conditions the stability of polymeric membranes puts a question mark on the feasibility of the recycling process. But in contrast to currently known nanofiltration systems for recycling of homogeneous catalysts, the overall catalyst recycling system in this thesis relies on an inorganic membrane, which is chemically much more stable. In this thesis I showed that recovery of toluene soluble POM catalyst is almost quantitative. The organic solution (containing solvent, reactants, products and catalyst) permeability is lower than that of pure toluene solvent. This effect has been attributed to the capillary condensation of water from the solution as well as concentration polarization of the POM molecules on the solution/membrane interface.

In chapter 3 I described the formation of an ordered porous silica layer on different substrates with different pore architectures. In the literature it is found that successful deposition of surfactant templated silica layers on porous supports is possible. But in most of these cases, structural characterization was carried on powders derived from the same sol that was used to form the thin film on the porous support. Though, it is well accepted in materials science that the structure of thin films may differ considerably from that of powders. In this chapter I also showed systematically that the powders and thin films, derived from same sol, could be structurally different. In chapter 3, I showed that when a surfactant templated silica layer was deposited on a porous support, XRD and TEM

characterization directly on the membrane could be carried out successfully. I also showed a unique feature of templated film growth on mesoporous supports. In literature it has been shown that ordering of the surfactant templated silica layer starts directly from the surface of the dense substrate (5). In this thesis we saw that in the case of a mesoporous support, the situation differs considerably. The ordered silica layer does not grow directly on the porous support; instead it grows on an amorphous intermediate layer.

Recommendations

a) Solvent transport through porous media

To further explore these effects it may be useful to try to control the water content of hydrocarbons by equilibrating them with salt solutions of known osmotic pressure, either via direct contact or through vapor. If a quantitative dependence of the permeability on the water activity could be established that would be a very interesting study.
A comparison between aromatic and aliphatic hydrocarbons might also be interesting. Aromatics will typically dissolve ten times more water than aliphatics - does this have an effect, or is it only the relative degree of water saturation in the liquid that is important?
To observe liquid behavior in confined spaces, we can simulate the membrane pore environment by coating flat surfaces of mica and an AFM tip with a γ-alumina layer by pulsed laser deposition (PLD). The advantage of PLD is that depending upon deposition conditions, the alumina layer roughness can be varied in a controlled way. Using a liquid cell AFM, we can observe force law in the liquids in the presence of a second species.

b) Nanofiltration

In this thesis successful recycling of an oxidation catalyst from the reaction mixture has been demonstrated. Entire experiments have been carried out on laboratory scale using flat plate membrane geometry. In future it would be nice to see the recycling efficiency on large scale (~ 5L) using tubular modules of γ-alumina membranes.

c) Surfactant templated silica layer

This thesis shows that on a mesoporous support, ordered growth in the thin silica layer starts on top of an intermediate layer. It would be interesting to see if the

same observation can be made on macroporous supports. In other words, does pore dimension of the support have any effect on the observed phenomenon? Another issue that would be interesting to study further is if there is any effect of the intermediate layer thickness on the liquid permeability through mesoporous silica membranes. The intermediate layer thickness may be varied by different coating rates. From a transport point of view it is also important to know the nature of the pores in the intermediate layer. If the intermediate layer is microporous in nature, liquid permeation through this layer may be the rate-determining step in the entire process.

References

1. W.A. Patrick, N.F. Eberman, Studies in adsorption from solution from the stand point of capillarity- II, *J. Phys. Chem.*, **29** (1925) 220.
2. T. Tsuru, H. Kondo, T. Yoshioka, M. Asaeda, Permeation of nonaqueous solution through organic/lnorganic hybrid nanoporous membranes, *AIChE J.* **50** (2004), 1080.
3. L. Bocquet, E. Charlaix, S. Ciliberto, J. Crassous, Moisture-induced ageing in granular media and the kinetics of capillary condensation, *Nature*, **396** (1998) 735.
4. H.K. Christenson, J, Fang, J.N. Israelachvili, Experimental-study of phase-separation in films of molecular dimensions, *Physical Rev. B,* **39**, (1989) 11750.
5. Y.F. Lu, R. Ganguli, C.A. Drewien, M.T. Anderson, C.J. Brinker, W.L. Gong, Y.X. Guo, H. Soyez, B. Dunn, M.H. Huang, J.I. Zink, Continuous formation of supported cubic and hexagonal mesoporous films by sol gel dip-coating, *Nature*, **389** (1997) 364.

Now this is not the end. It is not even the beginning of the end.
But it is, perhaps, the end of the beginning
- Sir Winston Churchill

Acknowledgements

Time flies. Four years ago when I started my Ph.D. work here, in Enschede, I knew almost nothing about inorganic membranes and life in cold western countries. In the last four years I went through several experiences and I shared them with you - not all events with all of you but in each event with some of you.

My first sincere thanks go to my supervisor Andre, who has been with me since I started working in IMS. Andre - I learned a lot from you and still have a lot to learn from you. We had regular discussions not only on scientific matters but also on different topics [jealous people say "arguments"☺]. You read me very well and steered [? at times you were confused about it ☺] me accordingly. Thank you for all that you have done.

Dave – thank you for all the support you have provided me with. You have been a great promoter. In last two years, especially in the final year of my Ph.D., when I had to go back to India for family matters you said, "don't worry, go home, they need you, we will take care here". It was a great relief.

Klaas - I really appreciate your laughter, passion for materials science and red wine. I am grateful to you for enlightening me on the philosophical part of scientific research.

Peter (Witte) – thank you for all the organic synthesis and analysis presented in chapter 6. I really enjoyed our email correspondence on experimental planning and discussion on the experimental findings. Paul (Alsters) - thank you for being a very good coordinator between DSM and Twente. Dorit and Ronny (Weizmann Institute of Science) thank you for initial catalyst (POM) supply and NMR measurements. Alisia (Peters) - thank you for your 10 months hard work that contributes to a significant part of chapter 3 and my thesis cover page. Joska, thank you for γ-alumina thin film deposition by PLD on Si-wafer, with which, I started working on my recommendations presented in chapter 7. Guus, thank you for your eye opening discussions on how PLD can be used to tailor the surface roughness. Michel (Kappl) (MPI polymer research, Mainz) - thank you for giving me the first opportunity to learn the basics of experimental liquid dynamics in confined space using AFM. Rico (Keim) and Albert - thank you for all time help for TEM and XPS. Both of you spent a lot of time in understanding the problem and delivering the best results.

Mieke, Cindy, Wika, Attila, Gerrit, Herman - thank you all for your laboratory supports. You never said "no" to me whenever I asked for favour. Henk, thank you for money matters. Cis - I will remember your "survival package" for my first three days in Netherlands. Marion - thank you for official matter handling. Louis - thank

you for discussion on nanofiltration at the very end of my thesis. Warner - you were the first person, who invited me to the University of Twente for interview, four years ago. Thank you for giving me that opportunity. Jose - thank you for all computer-related help and giving me tips on buying nice coffee mugs and children books.

My current officemates Richard and Ahmed - thank you for sharing the pain of dealing with Dutch immigration office, IND. I remember that from time-to-time we acted as a single team member when any one of us was fighting against IND over the phone. My past officemates, Mark (Hendricks), Ashima and Tijana - thank you all for sharing your experience inside and outside LA 1751 (or CT 1751?).

Tim - you reminded me of the story of Forrest Gump, but with a difference - you know where to stop. Thank you for sharing your research excitements with me. Monse, I was supposed to work in your project at the beginning (which I didn't). While I was formatting my thesis, I used your thesis as a model and still envy your perfectionism. I specially thank you for giving me the first opportunity to prepare "biriyani" at your kitchen!!! Samuel - thank you for providing interesting literatures on surface science and showing me the first time that the Dutch can also eat real hot Indian curry! Steven, Beatriz, Mai, Thang, Jelena, Krisztina - thank you for sharing your views with me on critical issues like criticizing Dutch people☺. Riaan - thank you for making me partially addicted towards passive smoking in the Alembic Borrel room☺. Fredo – thank you for exquisite French foods and also for the list of ten important French words (and their English translations, of course) used on French highways☺. Vittorio - thank you for being one of my paranymfs. Frank, Matthijn, Paul, Arjen (J and M), Koray - thank you for nice BBQ. Monique (Smaihi), University of Montpellier II - thank you helping me explore all possibilities for getting a position in France not only for me but also for my wife, Saheli.

Outside university a huge Indian community made my stay in The Netherlands more pleasant - diverse experiences I had with them. Those made my last four years very colourful. Kinsuk, Subhas da - thank you for being part of the same cooking group and for a host of other activities. Anurag, Kausik, Rituparna (Mandal), Raja da, Sharmishtha di, Mousumi di, Partha da, Diptish, Vipin, Richa, Pranab da, Nely, Kanya di, Tamalika, Ravi, Madhavi, Nikhil da, Rituparna boudi, Swapan babu, Anjana, Arup Nandi - thank you all for helping me make Netherlands as a (temporary) second home (E parobaas e robe ke!). Pratip, I should not thank you☺. Why should I? Give me a good reason…. Actually we have been so close in the last four years, I guess we crossed the border of any formality. Arup da and boumoni – thank you for encouraging me at all times when I am depressed or making me calm when I am angry.

Away from the university, in the last four years I spent a lot of time with German railways, Dutch railways and Swiss railways. Although I did not have pleasant experience with these carriers always but the experiences I gathered with them were invaluable.

Ma, Babin – had you not allowed me to “go, as you like”, I would not have been here today. I know you suffered a lot emotionally and physically but you should know I am here today only because of you. Didi, Uttam da - I could spend these four years here because I know, if something happens there, you will take care of Ma, Babin with unparalleled efficiency. Chhotomama - how do I forget those hectic days of getting visa from Dutch embassy at New Delhi? We were running like headless chickens to recover misplaced files from the embassy. At this point those days are like nightmares. You and chhoto mamima were always there with me.

Tuku, what to say to you? Are you really looking for thanks in this chapter? You deserve more than just that. Last two years you witnessed all my mood swings. You had been with me always.

Yours tomader

Sankho *Sankha, Sankha da*

Publications

Refereed Journal Articles:

1. P. T. Witte, **S. Roy Chowdhury**, J. E. ten Elshof, D. Sloboda-Rozner, R. Neumann, and P. L. Alsters, "Highly efficient recycling of a "sandwich" type polyoxometalate oxidation catalyst using solvent resistant nanofiltration", ***Chemical Communications***, 1206-1208 (2005).
2. R. Schmuhl, W. Nijdam, J. Sekulic, **S. Roy Chowdhury**, C.J.M. van Rijn, A. van den Berg, J.E. ten Elshof and D.H.A. Blank, "Si-supported Mesoporous and Microporous Oxide Interconnects as Electrophoretic Gates for Application in Microfluidic Devices", ***Analytical Chemistry***, 77 178-184 (2005).
3. **S. Roy Chowdhury**, K. Keizer, J.E. ten Elshof, and D.H.A. Blank, "Effect of trace amounts of water on organic solvent transport through gamma alumina membranes with varying pore sizes," ***Langmuir***, 20 4548- 4552 (2004).
4. R. Schmuhl, **S. Roy Chowdhury**, J.E. ten Elshof, A. van den Berg and D.H.A. Blank, "Nanostructured ion-selective MCM-48 membranes," ***Journal of. Sol-Gel Science and Technology***, 31 249-252 (2004).
5. R. Schmuhl, J. Sekulic, **S. Roy Chowdhury,** C.J.M. van Rijn, K. Keizer, A. van den Berg, J.E. ten Elshof, and D.H.A. Blank, "Si-compatible ion selective mesoporous and microporous oxide interconnects with high tuneability," ***Advanced Materials***, 16 900-904 (2004).
6. **S. Roy Chowdhury**, R. Schmuhl, K. Keizer, J. E. ten Elshof and D. H. A. Blank. "Pore size and surface chemistry effects on the transport of hydrophobic and hydrophilic solvents through mesoporous gamma alumina and silica MCM-48", ***Journal of Membrane Science***, 225 177- 186 (2003).
7. J.E. ten Elshof, C. Rubio Abadal, J. Sekulic, **S. Roy Chowdhury** and D.H.A. Blank, "Transport mechanisms of water and organic solvents through microporous silica in the pervaporation of binary liquids," ***Microporous Mesoporous Materials*** 65 197-208 (2003).
8. **S. Roy Chowdhury**, J.E. Ten Elshof, N.E. Benes and K. Keizer, "Development and comparative study of different nanofiltration membranes for highly charged large ion recovery", ***Desalination***, 144, 41-46 (2002).

Conference articles and abstracts

1. **S. Roy Chowdhury**, K. Keizer, J.E. ten Elshof, and D.H.A. Blank "Liquid transport through alumina membranes" Proc of Euromembrane 2004, ed. J. Hapke, C.N. Ranong, D. Paul, K.V. Peinemann. Hamburg, 2004.
2. **S. Roy Chowdhury**, R. Schmuhl, K. Keizer, A. van den Berg, J.E. ten Elshof, and D.H.A. Blank,"Tailor-made nanostructured ion selective MCM-48 membranes," Proc. Int. Symp. On Self-Assembled Nanostructured Materials, ed. C.J. Brinker, M. Antonietti, Y. Lu, and C. Bai, Mat. Res. Soc. Proc. 775,Materials Research Society, Pittsburg, 2003.
3. J.E. ten Elshof, **S. Roy Chowdhury,** "Template-directed synthesis of mesoporous ceramic membranes" 9th Aachen Membrane Colloquium, 18-20 March 2003.